Effect of addition of lithium salts on properties of poly(methyl methacrylate)

Asae Ito

Japan Advanced Institute of Science and Technology

Doctoral Dissertation

Effect of addition of lithium salts on properties of poly(methyl methacrylate)

Asae Ito

Supervisor: Prof. Dr. Masayuki Yamaguchi

Graduate School of Advanced Science and Technology

Japan Advanced Institute of Science and Technology

Materials Science

March 2019

Referee-in-chief: Professor Masayuki Yamaguchi
Japan Advanced Institute of Science and Technology

Referees: Professor Masayuki Yamaguchi
Japan Advanced Institute of Science and Technology

Professor Tatsuo Kaneko
Japan Advanced Institute of Science and Technology

Associate Professor Toshiaki Taniike
Japan Advanced Institute of Science and Technology

Associate Professor Ken-ichi Shinohara
Japan Advanced Institute of Science and Technology

Professor Akihiro Nishioka
Yamagata University

Effect of addition of lithium salts on properties of poly(methyl methacrylate)

Yamaguchi Laboratory
Asae Ito (s1620002)

Heat resistance and optical properties of amorphous polymers are important for engineering applications such as automobile parts, electrical devices, and displays. In general, a single plastic material often possesses poor physical properties for engineering application, so that the improvement of properties has been tried in decades. In particular, one of the promising processes to modify a polymer is mixing with low-molecular-weight compounds. Recently, it was found that the addition of a specific lithium salt enhances glass transition temperature (T_g) of poly(methyl methacrylate) (PMMA), which is a typical amorphous polymer. T_g is an index for heat resistance for amorphous polymers. Thus, the improvement of heat resistance of PMMA was achieved by the addition of the lithium salt as a simple way. However, it was not revealed that what kind of anion species of the salts powerfully affects T_g enhancement. In this study, I focused on the improvement of heat resistance of PMMA using this method. I found a lithium salt with the most effective anion for T_g increase of PMMA. Another salt that enhanced T_g and suppressed water absorbency of the blend film was also found. It was also attempted to investigate the mechanism of T_g enhancement of PMMA by adding such lithium salts. In the case of optical properties of polymers, orientation birefringence occurs during molding process of plastics. Furthermore, photoelastic birefringence is caused by elastic deformation of final products. It is required to suppress the birefringences for optical films. Therefore, orientation birefringence and photoelastic birefringence of the blend films were investigated.

In Chapter 2, the T_g enhancement of PMMA by the addition of various lithium salts was investigated using $LiNO_3$, $LiClO_4$, $LiCF_3SO_3$, $LiCOOCF_3$, and $LiN(CF_3SO_3)_2$ with 0.07 molar ratio of lithium cations per 1 molar of carbonyl groups in PMMA. As a result, $LiCF_3SO_3$ was the most effective on T_g enhancement for PMMA, which is due to ion–dipole interactions between the lithium cations and the carbonyl groups in PMMA molecules. However, at the same time, the addition of $LiCF_3SO_3$ also increased moisture absorption. Because water acted as a plasticizer in the case of $LiCF_3SO_3$, the T_g decreased with low modulus, even in the glassy region of PMMA/$LiCF_3SO_3$. In contrast, plasticization due to moisture absorption was not detected in the case of LiBr.

In Chapter 3, the mechanism of T_g enhancement by the addition of LiBr was investigated. It was found that a strong physical crosslinking occurs in PMMA/LiBr, leading to a prolonged relaxation mode. Furthermore, it was revealed that the prolonged relaxation mode is dominant to increase T_g in PMMA/LiBr. This phenomenon had not been reported that such strong crosslinking occurs only by the addition of a specific lithium salt. This technique could be applicable to provide strong physical crosslinking in various functional materials composed of PMMA.

In Chapter 4, the optical properties and thermal expansion of the blend films of PMMA with $LiCF_3SO_3$ were investigated. The orientation birefringence of films was decreased by addition of $LiCF_3SO_3$ when the film was stretched with same level of stress. The orientation birefringence of the blend was small since pure PMMA has a small intrinsic birefringence. Moreover, the addition of $LiCF_3SO_3$ reduced the photoelastic birefringence in the glassy state and the stress-optical coefficient. This may be attributed to the strong ion–dipole interactions between the lithium cations and the carbonyl groups of PMMA. The small thermal expansion was caused by such strong interactions. The modification of properties of PMMA by blending with salts is an attractive choice for optical applications including liquid crystal displays.

Keywords: Poly(methyl methacrylate), Salt, Glass transition temperature, Birefringence

Abstract

Poly(methyl methacrylate) (PMMA) has been applied to various products including optical usage, taking advantage of high durability and transparency. However, some properties such as heat resistance and birefringence do not satisfy the required conditions. Considering such situation, modification of the physical properties of PMMA has been tried so far. In this study, suppression of both birefringence and thermal expansion and improvement of heat resistance have been achieved by the addition of specific metal salts to PMMA. This is a very simple method without complicated process such as chemical synthesis. Therefore, it will be applicable in industry without any difficulties. This method can be established as next-generation functional materials by clarifying the relation between salt species and physical properties of polymer-salt blends. This can be applied to not only PMMA but also other polymers. I hope that this method will expand the application and the conditions of use of various plastics in industry.

Asae Ito

Acknowledgements

This work has accomplished under the cooperation of many people. I really appreciate receiving a lot of help in this two years.

First of all, I appreciate the supervision in my doctoral course by Prof. Dr. Masayuki Yamaguchi. I greatly thank him for being able to promote my doctoral studies in such a short period. I think it was impossible to finish my PhD without his appropriate advises.

I gratefully acknowledge many advises for my work by Prof. Dr. Tatsuo Kaneko. He gave me lots of helpful comments especially about the specific interaction in PMMA with LiBr. My doctoral thesis was further improved thanks to him. I am also grateful to Associate Prof. Dr. Toshiaki Taniike for helpful discussions. Associate Prof. Dr. Ken-ichi Shinohara, Prof. Dr. Akihiro Nishioka, and Prof. Dr. Noriyoshi Matsumi also gave me good suggestions about the thesis.

I would like to express my special thanks to Yusuke Sato and Maho Miyashita, who are master students in our laboratory. Mr. Sato helped me a lot to carry out XRD analysis. Ms. Miyashita also supported me to evaluate optical properties.

I thank Nobuaki Ito to measure my samples by XPS. Although the measurement did not succeed, it was a good experience for me.

I also would like to express my appreciation to my kind colleagues, Ryota Maeno, Naoya Tsugawa who is a visiting researcher from TOSOH corp., and Assistant Prof. Dr. Panitha Phulkerd. They gave me a lot of useful advises about my work.

I also appreciate Takumi Sako, who is another PhD student in our laboratory, for helping me a lot. He told me how to use many apparatus. Of course, I would like to express deep gratitude to other lab members. They encouraged me with heart-warming words and attitudes when I was sometimes depressed.

I express my gratitude to the Doctoral Research Fellow (DRF, JAIST) for financial support during my doctoral research.

Finally, I would like to express my deepest gratitude to my family for lots of support during my PhD.

Asae Ito

Contents

Chapter 1

General introduction

1.1. Basic properties of polymers

1.1.1. Crystalline and amorphous polymers

Polymers are widely used in industrial applications because of their wide-range properties. They are divided into two types such as crystalline and amorphous polymers, as shown in Figure 1.1 [1], [2].

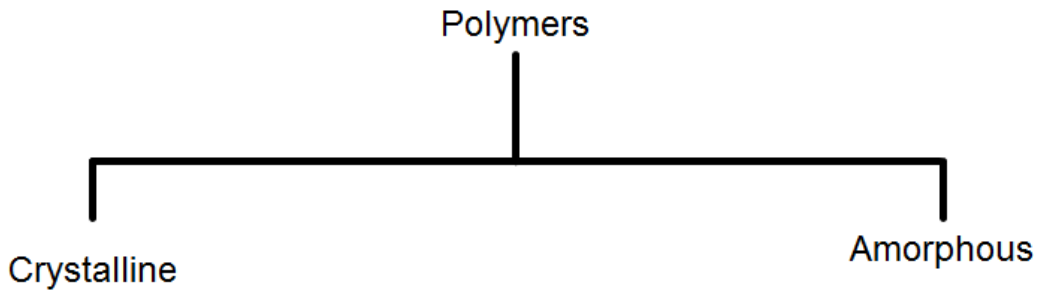

Figure 1.1. Classification of polymers [1], [2].

Crystalline polymers have highly organized structures. They are known to have high chemical resistance and high heat resistance. On the other hand, amorphous polymers show only short-range order like liquid phase of a low-molecular-weight compound. High transparency is a prominent feature of amorphous polymers.

1.1.2. Rubbery state and glassy state

There are rubbery state and glassy state in liquid phase of polymers, which are classified based on the molecular motions depending on time and temperature. In rubbery state, Brownian motion of polymer chains is allowed. As increasing the temperature, it is activated, leading to macroscopic flow under the stress. On the other hand, in glassy state, Brownian motion of polymer chains is frozen and only the molecular motions of side chains in polymers can occur.

1.1.3. Glass-to-Rubber transition

The change of specific volume as a function of temperature is shown in a schematic diagram in Figure 1.2.

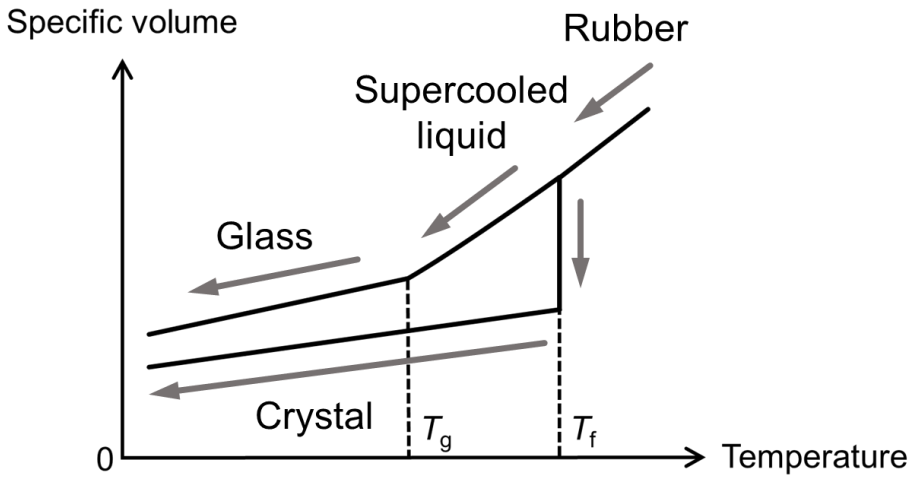

Figure 1.2. Schematic diagram of temperature dependence of specific volume in crystalline and amorphous polymers [1].

Starting from the rubbery state, a steady contraction in volume progresses at cooling, and sudden discontinuous drop occurs at the freezing point (T_f) when crystallization takes place as shown in the figure [1].

In certain crystallizable materials, liquid apparently solidifies below T_f by fast cooling and a discontinuous change in volume appears without crystallization [1]. Then, there is a change in the slope of the volume curve as a function of temperature as shown in the figure. This point is so called glass transition temperature (T_g). There is no discontinuous change in volume at T_g, but there is an apparent discontinuous change in quantities such as the specific heat, which is defined as the second derivative of the free energy [1]. Therefore, this is sometimes called as a second order transition (it is still open to discussion whether or not the T_g is related to a true second order transition) [1].

Certain polymers can never crystallize [1]. Such polymers are commonly defined as amorphous polymers. An amorphous polymer becomes a supercooled liquid, and it changes into glass below T_g.

1.1.4 Indicator of heat resistance of polymers

Recently, improvement of heat resistance is required for specific applications used under high temperatures. It is necessary to prevent flow and macroscopic deformation of polymer materials under an ambient temperature. Therefore, in polymers, T_f and T_g play a decisive role on the mechanical behavior.

As mentioned above, crystalline polymers easily crystallize below T_f, and thus, easily lose flowability. Therefore, the indicator of heat resistance for crystalline polymers is T_f.

In the case of amorphous polymers, Brownian motion of polymer chains is allowed beyond T_g, leading to macroscopic deformation and/or flow. Therefore, the indicator of heat resistance for amorphous polymers is T_g.

1.2. Modification of polymers using additive

1.2.1. General methods for polymer modification

Since physical properties of a single plastic material are sometimes not enough for engineering application, their improvement has been required in decades. As a means of improving physical or mechanical properties such as heat resistance, toughness, and processability, the following three methods are often employed: synthesis of new functionalized polymers [3]–[5], fabrication of polymer blends with different polymers [6], [7], and mixing with additives, i.e., low-molecular-weight compounds [8]–[10]. The first method can provide a special polymer on demand of specific applications. In comparison, the latter two methods are the easiest and the most useful methods. However, in polymer blends, there is a limitation of the combinations of different polymer species, since most blends are incompatible. Furthermore, even in compatible polymers, a sea-island structure is often formed on a microscale. Therefore, a miscible blend, which means mixing on molecular level, is almost impossible to obtain. Based on this situation, a current trend has focused on the additives with low-molecular-weight, because they can be miscible in a polymer.

1.2.2. Modification of polymers by inorganic fillers

In various additives, inorganic fillers are well known to improve various physical properties of polymers such as stiffness, strength, dimensional stability, and thermal stability [11]. There have been a lot of reports on the modification of physical properties for poly(propylene) (PP) by inorganic materials. For instance, talc is well known as one of the effective additives to improve various properties such as modulus and decomposition temperature of PP [12]. Mica also strongly improves the properties of PP [11], [13], [14]. Yazdani et al. reported that mica increases the stiffness of PP [11]. In addition, Zuiderduin et al. reported that PP with calcium carbonate shows higher stiffness and higher impact resistance than pure PP [15]. Furthermore, it was revealed that the addition of halloysite nanotubes (HNTs) improves thermal stability of PP [16].

A similar technique is also applicable for amorphous polymers. Rao et al. reported that poly(methyl methacrylate) (PMMA)-mineral composites show good mechanical strength [17]. Zhu et al. reported that thermal stability of PMMA is improved by doping only 3 % of sodium-montomorillionite-based-clay [18]. Another example was presented by Khan et al. They indicated that mechanical properties of polycarbonate (PC) are improved by blending with 32 % of jute [19].

In the case of the modification of amorphous polymers, it is often requested to maintain their high transparency for various applications including optical use. However, such inorganic fillers sometimes cause a reduction of transparency as the amount of fillers increases.

1.2.3. Modification of amorphous polymers by ionomers

As a way to modify physical properties of amorphous polymers without impairing their transparency, ionic interaction has been applied for practical usage. An ionomer is one of the most famous examples. Polymer materials including ionic bonds have been applied to practical use using metal salts.

Ma et al. reported that a PMMA-based ionomer with sodium and calcium ions shows higher storage modulus than pure PMMA [20].

Furthermore, the ionic interaction as physical crosslinking is one of the promising examples for T_g enhancement, that is, improvement of heat resistance, of amorphous polymers [21]–[24]. These materials are so called ionomers. In general, ionomers can be obtained by neutralizing polymers due to introducing a small amount of acid/base group, e.g., carboxyl or sulfone group, into a hydrophobic polymer by copolymerization.

The structure of ionomer is explained using the multiplet-cluster model [25]. The schematic illustration of a hierarchical structure of multiplet and cluster is shown in Figure 1.3 [26].

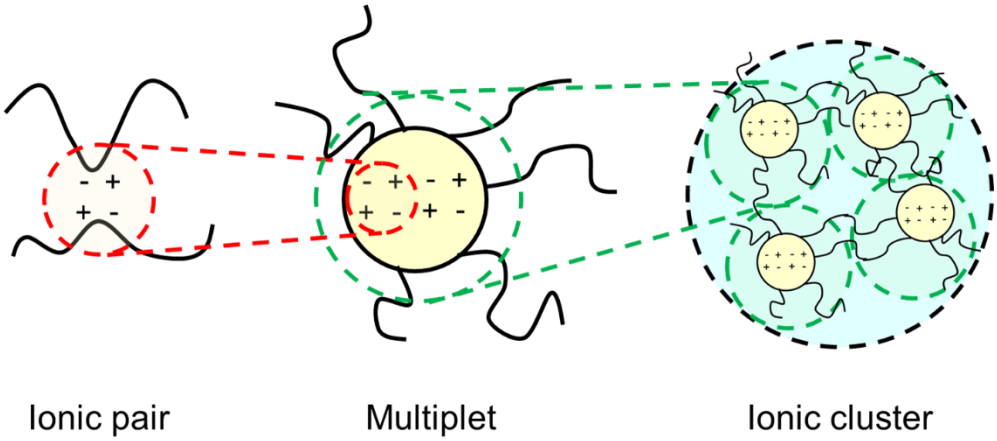

Figure 1.3. Schematic illustration representing hierarchical structure of ionomer [26].

Thus, mechanical properties of a matrix are improved by crosslinking between metal ions and functional groups in a polymer.

Figure 1.4 shows the dynamic mechanical properties of a PMMA-based ionomer, poly(methyl methacrylate-sodium methacrylate), with different sodium salt contents [20].

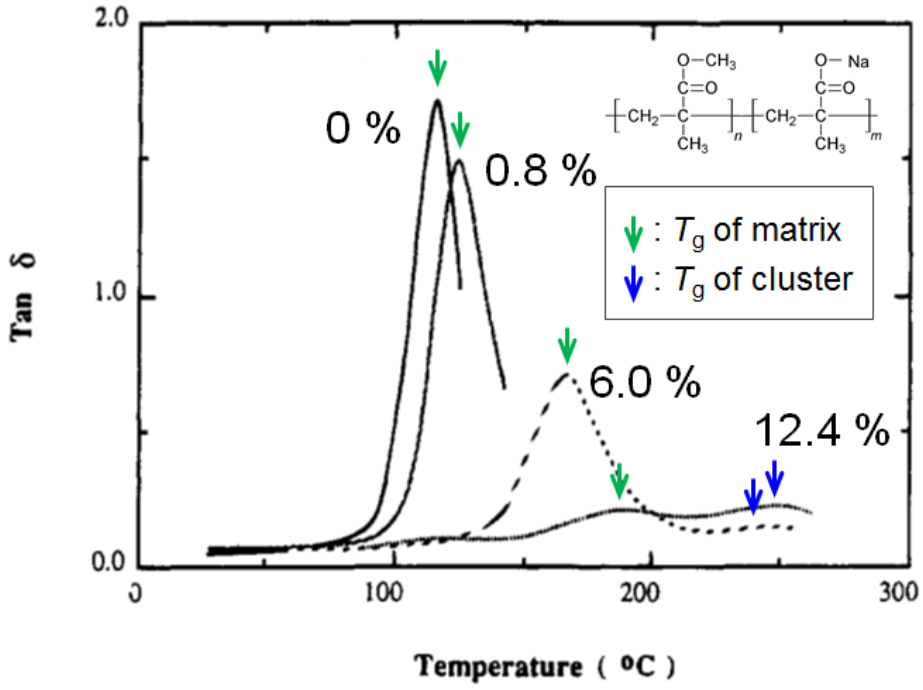

Figure 1.4. Temperature dependence of loss tangent (tan δ) of PMMA ionomers (sodium salt); poly(methyl methacrylate-co-sodium methacrylate) with different concentrations of 0, 0.8, 6.0, and 12.4 %. T_g was enhanced as the salt content increases [20].

There are two types of T_g, i.e., T_g of a matrix phase and T_g of a cluster phase. The peak located at the lower temperature is assigned as T_g of the matrix phase containing multiplets, ascribed to ionic aggregations. On the other hand, the high-temperature-peak in the curves of tan δ (The explanation of tan δ is described in chapter 2.) is assigned to T_g of the cluster phase, ascribed to ionic further aggregation into clusters as a second phase. As shown in Figure 1.4, T_g of the matrix is enhanced as the ion content increases. That is, heat resistance of the matrix is improved along with increase in the salt contents.

In ionomers, various properties can be improved with the high transparency as an advantage of amorphous polymers by introducing ionic interaction. At industrial applications, however, poor flowability of an ionomer causes a lack of molding

processability. Furthermore, it costs a lot for the process of ionization.

Considering these circumstances, it has been required to improve physical properties and to design new functional polymers using appropriate additives without impairing the high transparency and flowability of amorphous polymers.

1.3. Modification of PMMA

1.3.1. Application of PMMA

PMMA is one of the most useful amorphous polymers, which is well known as the material to be used for optical devices because of their high transparency. However, there are various demands to modify some properties of PMMA. For example, heat resistance is only around 100 ºC, which is not enough for engineering applications. Recently, especially for parts in automobiles, high heat resistance is required [27]. Takahashi pointed out that as the power densities of automobiles increased, the heat resistance at least at 200 ºC is demanded for their peripheral materials in automotive industry [27]. At present, in order to reduce the weight, all-plastic vehicles are being developed. As a part of this attempt, PMMA with both high heat resistance and transparency is desired for windshield and roof members [28].

It is also important to modify the optical properties of PMMA for various optical applications, e.g., diffusing plates for liquid crystal displays (LCDs) [29]–[31], substrates for optical disks [32], and optical fibers [33], [34], owing to its high transparency.

Therefore, this thesis aims to improve the heat resistance and optical characteristics of PMMA while maintaining its high transparency and flowability using an optimum additive, as described above.

1.3.2. Improvement of heat resistance of PMMA by lithium salts

Recently, Miyagawa et al. found that T_g of PMMA is enhanced by the addition of lithium trifluoromethanesulfonate ($LiCF_3SO_3$) which is indicated in Figure 1.5 [35].

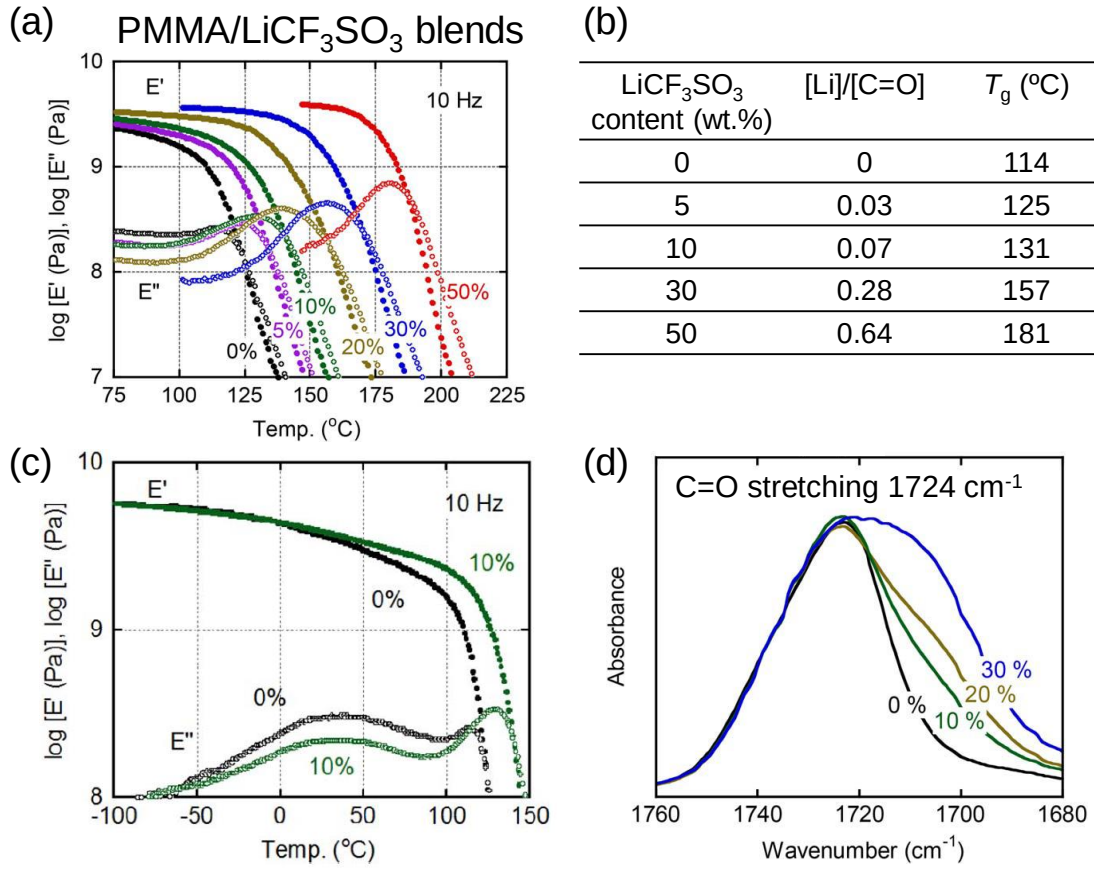

$LiCF_3SO_3$ content (wt.%)	[Li]/[C=O]	T_g (ºC)
0	0	114
5	0.03	125
10	0.07	131
30	0.28	157
50	0.64	181

Figure 1.5. (a) Temperature dependence of the oscillatory tensile moduli of PMMA/$LiCF_3SO_3$ blends with different molar ratios. (b) T_g enhancement of PMMA by the addition of $LiCF_3SO_3$ with different amounts. (c) Temperature dependence of the oscillatory tensile moduli of the blends with 0 and 10 wt.% of $LiCF_3SO_3$ at 10 Hz at the temperatures from -100 ºC to 150 ºC. (d) FT-IR spectra of stretching vibration mode of carbonyl group of PMMA at 1724 cm^{-1} in wavenumbers from 1680 cm^{-1} to 1760 cm^{-1} of the blends with 0, 10, 20 and 30 wt.% of $LiCF_3SO_3$ [35].

This phenomenon is attributed to the ion-dipole interaction between polymer and metal cations.

In this blend, T_g was enhanced gradually as the salt concentration increased (Figure 1.5. (a) and (b)). The T_g enhancement is due to physical crosslinking as ion-dipole interaction between lithium cations and carbonyl groups in PMMA, which is shown as a schematic illustration in Figure 1.6.

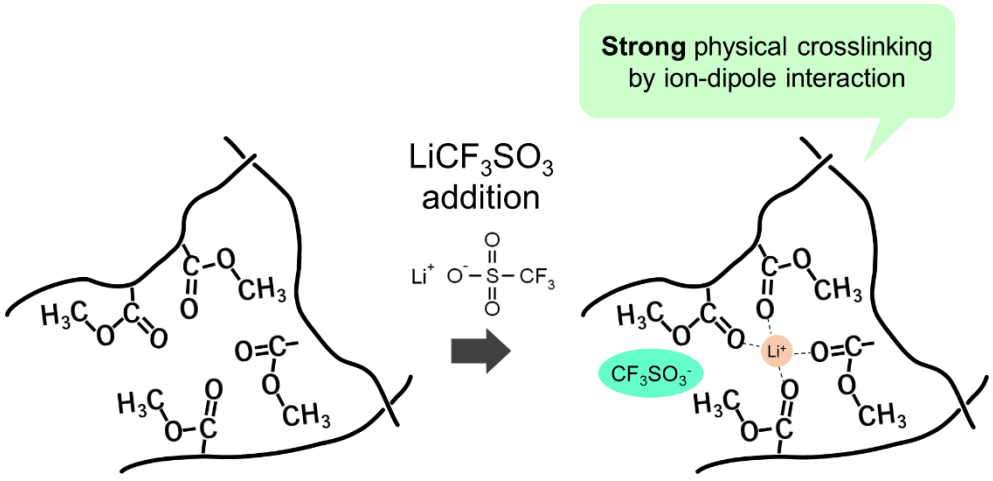

Figure 1.6. Schematic illustration of physical crosslinking by ion-dipole interaction between lithium cations and carbonyl groups in PMMA.

This phenomenon is suggested by the result of the reduction of β-relaxation mode, which is explained in chapter 2, of PMMA by the addition of 10 wt.% of $LiCF_3SO_3$ as seen in Figure 1.5 (c). Here, the β-relaxation mode is detected from -50 to 80 ºC, which is known to be ascribed to the local motion of the carbonyl group. This indicates that the local molecular motion is restricted by the strong electrostatic interaction between lithium cations and PMMA molecules. Figure 1.5 (d) shows the IR spectra of carbonyl stretching vibration at 1724 cm^{-1}. The peak becomes broad in the lower wavenumber region, i.e., higher energy region.

Although PMMA does not contain any acid/base groups like carboxyl or sulfonyl groups, T_g was effectively enhanced by the addition of the salt.

In this system, transparency can be kept even by the addition of 60 wt.% of the salt. In addition, this technique does not lose its high flowability, that is, thermoprocessability, because it is easily processed by compression-molding. Thus, T_g enhancement of PMMA can be achieved only by the addition of the lithium salt without any costly processes, and thus, this technique has a impact on industrial applications.

As mentioned above, it was revealed that the addition of lithium salts is quite effective to improve heat resistance of PMMA. However, it has not been clarified yet what kind of anion species affects the T_g enhancement for PMMA.

1.3.3. T_g enhancement of poly(ethylene oxide) (PEO) by lithium salts

The phenomenon in PMMA blends described above is also common in the field of solid electrolyte. The differential scanning calorimetry (DSC) trace curves of the crosslinked poly(ethylene oxide) (PEO)-lithium perchlorate ($LiClO_4$) complexes with different salt concentrations are shown in Figure 1.7 [36]. PEO is known as a promising material for solid electrolytes, and this is a rubbery polymer at room temperature. It can be seen from the figure that T_g of PEO-salt electrolyte is enhanced along the increase in the salt content.

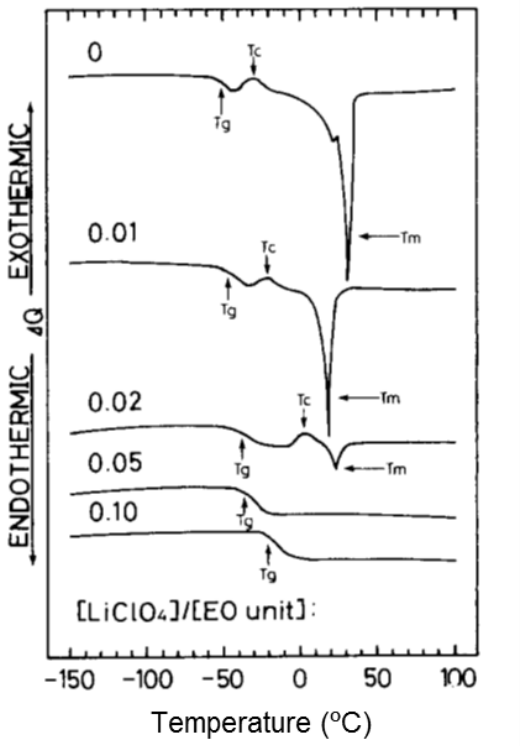

Figure 1.7. DSC heating curves of crosslinked PEO containing 0, 0.01, 0.02, 0.05, and 0.10 % of $LiClO_4$ [36].

1.3.4. Carrier transportation in PEO

The temperature dependence of ionic conductivity for the various PEO-alkali metal salt complexes in rubbery and amorphous states was known to be expressed by the following equation 1.1, where $\sigma_c(T)$ is the conductivity at the temperature T and, C_1 and C_2 are the constant values. This is so called Williams-Landel-Ferry (WLF)-type equation [37].

$$\log \frac{\sigma_c(T)}{\sigma_c(T_g)} = \frac{C_1(T-T_g)}{C_2+(T-T_g)} \quad (1.1)$$

In order to improve the reliability of the estimation of WLF parameters, $T_0 = T_g + 50$ (°C), was adopted as another reference temperature in this equation, because the conductivities near T_g could not be measured [38].

$$\log \frac{\sigma_c(T)}{\sigma_c(T_0)} = \frac{C_1'(T-T_0)}{C_2'+(T-T_0)} \quad (1.2)$$

The results of the WLF plots of PEO complexes with various alkali metal salts are indicated in Figure 1.8 [38] using the equation (1.2). As a result, the parameters for this master curve indicated by the solid line in the figure were C_1'= 4.6 and C_2'= 95.6. These values are comparable to the universal values, C_1'=8.86 and C_2'=101.6, which were reported by Williams et al [37]. This fact suggests that ionic migration does not occur by its Brownian motion itself but the segmental motion with associated ions brings the ionic migration.

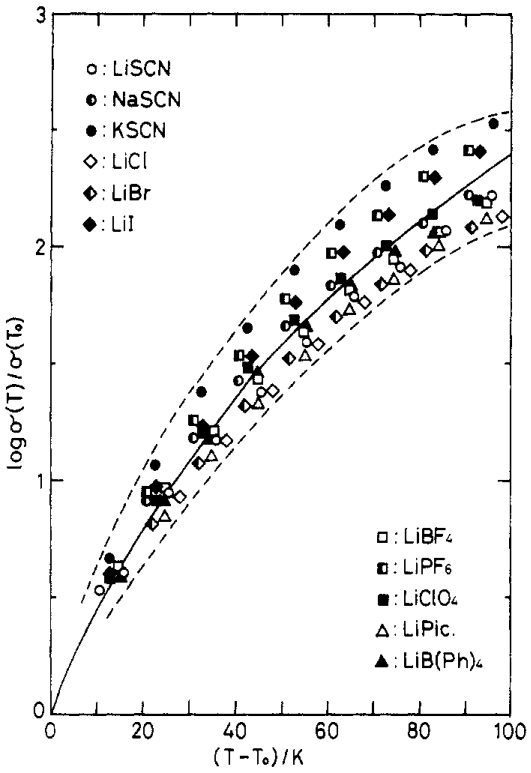

Figure 1.8. WLF plots of ionic conductivity for PEO-alkali metal salt complexes using a reference temperature T_0 with different kinds of lithium salts: lithium thiocyanate (LiSCN), sodium thiocyanate (NaSCN), potassium thiocyanate (KSCN), lithium chloride (LiCl), lithium bromide (LiBr), lithium iodide (LiI), lithium tetrafluoroborate ($LiBF_4$), lithium hexafluorophosphate ($LiPF_6$), $LiClO_4$, lithium picrate (Lipic), and lithium tetraphenylborate ($LiB(Ph)_4$) [38].

Thus, this segmental motion with ionic migration has been considered to occur by the strong ion-dipole interaction between carrier ions and PEO polymer chains [38]. Watanabe et al. indicated that the interaction of ions with the ether oxygen atoms in the PEO chain is an essential process for the carrier generation, and this interaction inhibits the crystallization of PEO chains. Considering ionic movement in solid electrolyte, Armand insisted that solvation-desolvation processes by polymer chains cause ionic conduction [39], as shown

in the schematic illustration in Figure 1.9.

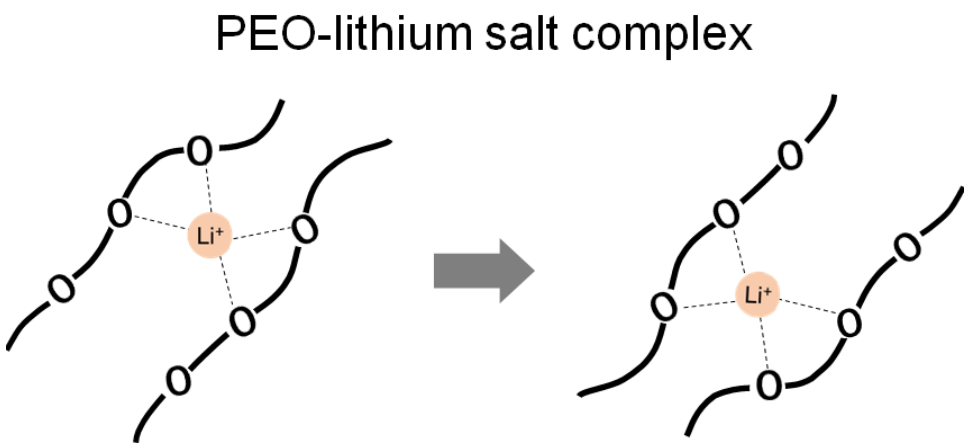

Figure 1.9. Molecular motion of PEO and transfer of lithium cation in PEO-based network polymer-lithium salt complex. Lithium cation moves with molecular segment motion simultaneously.

The cooperativity of such ion transfer and segmental motion of macromolecular chains indicates that T_g is highly related to the rate of ion transfer. In general, lithium cations are more easily solvated because they have larger charge densities, which is caused by their small ionic radius composed with that of anions. Thus, the contribution of lithium cations to T_g enhancement is considered to be stronger than that of anions.

Thus, T_g enhancement is considered to mainly occur due to ion-dipole interaction between lithium cations and the oxygen atoms in PEO. It has been known that the molecular motion occurs in cooperation with the ionic movement. Thus, the segmental motions of PEO are suppressed by this interaction, and as a result, T_g is enhanced.

In the field of lithium ion battery, T_g enhancement limits ionic conductivity. However, this disadvantage brings an advantage to the improvement of heat resistance of PMMA. Blending a polymer and specific metal salts makes it possible to control physical properties of the polymer simply.

1.3.5. Research objectives in this thesis

In summary, T_g enhancement by the addition of metal salts is also observed in typical solid electrolyte, and this phenomenon is thought to be caused by strong ion-dipole interaction between cations and polymer chains. It is well known that the degree of T_g enhancement in a system varies depending on the type of lithium salts in the field of lithium ion battery. However, it has not been known that what kind of anion species of the salts powerfully affects T_g enhancement.

Moreover, it is common that these salts easily associate in PEO. In general, especially when the ion concentration increases, ions make association easily. Such ionic association decreases the ionic conductivity. Based on this phenomena, Tominaga et al. have attempted to increase the ionic concentration by suppressing such ionic association and increasing the conductivity by processing in CO_2 under super critical conditions ($scCO_2$) [40], [41]. However, the mechanisms of dissociation/association of the salts in solid electrolytes have not yet been clarified. It is still unknown how the association of the salts affects T_g enhancement. Therefore, back to the topic in my thesis, it is difficult to predict the salt that mostly affects T_g enhancement of PMMA theoretically.

Therefore, in this study, the first purpose is to find a lithium salt with the most effective anion for T_g enhancement of PMMA. The influence of ionic association of the salts on T_g enhancement of PMMA is also investigated. In addition, the influence of the water absorbency on T_g enhancement is investigated. Another lithium salt capable of achieving both T_g enhancement and low water absorbability is found.

In Chapter 2, various lithium salts are added to PMMA. According to the temperature dependence of dynamic tensile moduli and IR spectra of the blends, the salt which can most affect T_g enhancement of PMMA has been found. Furthermore, another salt

which enhanced T_g and suppressed water absorbency of the blend film is also found.

In Chapter 3, the mechanism of T_g enhancement of PMMA is investigated by adding the lithium salts found in Chapter 2. According to the results of temperature dependence of viscoelastic properties, solvent immersion, and Infrared (IR) spectra, the possibility of a strong physical crosslinking structure is investigated.

In Chapter 4, the optical properties, that is, glassy and orientation birefringences, of PMMA is modified by the addition of the lithium salt found in Chapter 2. The basis about origins of such optical properties is written in this chapter. The effect of the salt content on thermal expansion of PMMA is also mentioned in this chapter.

In this thesis, physical properties, in other words, heat resistance, thermal expansion, and optical properties of PMMA are modified using lithium salts. This technique will be available for not only PMMA but also various types of polar polymers. Furthermore, there is a huge possibility to expand the applications of their materials with improved properties.

1.4. References

[1] M. M. Coleman and P. C. Painter, *Fundamentals of polymer science*, Second Ed. New York: CRC Press, 1998.

[2] R. J. Young and P. A. Lovell, *Introduction to polymers*, Third Ed. New York: CRC Press, 2011.

[3] M. Itoh, K. Inoue, K. Iwata, M. Mitsuzuka, and T. Kakigano, "New highly heat-resistant polymers containing silicon: Poly(silyleneethynylenephenyleneethynylene)s," *Macromolecules*, vol. 30, no. 4, pp. 694–701, 1997.

[4] Y. Ou, F. Yang, and Z. Z. Yu, "A new conception on the toughness of nylon6/silica nano composite prepaid via in situ polymerization," *J. Polym. Sci. Part B Polym. Phys.*, vol. 36, pp. 789–795, 1998.

[5] C. Cha, R. E. Kohman, and H. Kong, "Biodegradable polymer crosslinker: independent control of stiffness, toughness, and hydrogel degradation rate," *Adv. Funct. Mater.*, vol. 19, no. 19, pp. 3056–3062, 2009.

[6] Y. Li and H. Shimizu, "Improvement in toughness of poly(l-lactide) (PLLA) through reactive blending with acrylonitrile-butadiene-styrene copolymer (ABS): Morphology and properties," *Eur. Polym. J.*, vol. 45, no. 3, pp. 738–746, 2009.

[7] J. Wu, Y. Mai, and B. Cotterell, "Fracture toughness and fracture mechanisms of PBT/PC/IM blend Part I Fracture properties," *J. Mater. Sci.*, vol. 28, no. 12, pp. 3373–3384, 1993.

[8] X. L. Xie, Y. W. Mai, and X. P. Zhou, "Dispersion and alignment of carbon nanotubes in polymer matrix: A review," *Mater. Sci. Eng. R*, vol. 49, no. 4, pp. 89–112, 2005.

[9] Z. Bartczak, A. Argon, R. Cohen, and M. Weinberg, "Toughness mechanism in semi-crystalline polymer blends - I. HDPE toughened with rubber," *Polymer (Guildf).*, vol. 40, no. 9, pp. 2331–2346, 1999.

[10] H. Fischer, "Polymer nanocomposites: From fundamental research to specific applications," *Mater. Sci. Eng. C*, vol. 23, no. 6–8, pp. 763–772, 2003.

[11] H. Yazdani, J. Morshedian, and H. A. Khonakdar, "Effect of maleated polypropylene and impact modifiers on the morphology and mechanical properties of PP/Mica composites," *Polym. Compos.*, vol. 27, no. 6, pp. 614–620, 2006.

[12] Y. Zhou, V. Rangari, H. Mahfuz, S. Jeelani, and P. K. Mallick, "Experimental study on thermal and mechanical behavior of polypropylene, talc/polypropylene and polypropylene/clay nanocomposites," *Mater. Sci. Eng. A*, vol. 402, no. 1–2, pp. 109–117, 2005.

[13] H. G. Karian, *Handbook of Polypropylene and Polypropylene Composites*. New York: Wiley Interscience, 1999.

[14] J. Karger-Kocsis, *Polypropylene-Structure, Blends and Composites*. London: Springer, 1995.

[15] W. C. J. Zuiderduin, C. Westzaan, J. Huetink, and R. J. Gaymans, "Toughening of polypropylene with calcium carbonate particles," *Polymer (Guildf).*, vol. 44, no. 1, pp. 261–275, 2003.

[16] M. Du, B. Guo, and D. Jia, "Thermal stability and flame retardant effects of halloysite nanotubes on poly(propylene)," *European Polymer Journal*, vol. 42, no. 6. pp. 1362–1369, 2006.

[17] H. K. Rao, K. S. E. Forssberg, and W. Forsling, "Interfacial interactions and mechanical properties of mineral filled polymer composites: Wollastonite in PMMA polymer matrix," *Colloids Surfaces A Physicochem. Eng. Asp.*, vol. 133, no. 1–2, pp. 107–117, 1998.

[18] J. Zhu, P. Start, K. A. Mauritz, and C. A. Wilkie, "Thermal stability and flame retardancy of poly (methyl methacrylate)-clay nanocomposites," vol. 77, pp. 253–258, 2002.

[19] M. A. Khan, M. M. Hassan, and L. T. Drzal, "Effect of 2-hydroxyethyl methacrylate (HEMA) on the mechanical and thermal properties of jute-polycarbonate composite," *Compos. Part A Appl. Sci. Manuf.*, vol. 36, no. 1, pp. 71–81, 2005.

[20] X. Ma, J. A. Sauer, and M. Hara, "Poly(methyl methacrylate) based ionomers. 1. Dynamic mechanical properties and morphology," *Macromolecules*, vol. 28, no. 11, pp. 3953–3962, 1995.

[21] A. Eisenberg and J.-S. Kim, *Introduction to ionomers*. New York: Wiley Interscience, 1998.

[22] J. Kim, R. J. Jackman, and A. Eisenberg, "Filler and percolation behavior of ionic aggregates in styrene-sodium methacrylate ionomers," *Macromolecules*, vol. 27, no. 10, pp. 2789–2803, 1994.

[23] M. Hara and A. Eisenberg, “Miscibility enhancement via ion-dipole interactions. 2. LCST behavior in polystyrene ionomer/poly(alkylene oxide) systems.,” *Macromolecules*, vol. 20, no. 9, pp. 2160–2164, 1987.

[24] R. A. Weiss, J. J. Fitzgerald, and D. Kim, “Viscoelastic behavior of lightly sulfonated polystyrene ionomers,” *Macromolecules*, vol. 24, no. 5, pp. 1071–1076, 1991.

[25] A. Eisenberg, “Clustering of ions in organic polymers. A theoretical approach,” *Mucromolecules*, vol. 3, no. 2, pp. 147–154, 1970.

[26] M. A. Malmierca *et al.*, “Characterization of network structure and chain dynamics of elastomeric ionomers by means of ^{1}H low-field NMR,” *Macromolecules*, vol. 47, no. 16, pp. 5655–5667, 2014.

[27] A. Takahashi, “High heat resistant polymers for automotive electronics field,” *ネットワークポリマー(In Japanese)*, vol. 33, no. 1, 2012.

[28] Tomoyuki Endo, “Travel light: New polymers could help electric cars take flight,” *Nikkei Asian Review*, 2018. [Online]. Available: https://asia.nikkei.com/Business/Technology/Travel-light-New-polymers-could-help-electric-cars-take-flight. [Accessed: 27-Jan-2019].

[29] G. H. Kim, W. J. Kim, S. M. Kim, and J. G. Son, “Analysis of thermo-physical and optical properties of a diffuser using PET/PC/PBT copolymer in LCD backlight units,” *Displays*, vol. 26, no. 1, pp. 37–43, 2005.

[30] C. H. Chien, C. C. Chen, T. Chen, Y. M. Lin, and Y. C. Liu, “Thermal deformation of microstructure diffuser plate in LED backlight unit,” *J. Soc. Inf. Disp.*, vol. 24, no. 2, pp. 99–109, 2016.

[31] G. Kim, “A PMMA composite as an optical diffuser in a liquid crystal display backlighting unit (BLU),” *Eur. Polym. J.*, vol. 41, no. 8, pp. 1729–1737, 2005.

[32] N. Yamada, E. Ohno, K. Nishiuchi, N. Akahira, and M. Takao, “Rapid‐phase transitions of GeTe-Sb_2Te_3 pseudobinary amorphous thin films for an optical disk memory,” *J. Appl. Phys.*, vol. 69, no. 5, pp. 2849–2856, 1991.

[33] K. Kuriki, Y. Koike, and Y. Okamoto, “Plastic optical fiber lasers and amplifiers containing lanthanide complexes,” *Chem. Rev.*, vol. 102, no. 6, pp. 2347–2356, 2002.

[34] J. Zubia and J. Arrue, “Plastic optical fibers: An introduction to their technological processes and applications,” *Opt. Fiber Technol.*, vol. 7, no. 2, pp. 101–140, 2001.

[35] A. Miyagawa, V. Ayerdurai, S. Nobukawa, and M. Yamaguchi, “Viscoelastic properties of poly(methyl methacrylate) with high glass transition temperature by lithium salt addition,” *J. Polym. Sci. Part B Polym. Phys.*, vol. 54, no. 22, pp. 2388–2394, 2016.

[36] M. Watanabe, “Ion conduction mechanism in network polymers from poly(ethylene oxide) and poly(propylene oxide) containing lithium perchlorate,” *Solid State Ionics*, vol. 18 & 19, pp. 338–342, 1986.

[37] M. L. Williams, R. F. Landel, and J. D. Ferry, “The temperature dependence of relaxation mechanisms in amorphous polymers and other glass-forming liquids,” *J. Am. Chem. Soc.*, vol. 77, no. 14, pp. 3701–3707, 1955.

[38] M. Watanabe, M. Itoh, K. Sanui, and N. Ogata, “Carrier transport and generation processes in polymer electrolytes based on poly(ethylene oxide) networks,” *Macromolecules*, vol. 20, no. 3, pp. 569–573, 1987.

[39] M. Armand, "Polymer Solid Electrolytes-An overview," *Solid State Ionics*, vol. 9 & 10, pp. 745–754, 1983.

[40] Y. Tominaga, Y. Izumi, G. H. Kwak, S. Asai, and M. Sumita, "Effect of supercritical carbon dioxide processing on ionic association and conduction in a crystalline poly(ethylene oxide)-$LiCF_3SO_3$ complex," *Macromolecules*, vol. 36, no. 23, pp. 8766–8772, 2003.

[41] G. H. Kwak, Y. Tominaga, S. Asai, and M. Sumita, "Improvement of the ionic conductivity for amorphous polyether electrolytes using supercritical CO_2 treatment technology," *Electrochim. Acta*, vol. 48, pp. 1991–1995, 2003.

Chapter 2

Improvement of heat resistance of poly(methyl methacrylate) by addition of lithium salts

2.1. Introduction

2.1.1. T_g enhancement of polymers

As mentioned in Chapter 1, PMMA is one of the most useful polymers for various engineering applications. It is necessary to use an amorphous polymer having high T_g for practical reasons such as service temperature of plastic products. Therefore, up to now, various ways to increase T_g have been proposed. For example, there is a way of decreasing the number of chain ends, i.e., increasing the molecular weight [1]–[4] and adding a miscible polymer with higher T_g [5], [6]. Another way is suppressing molecular motion by introducing chemical/physical crosslinking points [7]–[10]. Chemical crosslinking to PMMA is usually performed using a polymer containing a specific monomer with a double bond in the side chain [11], [12]. Furthermore, X-ray [13] or electron [14] radiation is also employed. In addition to the chemical crosslinking, physical crosslinking is expected for some specific polymers, which includes hydrogen bonding [6], [10], [15], π–π stacking [16], and electrostatic interactions [17]. In this study, it has been aimed to enhance T_g of PMMA by a simple method that is, introducing physical crosslinking such as ion-dipole interaction.

In this chapter, the effect of anionic species on the T_g enhancement of PMMA is

discussed based on the results of temperature dependence of mechanical properties and IR spectroscopy analysis. In the next section, basis of mechanical properties, used in this research, is explained.

2.2. Mechanical properties of polymers

2.2.1. Viscoelastic measurement of polymers

In general, the properties of solid and liquid are discussed separately, and this separation is useful for various types of materials. However, polymers are much more complicated and they exhibit both elastic and viscous behaviors together depending on time and temperature, i.e., viscoelastic responses [18]. Therefore, the temperature and frequency dependence of mechanical properties are often measured to investigate the behavior of polymers. One of the most useful methods to determine the viscoelastic behavior is the measurement for dynamic mechanical properties. In this measurement, an oscillatory stress or strain is applied to the samples.

Here, the oscillatory strain is written as the following equation (2.1).

$$\gamma(t) = \gamma_0 e^{i\omega t} = \gamma_0(\cos\omega t + i\sin\omega t) \quad (2.1)$$

where γ(t) is the applied oscillatory strain as a function of time t, γ_0 is the constant strain, and ω is the angular frequency of the applied strain in radian/s (equal to $2\pi f$ where f the frequency in cycles/s).

Then, the relationship between stress and strain is written as the following equation (2.2).

$$\sigma(t) = [G'(\omega) + G"(\omega)]\gamma_0 e^{i\omega t} = [G'(\omega) + G"(\omega)]\gamma(t) \quad (2.2)$$

where σ(t) is stress, $G'(\omega)$ and $G''(\omega)$ are the storage modulus and loss modulus, respectively. In addition, loss tangent, so called tan δ, is indicated as below.

$$\tan\delta = \frac{G''(\omega)}{G'(\omega)} \tag{2.3}$$

The relaxation mechanism of the entanglement chains of a polymer can be estimated by examining the frequency dependence of storage modulus and loss modulus. The temperature region where the relaxation mechanism is observed reflects the molecular motion of the polymer chain.

2.2.2. Relaxation modes of polymers

There are mainly two kinds of structures in polymers: Primary structure and higher-order structure. Primary structures include the chemical structure, molecular weight, and its distribution. The higher-order structure means the structures with regularity except for the primary structure.

The dispersions of the dynamical relaxation modes, related to the local molecular motion in the primary structures, are usually observed in the lower temperature region. For example, β dispersion derived from local molecular motion of side chains of a polymer can be generally observed in the temperature region below T_g [18], [19]. On the other hand, the effects of the secondary structures become dominant in the high temperature region.

2.3. Experimental

2.3.1. Chemicals

The polymer utilized in this research was a commercially available PMMA (Acrypet VH; Mitsubishi Chemical Corp.). The number- and weight-average molecular weights, which were estimated using size-exclusion chromatography (HLC-8020; Tosoh Corp.) with chloroform as the solvent, were M_n = 54,000 and M_w = 120,000 (standard: polystyrene (PS)), respectively. The structure of PMMA is shown in Figure 2.1.

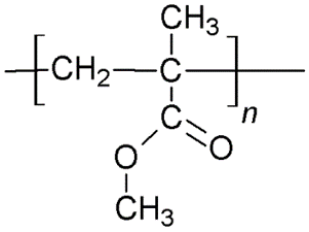

Figure 2.1. Chemical structure of PMMA.

Lithium nitrate ($LiNO_3$), lithium perchlorate ($LiClO_4$, purity was not identified), $LiCF_3SO_3$ (purity ≥ 98.0 %; Kanto Chemical Co., Ltd.), lithium trifluoroacetate ($LiCOOCF_3$, purity 97 %), lithium bis(trifluoromethane sulfonyl)imide ($LiN(CF_3SO_2)_2$, LiTFSI, purity ≥ 98.0 %; Tokyo Chemical Industry Co., Ltd. (TCI)) were used as lithium salts. Chemical structures of these lithium salts were shown in Figure 2.2. These lithium salts were used without further purification. Lithium bromide (LiBr, purity > 99.0 %; Tokyo Chemical

Industry Co., Ltd.)) was also utilized for another experiment.

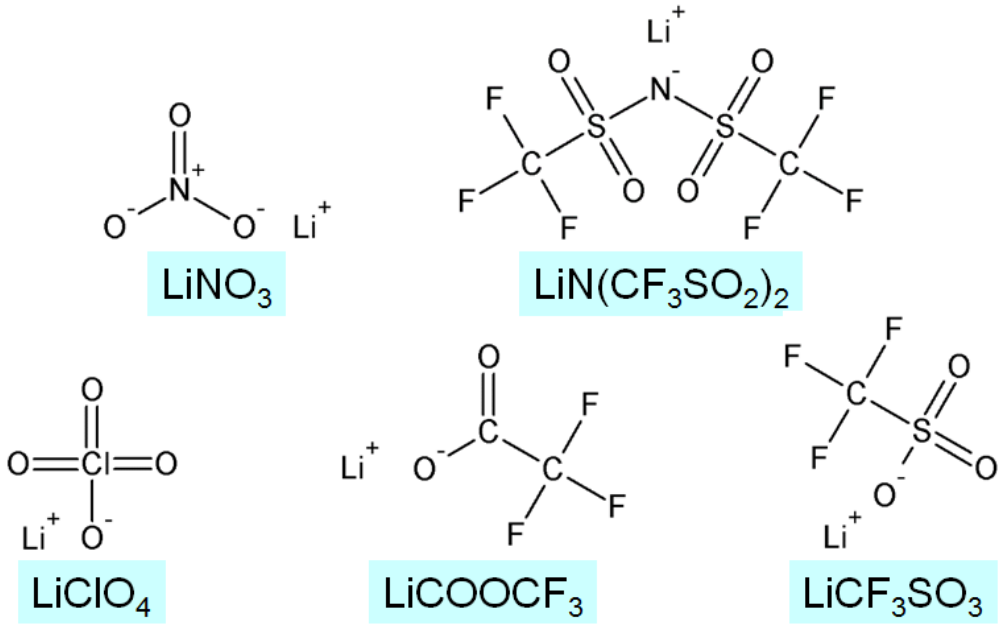

Figure 2.2. Chemical structures of various lithium salts, LiX (X=NO_3, ClO_4, CF_3SO_3, $COOCF_3$, $N(CF_3SO_2)_2$ (TFSI)).

2.3.2. Sample preparation

Fabrication of blend films

The PMMA and each lithium salt were completely dissolved in a mixed solution of dichloromethane and methanol in 9-to-1 weight ratio (total weight of the mixed solution: 10.8 g), and the mixture was stirred for 1 hour at r.t.. The concentration of the salts was fixed to 0.07 molar of lithium cations per 1 molar of carbonyl groups ([Li]/[C=O] ratio of 0.07) in PMMA, which corresponded to 5 wt.% of $LiNO_3$, 10 wt.% of $LiClO_4$, 10 wt.% $LiCF_3SO_3$, 8 wt.% of $LiCOOCF_3$, and 17 wt.% of LiTFSI, respectively. Each solution was cast onto a petri dish (diameter: 8 cm). After that, the samples were dried in air with increasing temperature to 160 °C, and then, in a vacuum chamber at 160 °C for 30 hrs. Then,

each sample was crushed into small pieces with a hammer and compression-molded into the film with a thickness of 300 μm. The compression-molding condition was as follows; heating at 200 °C for 10 min, and then quenching at 25 °C for 3 min. Some films were used for the following measurements immediately after compression-molding. The schematic illustration of this protocol is shown in Figure 2.3.

Water absorption test

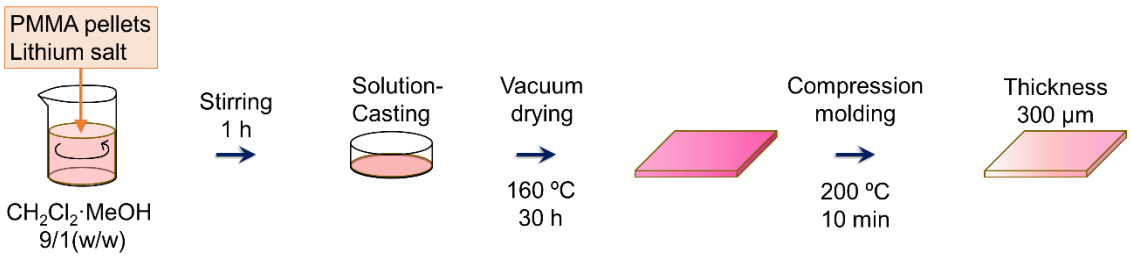

Figure 2.3. Schematic illustration of sample preparation of PMMA/lithium salt blends.

PMMA/$LiCF_3SO_3$ and PMMA/LiBr with a salt concentration with 0.07 molar ratio were prepared for this test. The method of film fabrication of these samples were the same as that noted above. The samples were kept at 25 °C and 50 % relative humidity (RH) in a temperature- and humidity-controlled chamber.

2.3.3. Measurements

The temperature dependence of the tensile storage modulus, *E'*, and loss modulus, *E"*, was measured in the temperatures from 30 to 200 °C by a dynamic mechanical analyzer (Rheogel-E4000, UBM Co., Ltd.). The frequency was set at 10 Hz and the heating rate was fixed to 2 °C/min.

A calorimeter (DSC 8500, PerkinElmer Co., Ltd.) was used as a differential scanning calorimetry (DSC) to investigate thermal properties of the polymer at a heating rate of 10 °C/min from room temperature to 200 ºC. Then the sample was cooled down to room temperature at 10 ºC/min. The second heating curve was used in this thesis to erase the processing history. Approximately 10 mg of each sample was encapsulated in an aluminum pan.

Absorption spectra were measured using Ultraviolet Visible (UV-Vis) spectroscopy (V650, Jasco). The measurement was held in the wavelength range between 400 nm and 700 nm.

Attenuated total reflection (ATR) measurements using a KRS-5 ATR prism were performed to evaluate infrared spectra under nitrogen flow. The accumulation counts were 16 times, and the resolution was 4 cm^{-1}.

X-ray diffraction (XRD) pattern was obtained by an X-ray diffractometer (SmartLab, Rigaku) with a Cu target as a source of X-ray emitting Cu Kα radiation. X-ray tube voltage and current were 40 kV and 30 mA, respectively. The measurement was carried out in the range of 2θ between 5 ° and 80 °. Scan step and duration time were 0.1 ° and 1.00 s, respectively.

Small angle X-ray scattering (SAXS) was measured by the X-ray diffractometer (SmartLab, Rigaku). The measurement was performed in the range of 2θ between 0.06 °

and 8.00 °. Scan step and scan speed were 0.02 ° and 3.97 degree/min, respectively.

X-ray photoelectron spectroscopy (XPS) was measured using an XPS spectroscopy (S-Probe TM2803, Fisons instruments) in order to compare the strength of the interaction between different salts from the peak shift of Li (1s). Another reason for using XPS was to estimate the distribution of each salt in the vertical direction of the film. However, the measurement was not succeeded because of charge-up of the samples. Since the blend films fabricated in this study had poor electrical conductivities, major electric measurements were not applicable.

2.4 Results and Discussion

2.4.1. Effect of anion species of various lithium salts on T_g of PMMA

Here, it should be noted that the process of compression-molding was available to all of the samples. This result indicates that the flowabilities of all samples was good enough to apply to actual processing operations used for thermoplastics. All of the samples except for PMMA/$LiNO_3$ were colorless and transparent which were shown in the UV-Vis spectra of the films, as shown in Figure 2.4.

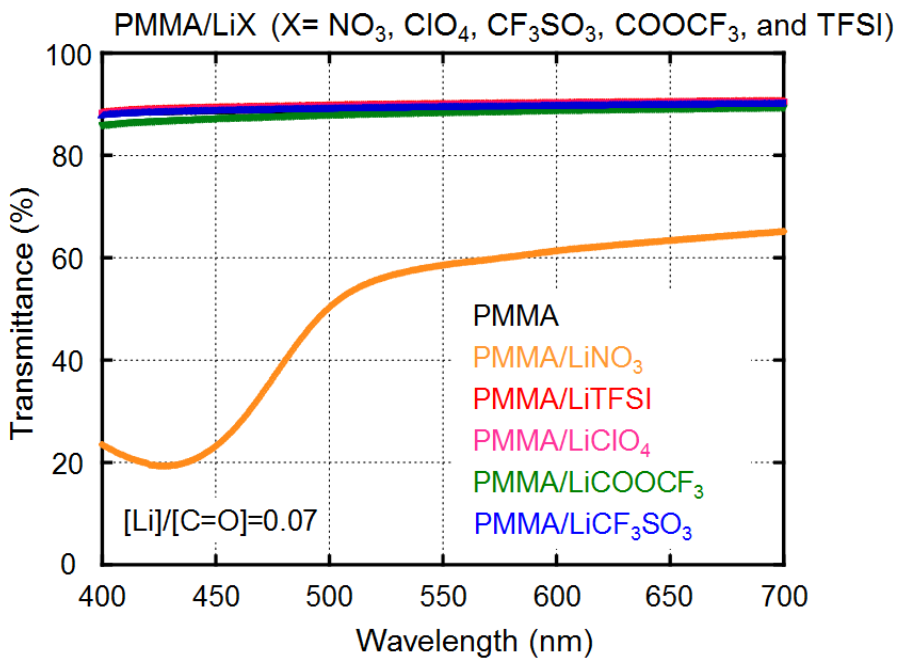

Figure 2.4. UV-Vis spectra of PMMA/LiX (X = NO_3, TFSI, ClO_4, $COOCF_3$, and CF_3SO_3, [Li]/[C=O] ratio of 0.07) films; (black) pure PMMA; (orange) PMMA/$LiNO_3$; (red) PMMA/LiTFSI; (pink) PMMA/$LiClO_4$; (green) PMMA/$LiCOOCF_3$; and (blue) PMMA/$LiCF_3SO_3$.

As a result, only PMMA/$LiNO_3$ had a large absorption in the wavelength region between 400 nm and 700 nm. This is also obvious in the photograph of the PMMA/$LiNO_3$ blend film in Figure 2.5.

Figure 2.5. Photograph of a blend film of PMMA/$LiNO_3$ ([Li]/[C=O] ratio of 0.07).

Furthermore, a diffraction peak derived from $LiNO_3$ was observed in the compressed film of PMMA/$LiNO_3$ ([Li]/[C=O] ratio of 0.07), as seen in the XRD results in Figure 2.6.

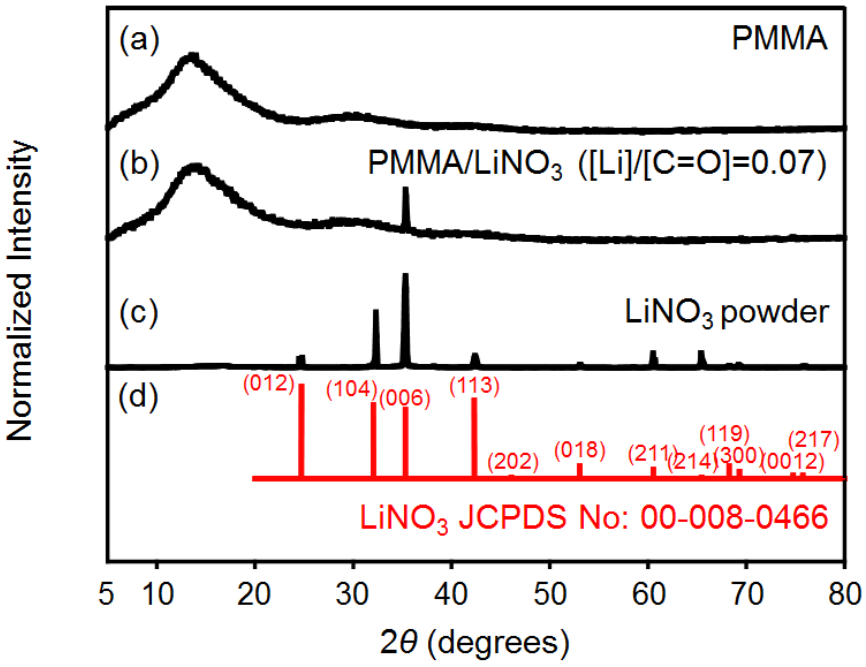

Figure 2.6. XRD pattern of (a) pure PMMA film, (b) PMMA/$LiNO_3$ ([Li]/[C=O] ratio of 0.07) film, (c) PMMA/$LiNO_3$ powder and (d) Standard pattern of $LiNO_3$ (JCPDS 00-008-0466).

This suggests that $LiNO_3$ is recrystallized and precipitated in PMMA by heating at 200 °C and quenching at 25 °C during compression molding. The recrystallization, if occurs, is responsible for the decrease in the transparency. Considering these results, PMMA/$LiNO_3$ does not satisfy the purpose of this research. As for the XRD patterns of the other films, there was no diffraction pattern derived from the powders of the lithium salts.

The temperature dependence of the dynamic tensile moduli and tan δ of the blends with various lithium salts is shown in Figure 2.7.

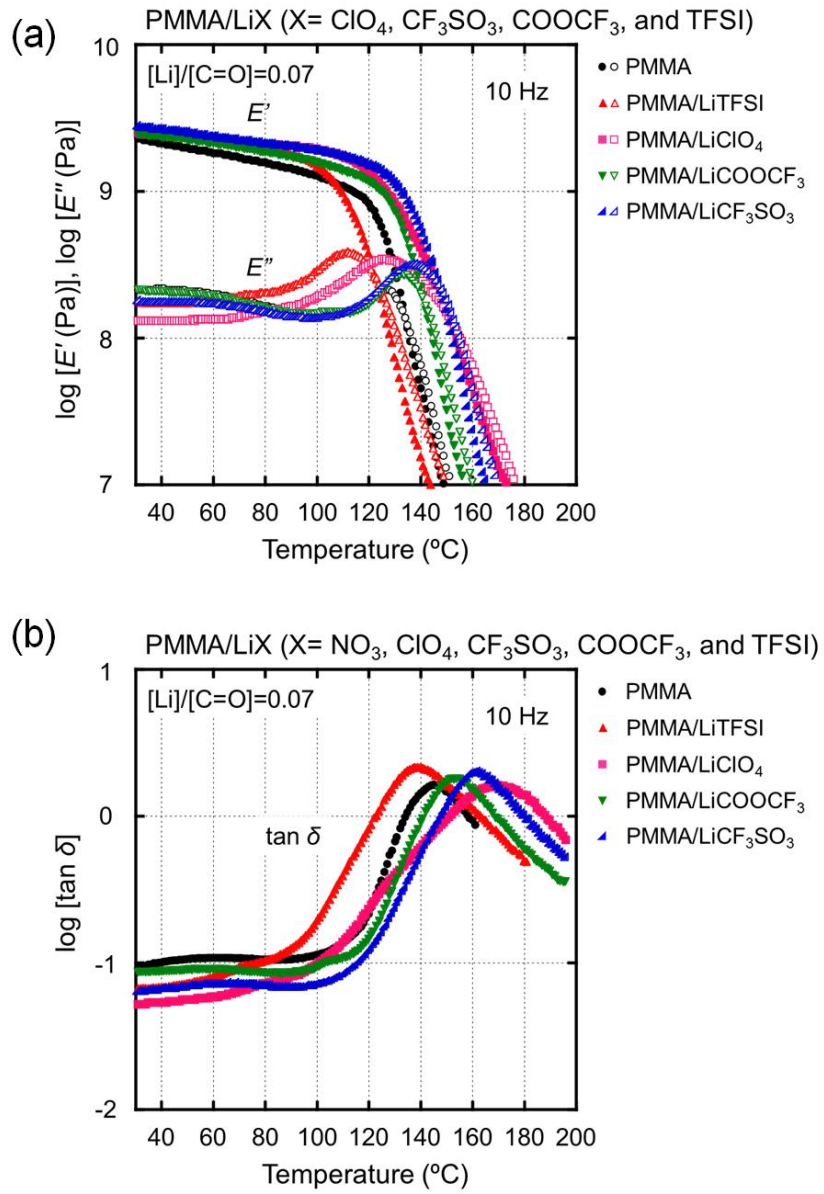

Figure 2.7. Temperature dependence of (a) dynamic tensile moduli and (b) tan δ at 10 Hz of PMMA/LiX (X = TFSI, ClO_4, $COOCF_3$, and CF_3SO_3, [Li]/[C=O] ratio of 0.07) films: (black) pure PMMA, (red) PMMA/LiTFSI, (pink) PMMA/$LiClO_4$, (green) PMMA/$LiCOOCF_3$, and (blue) PMMA/$LiCF_3SO_3$.

Furthermore, the values of T_g of these blends, estimated from the peak temperature of the *E''* curve, were summarized in Table 2.1.

Table 2.1. T_g of PMMA/LiX (X = TFSI, ClO_4, $COOCF_3$, and CF_3SO_3, [Li]/[C=O] ratio of 0.07).

Samples	[Li]/[C=O] (mol/mol)	wt. %	vol. %	T_g (°C)
PMMA	0.07	0	0	127
PMMA/LiTFSI	0.07	17	15	112
PMMA/$LiClO_4$	0.07	10	8	126
PMMA/$LiCOOCF_3$	0.07	8	5	133
PMMA/$LiCF_3SO_3$	0.07	10	-	137

As seen in the table, PMMA/$LiCF_3SO_3$ showed the highest T_g among the samples with a salt. T_g of the blend was increased by 10 °C as compared with that of pure PMMA only by the addition of 0.07 molar ratio of $LiCF_3SO_3$. Furthermore, this blend showed significantly higher *E'* than pure PMMA in the measurement temperature range. In other words, $LiCF_3SO_3$ has an ability to increase T_g of PMMA. On the other hand, T_g decreased by the addition of LiTFSI with low *E'* in the measurement range. In short, it acted as a plasticizer of PMMA.

Figure 2.8 shows ATR spectra of the blends with various salts. There were almost no difference among the blends in the ATR spectra in the wavenumber range between 2700 cm^{-1} and 3200 cm^{-1}, as seen in Figure 2.8 (a). There are three peaks at 2994, 2950, and 2924 cm^{-1}. Brinkhuis attributed the peak at 2994 cm^{-1} to the stretching vibration modes of α-CH_3 and OCH_3, and attributed the peak at 2950 cm^{-1} to the stretching vibration modes of α-CH_3,

OCH_3, CH_2 [20]. The peak at 2924 cm^{-1} was also derived from the stretching vibration mode of CH_2.

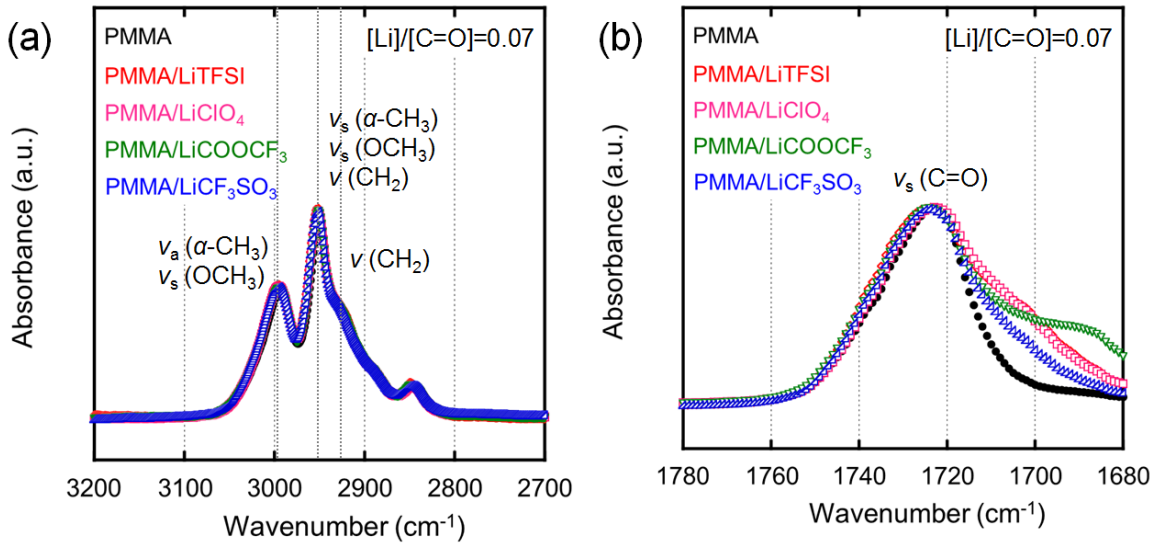

Figure 2.8. (a) Attenuated total reflection (ATR) spectra normalized with the peak height at 2950 cm^{-1} in wavenumber region from 2700 to 3200 cm^{-1} and (b) ATR spectra normalized with peak height at 1724 cm^{-1} in wavenumber region from 1680 to 1780 cm^{-1} of (black) pure PMMA; (red) PMMA/LiTFSI; (pink) PMMA/$LiClO_4$; (green) PMMA/$LiCOOCF_3$; (blue) PMMA/$LiCF_3SO_3$ with 0.07 molar ratios of salts.

In contrast, the peaks ascribed to the symmetry stretching vibration modes of carbonyl groups became broad in the lower wavenumber region, i.e., higher energy region, as shown in Figure 2.8 (b). This means that dissociated lithium cations of the salts interact with carbonyl groups in PMMA strongly. Thus, these interactions contribute to T_g enhancement of the blends by suppression of the local motion of the side chains in PMMA.

Here, the dissociation degree of the lithium salts in PMMA is estimated using the energy of

coulombic interactions described by the following equation [21]:

$$U(r) = \frac{Q_1 Q_2}{4\pi\varepsilon_0 \varepsilon r} \tag{2.4}$$

where Q_1 and Q_2 are charges, ϵ and ϵ_0 are the relative dielectric constants of the medium and dielectric constants of vacuum [22], [23], respectively, and r is the distance between cation and anion. The value of ϵ is 3.6 in PMMA [22]. Assuming that r is equal to the sum of the radius of the cation a_+ and the sum of the radius of the anion a_- , the coulombic interaction energies of the lithium salts, the absolute value of $U(r)$, is calculated as seen in Table 2.2. The ionic radii of lithium cation [24], [25] and anions [26]–[28] were used for r in equation (2.4). This calculation is performed assuming that PMMA is a medium.

Table 2.2. Ionic radii of lithium cation and $TFSI^-$, ClO_4^-, $COOCF_3^-$, and $CF_3SO_3^-$ from references. U means calculated coulomb interactions between cations [24], [25] and anions [26]–[28] assuming that PMMA is a medium. The absolute value of each calculated U is written in this table.

Salt	a_+ (nm)	a_- (nm)	$\lvert U(r)\rvert$ (J)
LiTFSI	0.073 [24], [25]	0.325 [27]	1.6×10^{-19}
$LiClO_4$	0.073 [24], [25]	0.225 [26]	2.2×10^{-19}
$LiCOOCF_3$	0.073 [24], [25]	0.348 [28]	1.5×10^{-19}
$LiCF_3SO_3$	0.073 [24], [25]	0.230 [26]	2.1×10^{-19}

Figure 2.9 shows deconvoluted peaks of the ATR spectra, which was carried out using Lorentzian function [29]. The stretching vibration modes of ClO_4^- are separated to a peak at 623 cm^{-1} and a peak at 635 cm^{-1} [30]. Each peak is attributed to free anions and a bound or contact ClO_4^- anions [30].

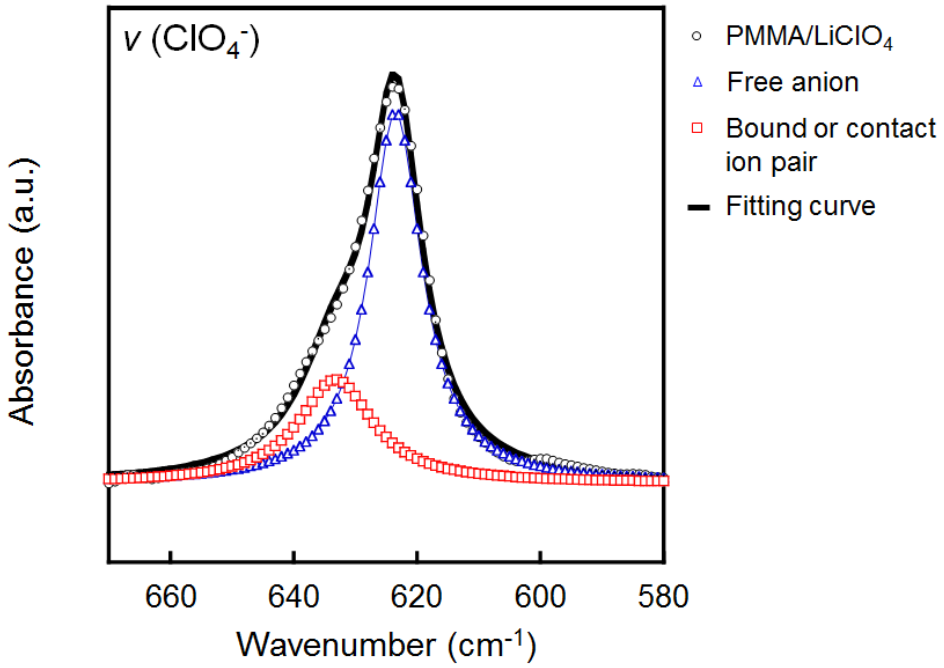

Figure 2.9. Peak deconvolution of ATR spectra of stretching vibration mode (ν (ClO_4^-)) for PMMA/$LiClO_4$ ([Li]/[C=O] ratio of 0.07) film. The IR band in the wavenumber range from 580 to 670 cm^{-1} was deconvoluted to peaks at 623 and 633 cm^{-1}.

Figure 2.10 shows the peak deconvolution of ATR spectra of a PMMA/$LiCOOCF_3$ blend film with 0.07 molar ratio of the salt. Since there was an overlap with the peak derived from pure PMMA at 1724 cm^{-1} attributed to the carbonyl symmetry stretching vibration mode, this peak was removed from the ATR spectra of PMMA/$LiCOOCF_3$ before the peak deconvolution. The peak deconvolution of the ATR spectra was carried out in the same way as that of PMMA/$LiClO_4$. The asymmetry stretching vibration modes of COO^- are composed of the contributions of peaks at 1695, 1736, 1710 cm^{-1}, and 1729 cm^{-1} [31]. Each peak is attributed to free ions and triplet anions, ion pairs, and aggregates, respectively [31].

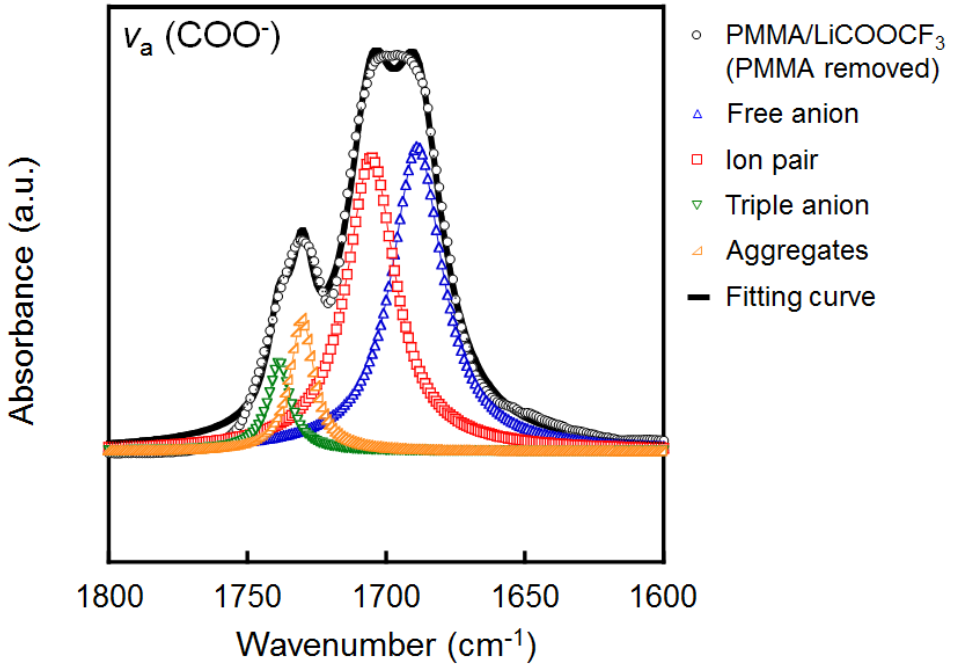

Figure 2.10. Peak deconvolution of ATR spectra of asymmetry stretching vibration mode (ν_a (COO^-)) for PMMA/$LiCOOCF_3$ ([Li]/[C=O] ratio of 0.07) film. IR band in the wavenumber range of 1600 to 1800 cm^{-1} was deconvoluted to the peaks at 1689, 1739, 1705, and 1730 cm^{-1}.

Figure 2.11 shows the result of the peak deconvolution of ATR spectra of a PMMA/$LiCF_3SO_3$ blend film with 0.07 molar ratio of the salt.

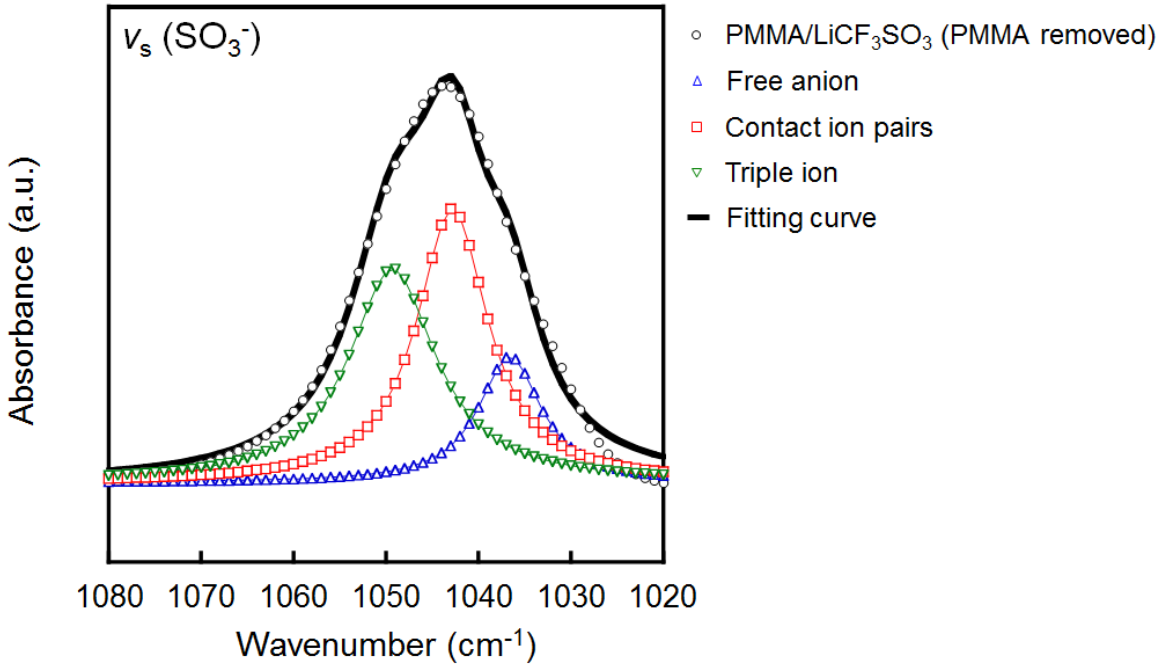

Figure 2.11. Peak deconvolution of ATR spectra of symmetry stretching vibration mode (ν_s (SO_3^-)) for PMMA/$LiCF_3SO_3$ ([Li]/[C=O] ratio of 0.07) film. IR band in the wavenumber range of 1020 to 1080 cm^{-1} was deconvoluted to the peaks at 1037, 1043, and 1050 cm^{-1}.

The peak deconvolution of the ATR spectra was carried out in the same way as that of PMMA/$LiClO_4$. The symmetry stretching vibration mode of SO_3^- are composed of the contributions of peaks at 1032, 1040, and 1045 cm^{-1}. Each peak is attributed to free ions, ion pairs, and triplet anions, respectively [32]. In the case of peak fitting of ATR spectra of this blend, background was corrected at first. In the wavenumber range of 1020 to 1080 cm^{-1}, there was an overlap with the peak derived from pure PMMA at 1060 cm^{-1}. Therefore, the normalized peak at 1060 cm^{-1} was removed before the peak deconvolution.

According to all of the peak deconvolution of ATR spectra of the blends, the ratio of the contribution of each structure of anionic species (ClO_4^-, $CF_3SO_3^-$, and $COOCF_3^-$) were calculated. They are summarized in Table 2.3.

Table 2.3. Contribution ratios of structure of anionic species (ClO_4^-, $CF_3SO_3^-$, and $COOCF_3^-$) calculated by area ratios of ATR peaks.

	Peak area (%)		
	PMMA/$LiClO_4$	PMMA/$LiCOOCF_3$	PMMA/$LiCF_3SO_3$
Free	72.3	44.1	17.3
Ion pair (Including bound and contact anions)	27.7	40.8	42.7
Triple ion	-	5.7	40.0
Aggregates	-	9.3	-

As a result, there was no reasonable correlation between the dissociation abilities of various lithium salts, as shown in Table 2.2. Considering the IR study of the blend films with the three different kinds of lithium salts, i.e., PMMA/$LiClO_4$, PMMA/$LiCOOCF_3$, and PMMA/$LiCF_3SO_3$, T_g of the blends increased as decreasing the contributions of the ratio of free anions.

LiTFSI, which is well known as a salt with high ionic conductivity in lithium ion battery, decreased T_g of PMMA. The peak deconvolution of ATR spectra in PMMA/LiTFSI could not carry out because there were many overlaps with the ATR spectra of pure PMMA. This is considered due to larger volume fraction of the salt in the blend film as shown in Table 2.1. It is assumed that PMMA is plasticized by a large volume of the salt in PMMA.

2.4.2. Hygroscopic property of PMMA/$LiCF_3SO_3$

Although it was revealed that the addition of $LiCF_3SO_3$ is quite effective on T_g enhancement of PMMA, it was easily predicted that the water absorption of the salt causes a substantial effect on properties. High water absorbency may sometimes change properties of a product. Therefore, the hygroscopic nature of PMMA and the effect of moisture on its T_g were investigated.

The temperature dependence of the dynamic mechanical moduli of PMMA/$LiCF_3SO_3$ with 0.07 molar ratio of the salt is shown in Figure 2.12.

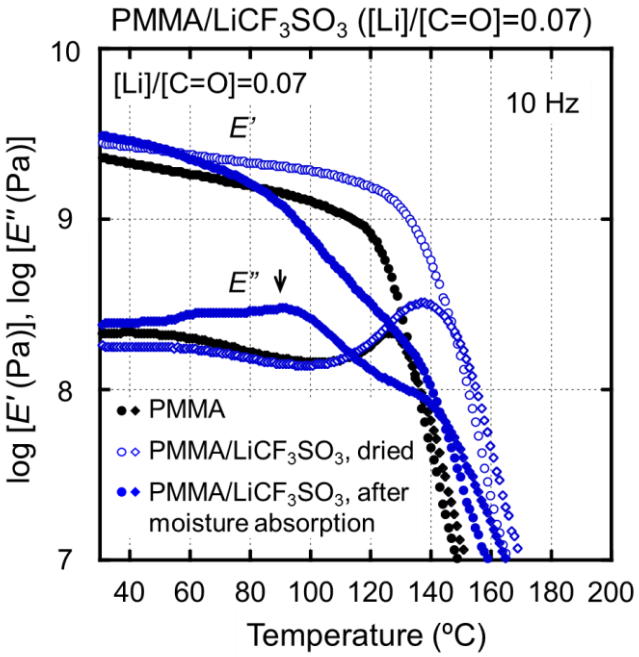

Figure 2.12. Temperature dependence of the dynamic tensile moduli at 10 Hz of PMMA/$LiCF_3SO_3$ ([Li]/[C=O] ratio of 0.07) blend; (black symbols) pure PMMA; (blue, open symbols) dried blend; and (blue, closed symbols) moisture-absorbed blend.

As demonstrated, the addition of $LiCF_3SO_3$ extended the glassy region to higher temperatures, i.e., increased the T_g. Furthermore, *E'* was high and insensitive to temperature

in the glassy region even at high temperatures. Consequently, the *E''* peak ascribed to the T_g was located at a high temperature with a strong intensity. However, after storage in a temperature- and humidity-controlled chamber (25 °C and 50 % RH) for 400 hrs, the *E'* in the glassy region decreased. Furthermore, in addition to the peak at 137 °C, there was an ambiguous broad peak in the *E''* curve at 90 °C, which is indicated by an arrow. The low-temperature-peak represents the T_g in the region containing a large amount of water, meaning the water molecules as a plasticizer [33]–[35], as discussed later. As a result, the *E'* of PMMA/$LiCF_3SO_3$ was much lower than that of pure PMMA over a wide temperature range after moisture absorption. Moreover, it was impossible to define the rheological glassy and transition region clearly. This demonstrates that, following moisture absorption, the addition of $LiCF_3SO_3$ reduces the service temperature of PMMA and limits its applicability at high temperatures.

According to Figure 2.12, The *E''* in the moisture-absorbed blend showed two different values of T_g, i.e., a broad peak at 90 °C and a peak at 137 °C. Here, the reason for the phenomenon is briefly discussed. In general, as shown in Figure 1.4 [36], there are two values of T_g. One is derived from matrix phase and the other one is derived from cluster phase depending on the different structures of ionomer in Figure 1.3 [37]. Presumably, the same phenomenon also occurs in the blends in this study. As mentioned above in this chapter, there are at least three structures in PMMA/$LiCF_3SO_3$ blend. Because of the differences in the ease of water absorption depending on such ionic structures, two values of T_g were observed. In other words, some parts are easily plasticized by water molecules and the other parts are hardly plasticized. If such ionic structures are hierarchical and periodic, they should be detected by SAXS. Figure 2.13 shows the SAXS profile of PMMA/$LiCF_3SO_3$ ([Li]/[C=O] ratio of 0.07) as compared with that of pure PMMA.

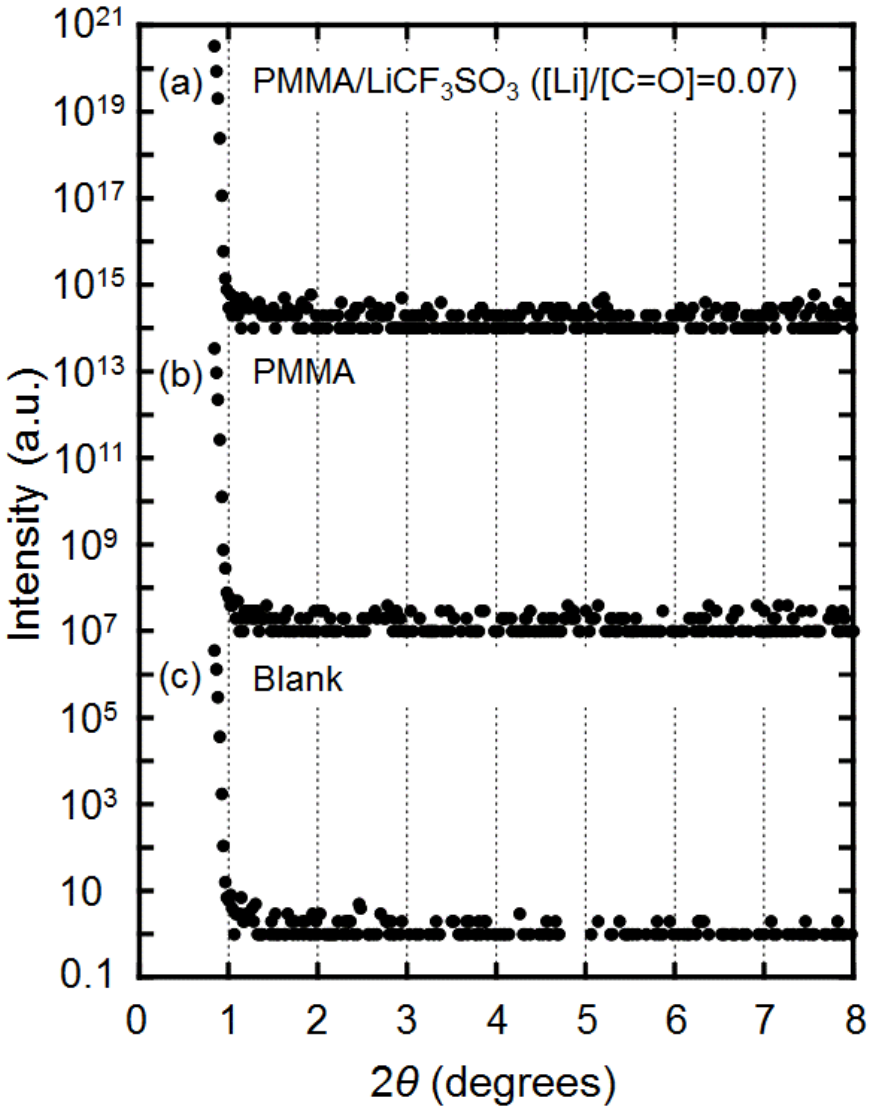

Figure 2.13. SAXS profiles of (a) PMMA/$LiCF_3SO_3$ ([Li]/[C=O] ratio of 0.07) blend, (b) pure PMMA, and (c) blank as a reference.

As a result, no scattering was observed in the profiles in Figure 2.13. It is considered that each structure is not periodical to be detected using X-ray.

How water molecules absorb the blends is additionally explained here. Referring to the report by Hagiwara et al. [38], the average free volume size of PMMA at room temperature can be estimated as a sphere with a diameter of around 10 Å. Since the 2.8 Å [39] diameter size of a water molecule is one order of magnitude smaller than the average free volume size of PMMA, water molecules are supposed to diffuse easily in the film.

Filipe et al. compared the differences of sodium trifluoromethanesulfonate ($NaCF_3SO_3$) and sodium bromide (NaBr) in the effects on surface tension of water which was calculated by MD (MD; Molecular Dynamics) simulations. They suggested that $CF_3SO_3^-$ (Tf^-) showed strong affinity to the air/water interface as shown in Figure 2.14 (A) to (D).

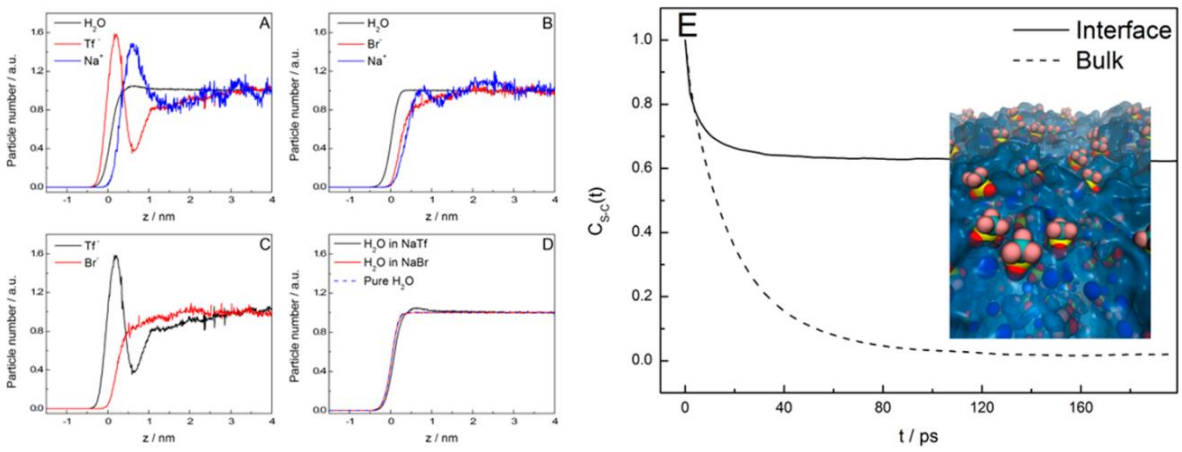

Figure 2.14. Normalized densities of water, sodium, and anion in the air/water simulation calculated by MD simulation which was held by Filipe et al.: (A) $NaCF_3SO_3$; (B) NaBr; (C) comparison between $CF_3SO_3^-$ (Tf^-) and Br-; (D) water from the two systems and pure water. (E) Rotational autocorrelation function of $CF_3SO_3^-$ at the interface and bulk solution. (Inset) Snapshot of the air/water interface from simulation of a water/triflate/sodium. Water is represented as the blue surface. (Pink) F; (light green) C; (yellow) S; (red) O; and (blue) Na [40].

Furthermore, it was revealed from their simulation that the CF_3 groups were exposed to the less polar environment while SO_3 groups were immersed in water as shown in the schematic illustration in the inserted snapshot in Figure 2.14 (E). Therefore, $CF_3SO_3^-$ exists at the air/water interface rather than bulk as compared with Br^-. It is estimated that hydrogen bonding occurs between SO_3 groups and water molecules, and thus, $NaCF_3SO_3$ should have higher hydrophilicity than NaBr. Although this paper reported about sodium salts, the same tendency may be detected in our system. Therefore, there is a possibility to reduce the water absorption by changing the species of anion of a salt. Considering this result, it has been attempted to add LiBr to our system [40].

Based on these results, it was decided to develop of PMMA having both high heat

resistance and low water absorption by the addition of another lithium salt, i.e., lithium bromide (LiBr).

2.4.3. Comparison of hygroscopic properties of PMMA/$LiCF_3SO_3$ and PMMA/LiBr

After compression-molding, the DSC was measured immediately. The molar ratio of the salt to the carbonyl groups in PMMA was set at 0.07 in both blends. As shown in Figure 2.15, the glass-to-rubber transition in the blends were observed at higher temperatures. The addition of $LiCF_3SO_3$ caused an intense change in the increase of transition temperature.

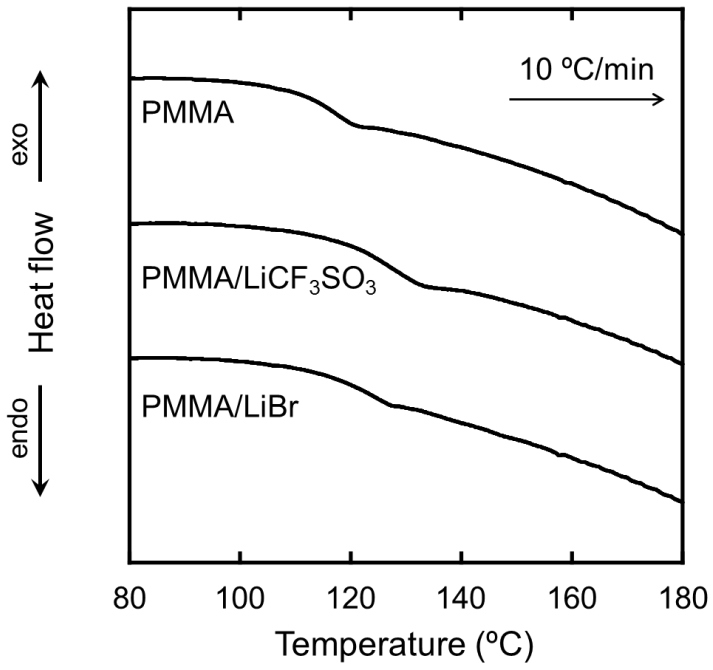

Figure 2.15. Differential scanning calorimetry (DSC) heating curves obtained at 10 °C/min for pure PMMA, PMMA/$LiCF_3SO_3$ ([Li]/[C=O] ratio of 0.07), and PMMA/LiBr ([Li]/[C=O] ratio of 0.07).

The dynamic mechanical properties of PMMA/LiBr, as seen in Figure 2.16, were different from those of PMMA/$LiCF_3SO_3$. In the glassy region, the *E'* slightly decreased as the temperature increased.

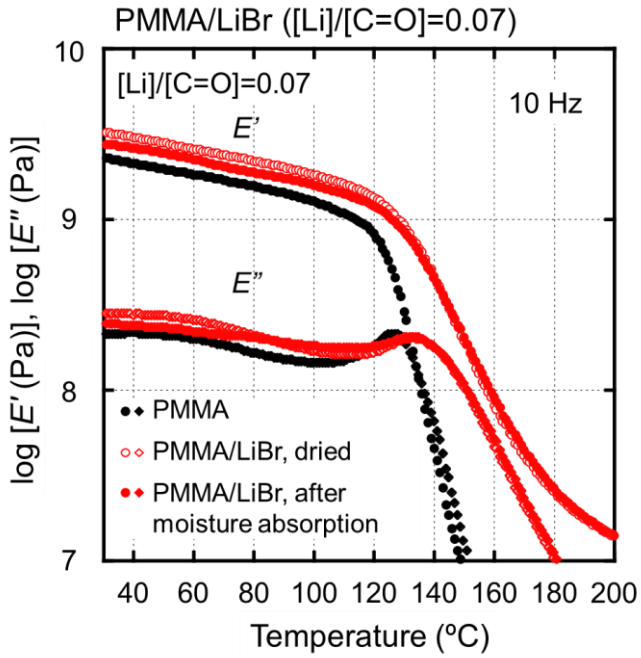

Figure 2.16. Temperature dependence of the dynamic tensile moduli at 10 Hz of PMMA/LiBr ([Li]/[C=O] ratio of 0.07) films; (black symbols) pure PMMA; (red, open symbols) dried blends; and (red, closed symbols) moisture-absorbed blends.

This is a similar trend to that of pure PMMA. However, the *E'* of PMMA/LiBr was significantly higher than that of pure PMMA beyond the glass-to-rubber transition. Furthermore, the *E"* peak of PMMA/LiBr became broad, especially in the high temperature region, suggesting a prolonged relaxation mode. This is important that the dynamic mechanical properties of PMMA/LiBr were not substantially affected by moisture absorption. This implies that LiBr can be used to increase the T_g of PMMA in industrial

applications. T_g of these two blends, which were estimated from the temperature at the peak top of *E"* in the graphs, were summarized in Table 2.4. As seen in Table 2.1 and 2.4, PMMA/LiBr showed the second highest T_g.

Table 2.4. T_g of the blends of PMMA, PMMA/$LiCF_3SO_3$ and PMMA/LiBr ([Li]/[C=O] ratio of 0.07) estimated from the results of temperature dependence of the dynamic tensile moduli.

Sample	[Li]/[C=O] (mol/mol)	wt. %	vol. %	T_g (°C)
PMMA	0.07	0	0	127
PMMA/$LiCF_3SO_3$	0.07	10	-	137
PMMA/LiBr	0.07	6	2	133

The dynamic mechanical properties of the samples with [Li]/[C=O] ratio of 0.01 are shown in Figure 2.17. Because the moisture contents were low, the added salt did not have a substantial impact on the dynamic mechanical properties in the case of PMMA/LiBr.

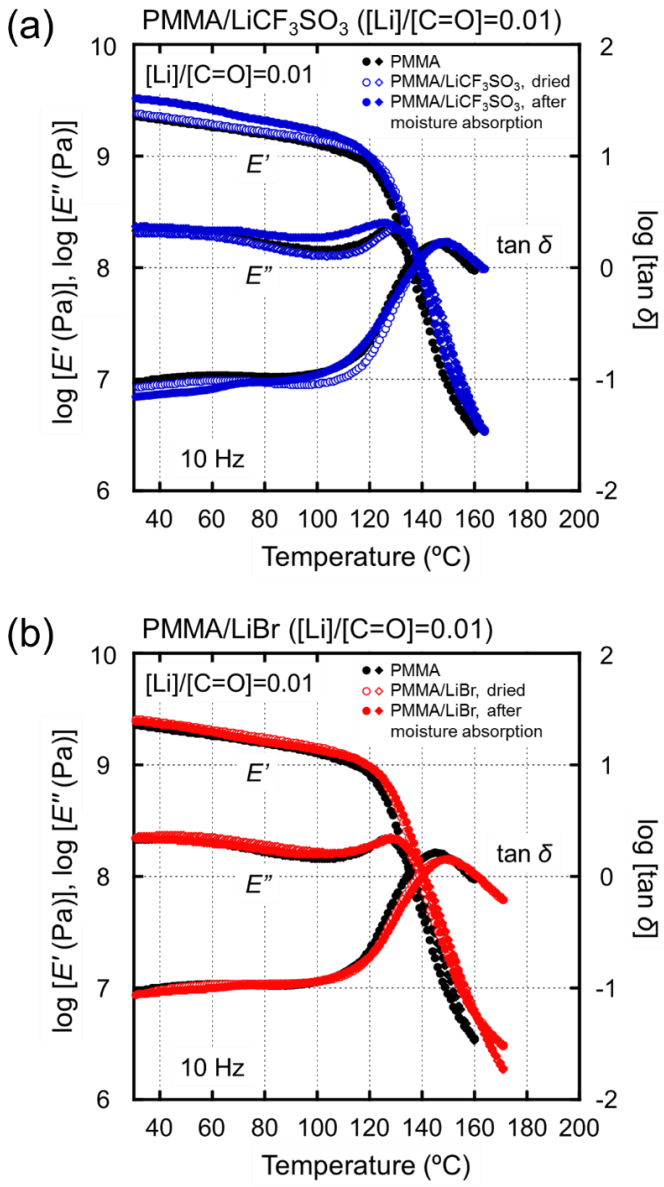

Figure 2.17. Temperature dependence of the dynamic tensile moduli at 10 Hz of (a) PMMA/$LiCF_3SO_3$ ([Li]/[C=O] ratio of 0.01) and (b) PMMA/LiBr ([Li]/[C=O] ratio of 0.01) films; (black symbols) pure PMMA; (open symbols) dried blends; and (closed symbols) moisture-absorbed blends.

The growth curves of the sample weight measured using a chemical balance at 25 °C and 50 % RH are shown in Figures 2.18 and 2.19.

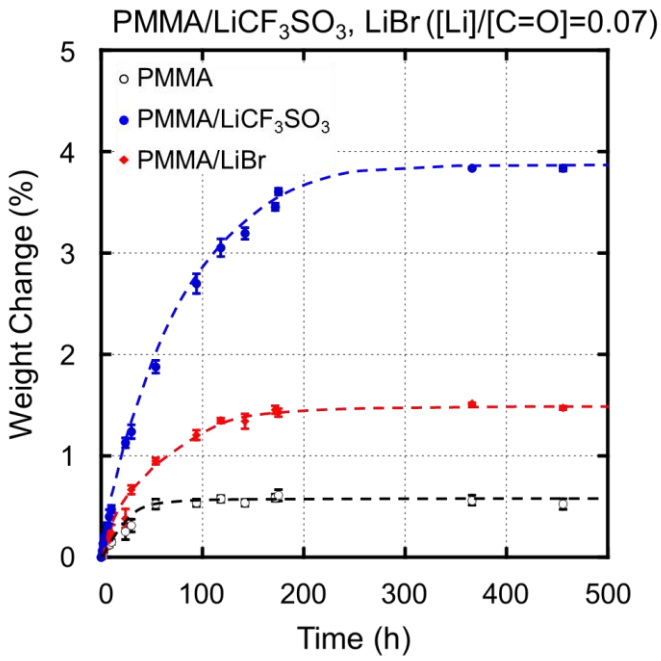

Figure 2.18. Growth curves of the weight change for (black, open circles) pure PMMA; (blue, closed circles) PMMA/$LiCF_3SO_3$ ([Li]/[C=O] ratio of 0.07) and (red, closed diamonds) PMMA/LiBr films ([Li]/[C=O] ratio of 0.07) after being stored at 25 °C and 50 % RH.

Figure 2.18 reveals that the moisture content became a constant, i.e., reached equilibrium after several hundred hrs. The equilibrium moisture content of PMMA/$LiCF_3SO_3$ was approximately 4 %. In contrast, PMMA/LiBr had a moisture content of only 1.5 % at equilibrium. Because both values were larger than that of pure PMMA (approximately 0.5 %), the salt strongly affects the hygroscopicity of the polymer. The same

tendency was observed in the samples with a lower salt concentration. The equilibrium moisture contents of the samples with an [Li]/[C=O] ratio of 0.01 were found to be 1.3 % for PMMA/$LiCF_3SO_3$ and 0.8 % for PMMA/LiBr as shown in Figure 2.19.

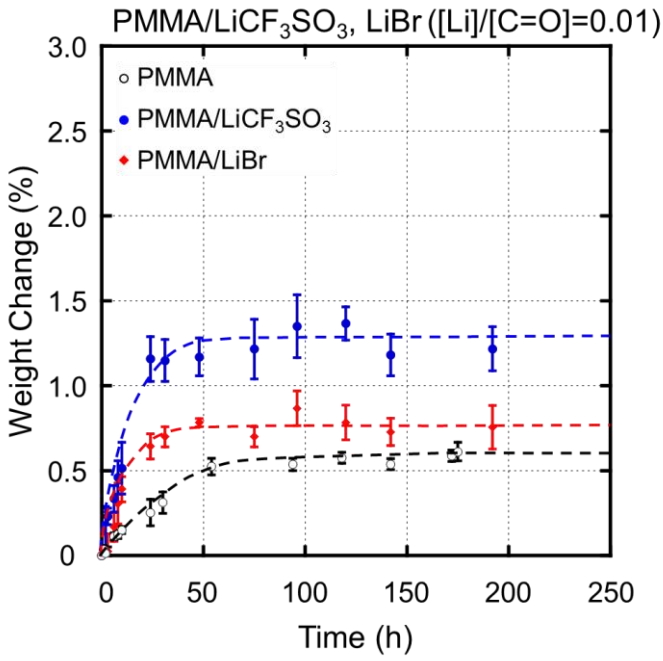

Figure 2.19. Growth curves of the weight change for (black, open circles) pure PMMA; (blue, closed circles) PMMA/$LiCF_3SO_3$ ([Li]/[C=O] ratio of 0.01) and (red, closed diamonds) PMMA/LiBr films ([Li]/[C=O] ratio of 0.01) after being stored at 25 °C and 50 % RH.

The ionic radii of the ionic crystals of $LiCF_3SO_3$ and LiBr are shown in Table 2.5. Smaller ions tend to be more easily solvated by the surrounding molecules because of their higher charge density. Therefore, lithium cations are strongly solvated, whereas strong solvation is not expected for $CF_3SO_3^-$. Moreover, water adsorption by the lithium cation and Br^- was prevented by the strong interaction between them due to their relatively higher charge density. However, $CF_3SO_3^-$ was “naked”, which increased its solvation by water

molecules. This is reasonable because metal trifluoromethanesulfonates act as Lewis acids in water [41], and are therefore stable in aqueous media.

Table 2.5. Ionic radii of lithium cation and $CF_3SO_3^-$/bromide anion from references.

Salt	a_+ (nm)	a_- (nm)
$LiCF_3SO_3$	0.073 [25]	0.230 [26]
LiBr	0.073 [25]	0.196 [26]

2.5. Conclusion

In this chapter, the T_g enhancement of PMMA by the addition of various lithium salts, was investigated using $LiNO_3$, LiTFSI, $LiClO_4$, $LiCOOCF_3$, and $LiCF_3SO_3$ ([Li]/[C=O] ratio of 0.07). $LiNO_3$ decreased the transparency of the blend. LiTFSI acted as plasticizers and decreased T_g of PMMA. In the case of the addition of $LiClO_4$, T_g was almost the same as that of pure PMMA. $LiCOOCF_3$ enhanced T_g of PMMA. $LiCF_3SO_3$ was the most effective on T_g enhancement for PMMA, which was due to ion–dipole interactions between the lithium cations and the carbonyl groups in PMMA molecules. However, at the same time, the addition of $LiCF_3SO_3$ also increased moisture absorption. Because water acts as a plasticizer in the case of $LiCF_3SO_3$, the T_g decreased with low modulus even in the glassy region of PMMA/$LiCF_3SO_3$. In contrast, plasticization due to moisture absorption was hardly detected in the case of LiBr. There are two reasons for the higher water absorbency of PMMA/$LiCF_3SO_3$. The first reason is that $CF_3SO_3^-$ has higher affinity to the air/water interface than Br^-. Another reason is that $CF_3SO_3^-$ exist as many "naked anions" in PMMA as compared with bromide anions due to their higher dissociation degree. "Naked

triflate anions" increased their solvation by water molecules because metal trifluoromethanesulfonates are well known as a Lewis acid in water and stably exist in water.

2.6. References

[1] J. M. G. Cown, "Some general features of T_g-M relations for oligomers and amorphous polymers," *Eur. Polym. J.*, vol. 11, no. 4, pp. 297–300, 1975.

[2] K. Tadlaoui, Y. Pietrasanta, A. Michel, and V. Verney, "Influence of molecular weight on the glass transition temperature and the melt rheological behaviour of methyl methacrylate telomers," *Polymer (Guildf).*, vol. 32, no. 12, pp. 2234–2237, 1991.

[3] K. L. Wooley, C. J. Hawker, J. M. Pochan, and J. M. J. Fréchet, "Physical properties of dendritic macromolecules: a study of glass transition temperature," *Macromolecules*, vol. 26, pp. 1514–1519, 1993.

[4] J. A. Forrest, K. Dalnoki-Veress, and J. R. Dutcher, "Interface and chain confinement effects on the glass transition temperature of thin polymer films," *Phys. Rev. E*, vol. 56, no. 5, pp. 5705–5716, 1997.

[5] P. C. Painter, J. F. Graf, and M. M. Coleman, "Effect of hydrogen bonding on the enthalpy of mixing and the composition dependence of the glass transition temperature in polymer blends," *Macromolecules*, vol. 24, no. 20, pp. 5630–5638, 1991.

[6] T. P. Lodge and T. C. B. McLeish, "Self-concentrations and effective glass transition temperatures in polymer blends," *Macromolecules*, vol. 33, no. 14, pp. 5278–5284, 2000.

[7] A. Shefert and M. Gottlieb, "Effect of cross-links on the glass transition temperature of end-linked elastomers," *Macromolecules*, vol. 25, pp. 4036–4042, 1992.

[8] H. Liu and S. Zheng, "Polyurethane networks nanoreinforced by polyhedral oligomeric silsesquioxane," *Macromol. Rapid Commun.*, vol. 26, no. 3, pp. 196–200, 2005.

[9] B. D. Fairbanks, T. F. Scott, C. J. Kloxin, K. S. Anseth, and C. N. Bowman, "Thiol-yne photopolymerizations: Novel mechanism, kinetics, and step-growth formation of highly cross-linked networks," *Macromolecules*, vol. 42, no. 1, pp. 211–217, 2009.

[10] T. Y. Juang *et al.*, "A reactive modifier that enhances the thermal mechanical properties of epoxy resin through the formation of multiple hydrogen-bonded network," *J. Polym. Res.*, vol. 18, no. 5, pp. 1169–1176, 2011.

[11] M. A. Hussein, R. M. El-Shishtawy, B. M. Abu-Zied, and A. M. Asiri, "The impact of cross-linking degree on the thermal and texture behavior of poly(methyl methacrylate)," *J. Therm. Anal. Calorim.*, vol. 124, no. 2, pp. 709–717, 2016.

[12] W. Ming, Y. Zhao, J. Cui, S. Fu, and F. N. Jones, "Formation of irreversible nearly transparent physical polymeric hydrogels during a modified microemulsion polymerization," *Macromolecules*, vol. 32, no. 2, pp. 528–530, 1999.

[13] S. Iqbal, M. S. Rafique, N. Iqbal, S. Bashir, S. Arif, and R. Ahmad, "Impact of radiation induced crosslinking on structural, morphological, mechanical and optical properties of Polymethylmethacrylate thin films," *Prog. Org. Coatings*, vol. 111, no. June 2016, pp. 202–209, 2017.

[14] W. H. Teh, C. Te Liang, M. Graham, and C. G. Smith, "Cross-linked PMMA as a low-dimensional dielectric sacrificial layer," *J. Microelectromechanical Syst.*, vol. 12, no. 5, pp. 641–648, 2003.

[15] Y. Shangguan, J. Yang, and Q. Zheng, "Rheology of nitrile rubber with hybrid crosslinked network composed of covalent bonding and hydrogen bonding," *RSC Adv.*, vol. 7, no. 26, pp. 15978–15985, 2017.

[16] B. Pépin-Donat, A. Viallat, J. F. Blachot, and C. Lombard, "Electromechanical polymer gels combining rubber elasticity with electronic conduction," *Adv. Mater.*, vol. 18, no. 11, pp. 1401–1405, 2006.

[17] S. Yang, H. Fan, Y. Jiao, Z. Cai, P. Zhang, and Y. Li, "Improvement in mechanical properties of NBR/$LiClO_4$/POSS nanocomposites by constructing a novel network structure," *Compos. Sci. Technol.*, vol. 138, pp. 161–168, 2017.

[18] M. M. Coleman and P. C. Painter, *Fundamentals of polymer science*, Second Ed. New York: CRC Press, 1998.

[19] 日本レオロジー学会, *講座・レオロジー (in Japanese)*. 高分子刊行会, 1992.

[20] R. H. G. Brinkhuis and A. J. Schouten, "Thin-film behavior of poly(methyl methacrylates). 2. An FT-IR study of Langmuir-Blodgett films of isotactic PMMA," *Macromolecules*, vol. 24, no. 7, pp. 1496–1504, 1991.

[21] Jacob N. Israelachvili, *Intermolecular and Surface Forces*. Amsterdam: Elsevioer Inc., 2011.

[22] J. Brandrup, E. H. Immergut, and E. A. Grulke, *Polymer Handbook*. Hoboken: Wiley-Interscience, 1999.

[23] P. W. Atkins, *Atkins' Physical Chemistry*. Oxford: Oxford University Press;, 1998.

[24] The Chemical Society of Japan, Ed., *Handbook of Chemistry: Pure Chemistry*. Tokyo: Maruzen, 2004.

[25] Y. Saito *et al.*, "Determination of ionic self-diffusion coefficients of lithium electrolytes using the pulsed field gradient NMR," *J. Power Sources*, vol. 81–82, pp. 772–776, 1999.

[26] R. Custelcean and B. A. Moyer, "Anion separation with metal-organic frameworks," *Eur. J. Inorg. Chem.*, no. 10, pp. 1321–1340, 2007.

[27] M. Ue, "Mobility and ionic association of lithium salts in a propylene carbonate-ethyl methyl carbonate mixed solvent," *J. Electrochem. Soc.*, vol. 142, no. 8, p. 2577, 1995.

[28] John B. Milne, "The trifluoroacetic acid solvent system. Part VI. Density measurements," *Can. J. Chem.*, vol. 58, pp. 283–287, 1980.

[29] G. Giraud, C. M. Gordon, I. R. Dunkin, and K. Wynne, "The effects of anion and cation substitution on the ultrafast solvent dynamics of ionic liquids: A time-resolved optical Kerr-effect spectroscopic study," *J. Chem. Phys.*, vol. 119, no. 1, pp. 464–477, 2003.

[30] W. Wieczorek, P. Lipka, G. Żukowska, and H. Wyciślik, "Ionic Interactions in Polymeric Electrolytes Based on Low Molecular Weight Poly(ethylene glycol)s," *J. Phys. Chem. B*, vol. 102, no. 36, pp. 6968–6974, 1998.

[31] A. Regis and J. Corset, "IR study of solutions of lithium trifluoroacetate in non-aqueous solvents. Structure of ion pairs and triple ions," *Chem. Phys. Lett.*, vol. 32, no. 3, 1975.

[32] R. Frech, S. Chintapalli, P. G. Bruce, and C. A. Vincent, "Crystalline and Amorphous Phases in the Poly(ethylene oxide)−$LiCF_3SO_3$ System," *Macromolecules*, vol. 32, no. 3, pp. 808–813, 1999.

[33] J. Zhou and J. P. Lucas, "Hygrothermal effects of epoxy resin. Part II: Variations of glass transition temperature," *Polymer (Guildf).*, vol. 40, no. 20, pp. 5513–5522, 1999.

[34] J. Shen, C. C. Chen, and J. A. Sauer, "Effects of sorbed water on properties of low and high molecular weight PMMA: 1. Deformation and fracture behaviour," *Polymer (Guildf).*, vol. 26, no. 4, pp. 511–518, 1985.

[35] L. S. A. Smith and V. Schmitz, "The effect of water on the glass transition temperature of poly(methyl methacrylate)," *Polymer (Guildf).*, vol. 29, no. 10, pp. 1871–1878, Oct. 1988.

[36] X. Ma, J. A. Sauer, and M. Hara, "Poly(methyl methacrylate) based ionomers. 1. Dynamic mechanical properties and morphology," *Macromolecules*, vol. 28, no. 11, pp. 3953–3962, 1995.

[37] M. A. Malmierca *et al.*, "Characterization of network structure and chain dynamics of elastomeric ionomers by means of ^{1}H low-field NMR," *Macromolecules*, vol. 47, no. 16, pp. 5655–5667, 2014.

[38] K. Hagiwara, T. Ougizawa, T. Inoue, K. Hirata, and Y. Kobayashi, "Studies on the free volume and the volume expansion behavior of amorphous polymers," *Radiat. Phys. Chem.*, vol. 58, no. 5–6, pp. 525–530, 2000.

[39] K. Murata *et al.*, "Structural determinants of water permeation through aquaporin-1 Actin cytoskeleton View project Structural determinants of water permeation through aquaporin-1," *Nature*, pp. 599–605, 2000.

[40] F. S. Lima, H. Chaimovich, I. M. Cuccovia, and D. Horinek, "Molecular dynamics shows that ion pairing and counterion anchoring control the properties of triflate

micelles: A comparison with triflate at the air/water interface," *Langmuir*, vol. 30, no. 5, pp. 1239–1249, 2014.

[41] S. Kobayashi, S. Nagayama, and T. Busujima, "Lewis acid catalysts stable in water. Correlation between catalytic activity in water and hydrolysis constants and exchange rate constants for substitution of inner-sphere water ligands," *J. Am. Chem. Soc.*, vol. 120, no. 32, pp. 8287–8288, 1998.

Chapter 3

Effect on T_g enhancement of poly(methyl methacrylate) by addition of LiBr

3.1. Introduction

3.1.1. T_g enhancement of PMMA by addition of lithium salts

As mentioned in Chapter 2, $LiCF_3SO_3$ is the most effective salt on T_g enhancement for PMMA among various lithium salts. However, after being stored in a temperature- and humidity-controlled chamber at 25 ºC and 50 % RH, T_g of PMMA/$LiCF_3SO_3$ was decreased by moisture absorption. In other words, PMMA was significantly plasticized by the addition of $LiCF_3SO_3$ under the conditions of high humidity. This is due to the high hydrophilicity of $LiCF_3SO_3$.

It was also demonstrated that T_g was also enhanced by the addition of LiBr. Furthermore, plasticization by water molecules was not significant for the blend. However, the mechanism of T_g enhancement by the addition of LiBr has not been elucidated yet. Therefore, in this chapter, the mechanism of T_g enhancement of PMMA/LiBr was investigated. PMMA/$LiCF_3SO_3$ was used as a reference for a comparison with PMMA/LiBr.

3.2. Experimental

3.2.1. Chemicals

The polymer utilized in this research was a commercially available PMMA (Acrypet VH; Mitsubishi Chemical Corp.). The number- and weight-average molecular weights, which were estimated using size-exclusion chromatography (HLC-8020; Tosoh Corp.) with chloroform as the solvent, were M_n = 54,000 and M_w = 120,000 (standard: polystyrene (PS)), respectively.

Two kinds of lithium salts, i.e., $LiCF_3SO_3$ (purity ≥ 98.0 %; Kanto Chemical Co., Ltd.) and lithium bromide (LiBr, purity > 99.0 %; Tokyo Chemical Industry Co., Ltd.)), were used without further purification.

3.2.2. Sample preparation

Blend film fabrication

The PMMA and each lithium salt were completely dissolved in a mixed solution of dichloromethane and methanol in 9-to-1 weight ratio, and the mixture was stirred for 1 hour. The molar ratios of lithium ions per 1 mole of carbonyl groups of PMMA were fixed to 0, 0.01, 0.03, and 0.07 of both lithium salts. These molar ratios were corresponded to 0, 2, 5, and 10 wt.% for $LiCF_3SO_3$, and 0, 1, 3, and 6 wt.% for LiBr, respectively. Each solution was cast onto a petri dish, and dried in a vacuum chamber at 160 °C for 30 hrs. Then, each sample was compression-molded into the film with the thickness of 300 μm. The compression-molding condition was as follows; heating at 200 °C for 10 min and quenching at 25 °C. These samples were measured immediately after compression-molding.

3.2.3. Measurements

The temperature dependence of the storage modulus *E'*, and loss modulus *E"*, were measured in the temperatures from 30 to 200 °C by Rheogel-E4000 dynamic mechanical analyzer (UBM Co., Ltd.). The frequency was set at 10 Hz. Heating rate was fixed to 2 °C/min.

The frequency dependences on the oscillatory shear moduli, i.e., the storage modulus *G'* and loss modulus *G"*, were measured using an AR2000ex cone-and-plate rheometer (TA Instruments Co., Ltd.) under nitrogen flow at 200, 220, and 240°C. The steady-flow properties were also measured using the same plate under nitrogen flow at 240°C.

XRD pattern was obtained by X-ray diffractometer (Rigaku, SmartLab) with a Cu target as a source of X-ray emitting Cu Kα radiation. X-ray tube voltage and current were 40 kV and 30 mA, respectively. The measurement was held in the range of 2θ between 5 ° and 80 °. Scan step and duration time were 0.1 ° and 1.00 s, respectively.

In order to investigate the strength of ion-dipole interaction between lithium cations and carbonyl groups in PMMA, ATR measurements using a KRS-5 ATR prism were held to evaluate infrared spectra under nitrogen flow. The accumulation counts were 16 times, and the resolution was 4 cm^{-1}.

3.3. Results and Discussion

3.3.1. T_g enhancement of PMMA by addition of LiBr

The dynamic tensile moduli of PMMA/$LiCF_3SO_3$ and PMMA/LiBr with different salt concentrations are shown in Figures 3.1 (a) and (b), respectively. As seen in the figures, T_g was gradually enhanced as the salt concentration increased for both cases. The values of

T_g, which were characterized as the peak temperature of *E"*, are summarized in Table 3.1 and Table 3.2.

Table 3.1. T_g of the PMMA/$LiCF_3SO_3$ ([Li]/[C=O] ratio of 0, 0.01, 0.03, and 0.07, which correspond to 0, 2, 5, and 10 wt.%).

[Li]/[C=O] (mol/mol)	wt.%	T_g (°C) of PMMA/$LiCF_3SO_3$
0	0	127
0.01	2	130
0.03	5	133
0.07	10	137

Table 3.2. T_g of the PMMA/LiBr ([Li]/[C=O] ratio of 0, 0.01, 0.03, and 0.07, which correspond to 0, 1, 3, and 6 wt.%).

[Li]/[C=O] (mol/mol)	wt.%	T_g (°C) of PMMA/LiBr
0	0	127
0.01	1	128
0.03	3	132
0.07	6	133

As shown in Figure 3.1 (a), the glass-to-rubber transition was shifted to a high temperature as the salt concentration increased in the case of PMMA/$LiCF_3SO_3$. On the other hand, PMMA/LiBr, the glass-to-rubber transition occurred in the wide temperature range with the slight shift of the peak temperature of *E"*. In other words, the prolonged relaxation mode appeared in the case of PMMA/LiBr.

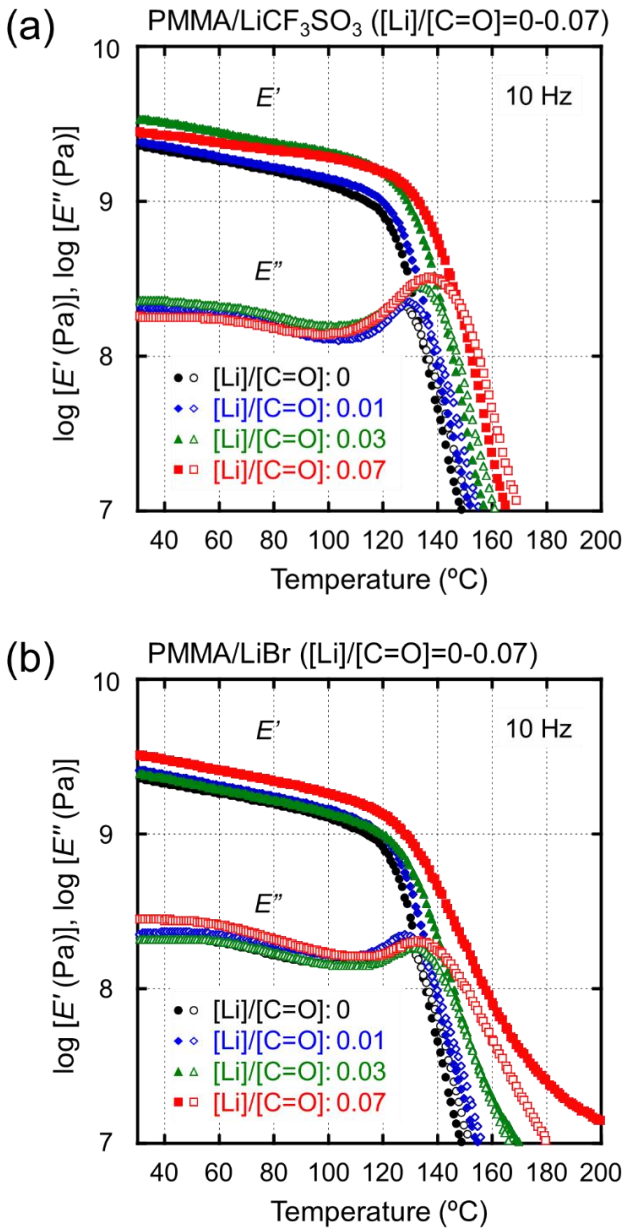

Figure 3.1. Temperature dependence of the dynamic tensile moduli at 10 Hz of (a) PMMA/$LiCF_3SO_3$ and (b) PMMA/LiBr films with different salt concentrations. The salt concentrations were 0–0.07 molar ratios of lithium ions to PMMA carbonyl groups; (black) [Li]/[C=O] ratio of 0, (blue) [Li]/[C=O] ratio of 0.01, (green) [Li]/[C=O] ratio of 0.03, and (red) [Li]/[C=O] ratio of 0.07.

In Figure 3.2, the average strength of ion-dipole interaction between carbonyl group in PMMA and lithium cations was estimated by infrared spectroscopy.

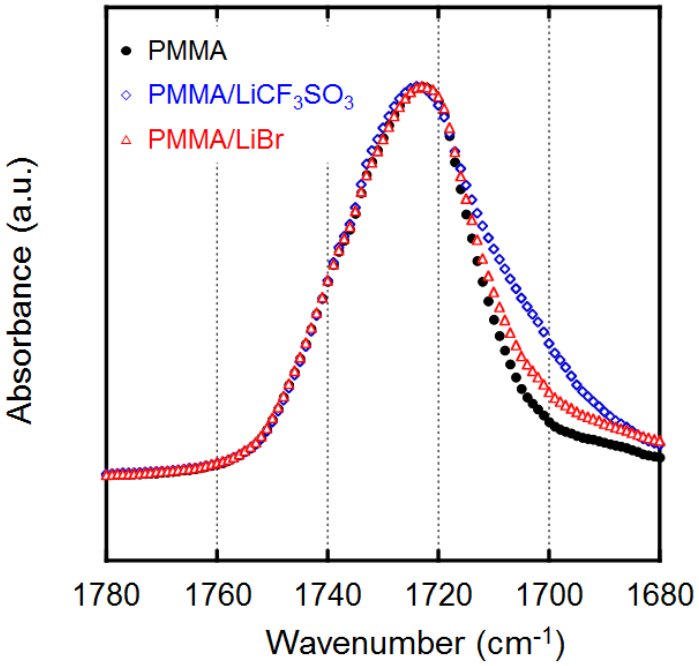

Figure 3.2. Attenuated total reflection (ATR) spectra of (black) PMMA, (blue) PMMA/$LiCF_3SO_3$ ([Li]/[C=O] ratio of 0.07), and (red) PMMA/LiBr ([Li]/[C=O] ratio of 0.07).

As shown in Figure 3.2, the peak of PMMA/$LiCF_3SO_3$ was broadened to the lower wavenumber region, i.e., higher energy region. In contrast, the peak of PMMA/LiBr was located at almost the same wavenumber as that of PMMA. This suggests that the ion–dipole interaction between the lithium cation and the carbonyl groups in PMMA/$LiCF_3SO_3$ was stronger than that in PMMA/LiBr on average. This corresponds with the previous result in Figure 3.1, i.e., the addition of $LiCF_3SO_3$ remarkably affected increasing T_g of PMMA. However, the origin of the prolonged relaxation mode in PMMA/LiBr can not be explained from this result. This phenomenon occurred remarkably in the high temperature region, that

is, in the region of the molten state of the blends.

Therefore, the rheological properties in the molten state of the samples were investigated for pure PMMA and both blends in high temperatures to evaluate the origin of this phenomenon. The salt concentration in both blends was 0.01 molar ratio of lithium ions to PMMA carbonyl groups, which was determined considering the experimental difficulty of PMMA/LiBr. In the case of PMMA/LiBr, it was almost impossible to prepare flat films without strong molecular orientation when the salt ratio is beyond [Li]/[C=O] ratio of 0.01. Consequently, marked shrinkage occurs during the rheological measurements.

The master curves of the oscillatory shear moduli are shown in Figure 3.3 at the reference temperature (T_r) of 200°C.

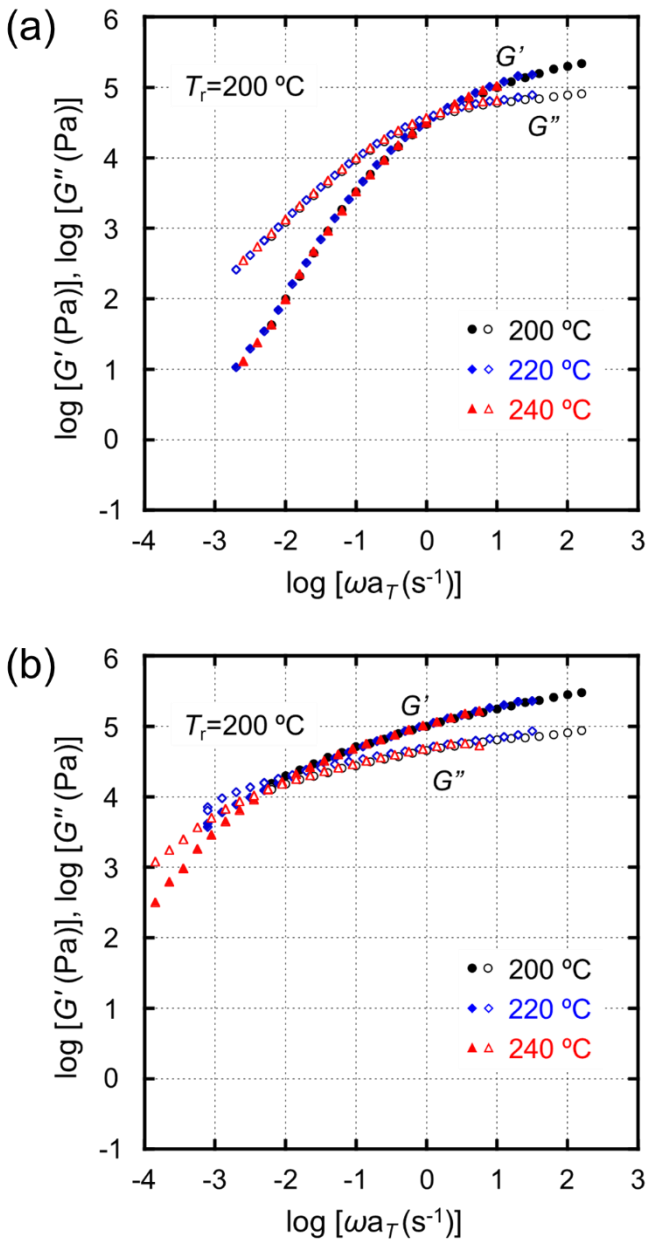

Figure 3.3. Master curves of frequency dependence of oscillatory shear moduli of (a) PMMA/$LiCF_3SO_3$ ([Li]/[C=O] ratio of 0.01) and (b) PMMA/LiBr ([Li]/[C=O] ratio of 0.01) at the reference temperature T_r of 200°C; (black) 200°C, (blue) 220°C, and (red) 240°C.

As shown in Figure 3.3 (a), the time–temperature superposition (TTS) principle was applicable to PMMA/$LiCF_3SO_3$. This phenomenon was detected because the contribution of the ion–dipole interaction to the oscillatory moduli was much smaller than that of reptation motion. When the molecular weight of PMMA is low, a thermorheological complex is observed, as shown in the previous report [1]. On the other hand, it was not applicable to PMMA/LiBr as shown in Figure 3.3 (b).

The shift factors of pure PMMA and the blends are summarized in Table 3.3. For PMMA/LiBr, the shift factor was conveniently determined by horizontal shift in the high frequency region.

Table 3.3. Shift factors of pure PMMA, PMMA/$LiCF_3SO_3$ ([Li]/[C=O] ratio of 0.01) and PMMA/LiBr ([Li]/[C=O] ratio of 0.01) at the reference temperature T_r of 200°C.

Sample	a_T (220 ºC)	a_T (240 ºC)
Pure PMMA	0.77	1.40
PMMA/$LiCF_3SO_3$	0.90	1.40
PMMA/LiBr	0.90	1.65

These trends in both blends can be also assumed from the van Gurp-almen plot [2]–[4] in Figure 3.4. The van Gurp-Palmen plot represents the phase angle δ against the absolute value of complex modulus $|G^*|$, which yields temperature independent curves if TTS is applicable [2]. As seen in Figure 3.4 (b), the data of PMMA/LiBr were not on the same line, suggesting that TTS principle was not applicable for PMMA/LiBr.

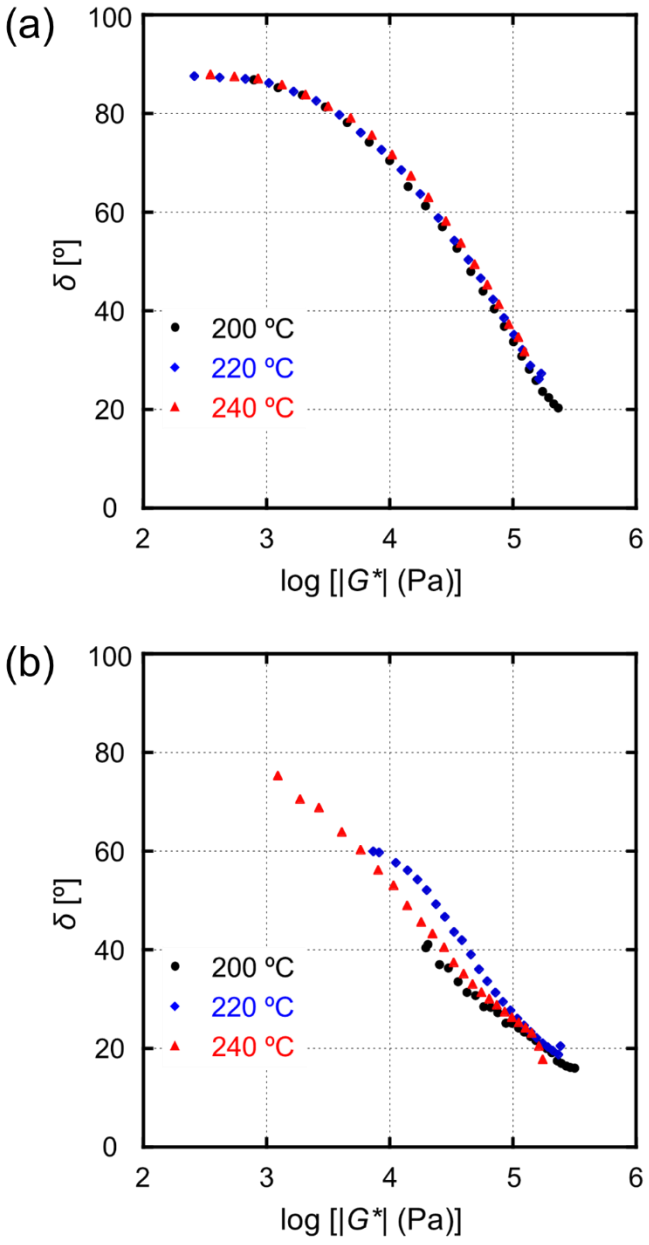

Figure 3.4. van Gurp-Palmen plots of (a) PMMA/$LiCF_3SO_3$ ([Li]/[C=O] ratio of 0.01) and (b) PMMA/LiBr ([Li]/[C=O] ratio of 0.01); (black) 200°C, (blue) 220°C, and (red) 240°C.

Furthermore, it was revealed that the rubbery region of PMMA/LiBr was significantly broad, demonstrating that the ion–dipole interaction prolongs the reptation motion of polymer chains, even at 240°C. The longer relaxation of PMMA/LiBr was also suggested quantitatively by the fact that the inverse of the angular frequency at the cross point of *G'* and *G"*, that is, an average relaxation time, for PMMA/LiBr, 180 s, was significantly longer than that for PMMA/$LiCF_3SO_3$, 0.63 s, as summarized in Table 3.4. The average relaxation time for PMMA/$LiCF_3SO_3$ was almost the same as that for pure PMMA.

The values of steady-state shear stress at 240 °C were shown in Figure 3.5 for pure PMMA and both blends at [Li]/[C=O] ratio of 0.01.

Table 3.4. Average relaxation time of pure PMMA, PMMA/$LiCF_3SO_3$ ([Li]/[C=O] ratio of 0.01) and PMMA/LiBr ([Li]/[C=O] ratio of 0.01).

Sample	Average relaxation time (s)
Pure PMMA	0.40
PMMA/$LiCF_3SO_3$	0.63
PMMA/LiBr	180

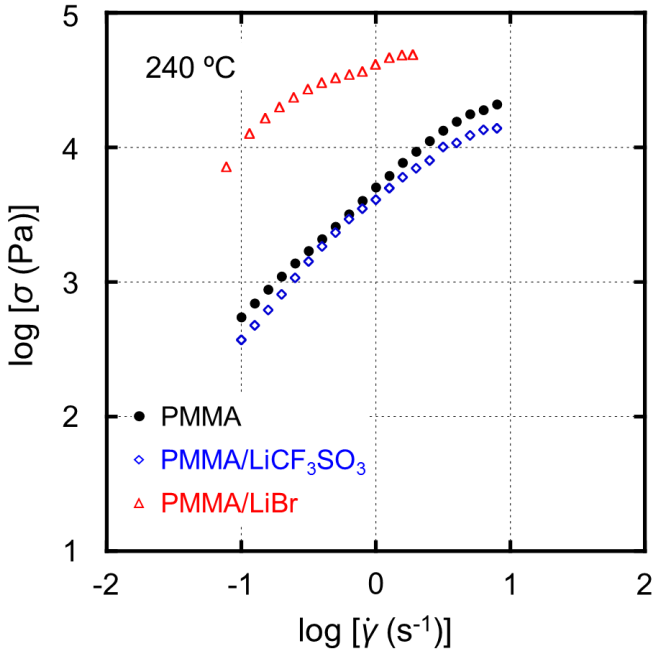

Figure 3.5. Relationship between shear rate $\dot{\gamma}$ and shear stress σ at 240 °C for PMMA/$LiCF_3SO_3$ and PMMA/LiBr with 0.01 molar ratio of salts at 240 °C; (black) PMMA, (blue) PMMA/$LiCF_3SO_3$, and (red) PMMA/LiBr.

As seen in Figure 3.5, the steady-state shear stress for PMMA/LiBr was an order of magnitude higher than those for the other blend. This indicates that the strong interaction acted as crosslinking points, even at 240 °C, as corroborated by the linear viscoelastic properties. Furthermore, the shear stress of PMMA/$LiCF_3SO_3$ was slightly lower than that of pure PMMA, indicating that $LiCF_3SO_3$ acts as a diluent for PMMA at high temperatures, although it behaved as an antiplasticizer which increases *E'* of the blend at the temperature around T_g.

3.3.2. Contribution of strong crosslinking to T_g enhancement in PMMA/LiBr

As demonstrated by the rheological properties, PMMA/LiBr has a longer relaxation mechanism, i.e., stronger interaction. It could not be explained by only physical crosslinking based on ion-dipole interaction between lithium cations and carbonyl groups in PMMA because the ion-dipole interaction is barely reduced even at high temperatures. These results are contradict from weaker average strength of interaction as suggested in Figure 3.2. This contradiction implies the possibility that the quite strong interaction such as chemical crosslinking was provided in PMMA/LiBr. Therefore, the solvent immersion test was performed as follows.

The films # 1 - # 3 were dipped in tetrahydrofuran (THF) to reveal the process for strong crosslinking such as chemical crosslinking.

1. Solution-cast film

2. Film dried at 160 ºC for 30 hrs after solution-casting

3. Film compressed at 200 ºC after drying at 160 ºC for 30 hrs

The scheme of this experiment is shown in Figure 3.6.

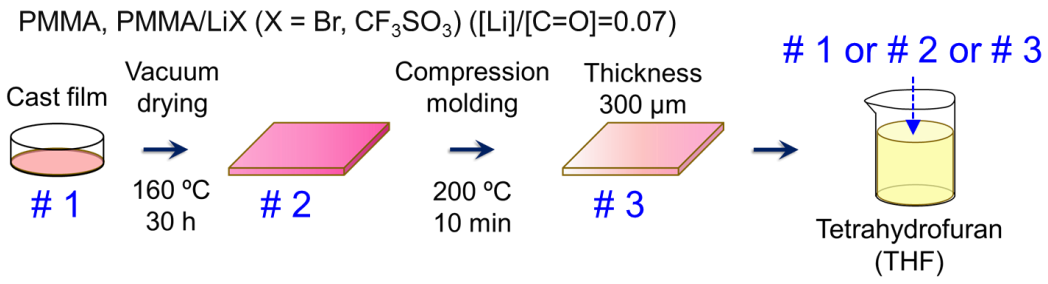

Figure 3.6. Experimental scheme of the solvent immersion tests.

Table 3.5. Solubility in THF of PMMA, PMMA/LiBr ([Li]/[C=O] ratio of 0.07), and PMMA/$LiCF_3SO_3$ ([Li]/[C=O] ratio of 0.07).

Sample	# 1	# 2	# 3
PMMA	dissolved	dissolved	dissolved
PMMA/$LiCF_3SO_3$	dissolved	dissolved	dissolved
PMMA/LiBr	dissolved	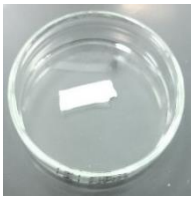 insoluble	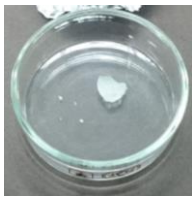 insoluble

As shown in Table 3.5, insoluble parts were detected in the samples of # 2 and # 3 of PMMA/LiBr. All of the others were dissolved in THF, suggesting that the strong interaction such as chemical crosslinking occurred by heating for PMMA/LiBr.

The gel fractions of both # 2 and # 3 for PMMA/LiBr were also evaluated from the weight of dried gel and the initial weight of the sample.

Table 3.6. Gel fractions of PMMA/LiBr ([Li]/[C=O] ratio of 0.07) in THF.

No.	# 1	# 2	# 3
Φ_{gel}	-	0.44	0.24

As shown in Table 3.6, the gel fraction of PMMA/LiBr sample # 3 is much smaller than that of PMMA/LiBr sample # 2. This indicates that both chain session and strong

interaction occurred simultaneously by additional heating during compression-molding at 200 ºC in the PMMA/LiBr sample # 3.

These results demonstrate that not only ion-dipole interaction between lithium cations and carbonyl groups in PMMA but other strong interaction such as chemical crosslinking also contribute to the T_g enhancement of PMMA in the case of PMMA/LiBr. Therefore, it is required to discuss the difference in the mechanism of T_g enhancement between PMMA/$LiCF_3SO_3$ and PMMA/LiBr. Here, the T_g enhancement of each film was compared for PMMA, PMMA/LiBr, and PMMA/$LiCF_3SO_3$, before discussion of the mechanism of T_g enhancement. The concentration of the salt was 0.07 molar ration per 1 molar of carbonyl groups in PMMA for the blends. In the loss modulus *E"* of the sample # 1 and the sample # 2, the two peaks were detected. One is T_g of the blend itself (under dry condition) and the other, located at the low temperature, is T_g of the plasticized region by water or the organic solvents. Because the peaks were overlapped each other, it was difficult to determine the T_g of the film itself from the loss modulus *E"*. Therefore, the T_g was evaluated by the peak temperature of loss tan δ. The values of T_g were summarized in Table 3.7. As seen in the second line of this table, T_g of the PMMA sample # 2 was increased by 14 ºC from that of the sample # 1.

Table 3.7. Contribution to T_g enhancement at each step of sample fabrication of PMMA, PMMA/LiBr and PMMA/$LiCF_3SO_3$ with 0.07 molar ratio of salts. T_gs were evaluated by the peak temperature of tan δ at the dynamic mechanical measurements at 10 Hz.

	# 1	# 2	# 3
T_g of PMMA	128 ºC	142 ºC	142 ºC
	Δ29 ºC	Δ18 ºC	Δ19 ºC
T_g of PMMA/$LiCF_3SO_3$	157 ºC	160 ºC	161 ºC
	Δ9 ºC	Δ10 ºC	Δ15 ºC
T_g of PMMA/LiBr	137 ºC	152 ºC	157 ºC
	↑ ion-dipole interaction	↑ chemical crosslink	↑ chemical crosslink

Here, it was revealed that a quite small amount of residual solvents affected the T_g of PMMA. As shown in Figure 3.7 (a), T_g (denoted as black symbols in the Figure) of the compression-molded film obtained from the pellets without any solvent treatment which was vacuum dried at room temperature for 30 hrs was 112 ºC. However, the T_g of the solution-cast film prepared using a mixture solvent of dichloromethane and methanol with weight fraction of 9 : 1 was 102 ºC. This result suggests that the tiny amount of organic solvent still remained in the sample even after compression-molding at 200 ºC and being dried under vacuum at room temperature. This T_g decrease is considered because the strong ion-dipole interactions between the solvent molecules and the carbonyl group in PMMA molecules reduced the T_g of PMMA. Such strong ion-dipole interaction suppressed the associated states of PMMA and greatly affected chain mobility of PMMA.

In contrast, as shown in Figure 3.7 (b), the most remaining solvents in the film were

successfully removed by heating at 160 ºC under vacuum for 30 hrs.

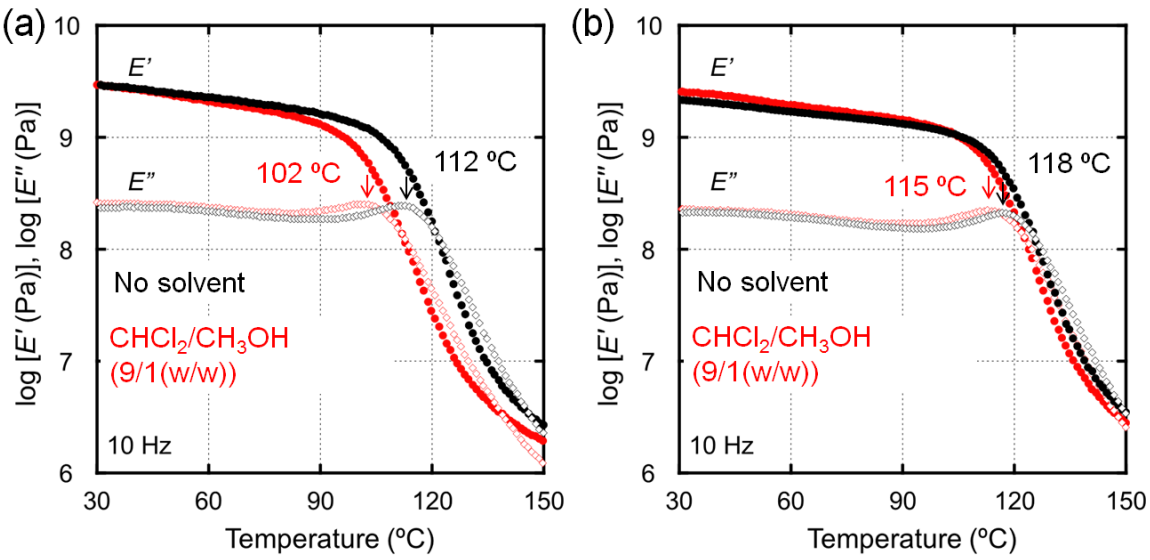

Figure 3.7. Temperature dependence of the dynamic tensile moduli at 10 Hz of (a) (black) compression-molded film of PMMA pellets and (red) solution-cast film of PMMA dried under vacuum at room temperature for 30 hrs after being treated with the mixture solvent of dichloromethane and methanol with a weight fraction of 9 : 1 and (b) (black) compression-molded film of PMMA pellets and (red) solution-cast film of PMMA dried under vacuum at 160 ºC for 30 h after being treated with mixture solvent of dichloromethane and methanol with a weight fraction of 9 : 1.

Therefore, this T_g enhancement by the process of drying at 160 ^{O}C for 30 hrs is due to the evaporation of the remaining solvents.

Furthermore, the temperatures of T_g of PMMA, PMMA/$LiCF_3SO_3$, and PMMA/LiBr under the processes # 1 to # 3 were compared. As a result, PMMA/$LiCF_3SO_3$ at each step showed higher T_g than the corresponding PMMA film.

In contrast, T_g of PMMA/$LiCF_3SO_3$ was barely affected by the film processing steps, i.e., # 1 to # 3, suggesting that T_g was enhanced at the first step; i.e., the annealing history does not affect T_g for PMMA/$LiCF_3SO_3$. This is reasonable because the T_g enhancement occurred by only ion-dipole interaction.

In contrast, T_g of the solution-cast film was not enhanced so much by the LiBr addition. (about 9 ºC, which is attributable to the ion-dipole interaction.) It should be notified that the T_g enhancement was detected after the heating history (# 2 and # 3). This suggests that the strong interaction was provided by heating at the second process and additional heating at the compression molding as a final process. T_g of the PMMA/LiBr was greatly enhanced by the heating processes.

3.3.3. Interaction in PMMA/LiBr

The origin of the strong interaction in PMMA/LiBr is discussed in this section. According to the solvent immersion experiment using THF, it was proposed that there is a strong interactions like chemical crosslinking in PMMA/LiBr, although it is not clarified well.

Thus, to elucidate the prolonged relaxation mode in PMMA/LiBr, ATR spectra were collected. Figure 3.8 shows the ATR spectra of PMMA and PMMA/LiBr with 0.07 molar ratio of lithium ions to PMMA carbonyl groups. The ATR spectra were normalized with a peak height at 1435 cm^{-1} assigned to the symmetry stretching vibration mode of OCH_3 [5]. The positions of absorption bands for ATR spectra and their assignments are listed in Table 3.8 [5]–[7].

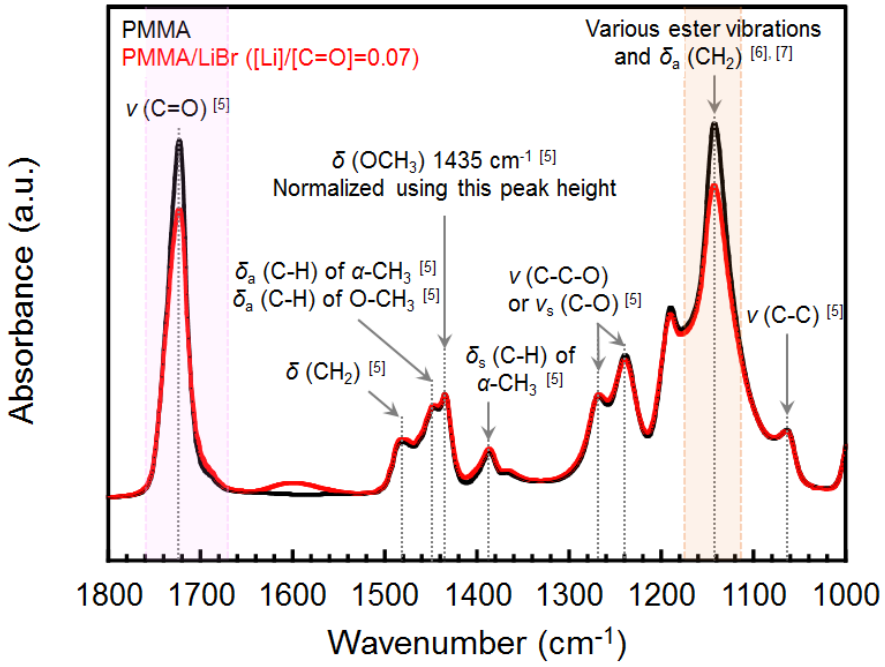

Figure 3.8. Attenuated total reflection (ATR) spectra normalized with peak height at wavenumber of 1435 cm^{-1} of (black) PMMA and (red) PMMA/LiBr ([Li]/[C=O] ratio of 0.07) in wavenumber range of 1000 to 1800 cm^{-1}.

Table 3.8. Wavenumbers and assignments of infrared absorption bands of PMMA [5-7].

Wavenumbers (cm^{-1}) in this result	Wavenumbers (cm^{-1}) reported in reference [5, 6]	Assignments
2994	2995 [5]	ν_a (C-H) of α-CH_3, ν_a (C-H) of OCH_3 [5]
2950	2948 [5]	ν_s (C-H) of OCH_3 with ν_s (C-H) of α-CH_3, and ν_a (CH_2) [5]
2924	2915-2920 [5]	Combination band involving OCH_3 and ν_s (CH_2) [5]
1724	1730 [5]	ν (C=O) [5]
1485	1483 [5]	δ (CH_2) [5]
1448	1452, 1465 [5]	δ_a (C-H) of α-CH_3, δ_a (C-H) of O-CH_3 [5]
1435	1438 [5]	δ (C-H) of OCH_3 [5]
1387	1388 [5]	δ_s (C-H) of α-CH_3 [5]
1268	1270 [5]	ν (C-C-O) or ν_s (C-O) [5]
1239	1240 [5]	
1190	1190 [5, 6], 1192 [7]	Under discussion [5-7]; possibly ν (C-O-C) [6]
1143	1150 [6], 1148 [7]	Combination of delocalized modes of various ester vibrations and CH_2 rocking modes [6], [7]
1064	1063 [5]	ν (C-C) [5]

As seen in Figure 3.8, a broad peak appeared at 1600 cm^{-1} in PMMA/LiBr. A functional group having a peak at 1600 cm^{-1} is possibly attributed to an amide group or a C=C double bond. However, it is impossible that amide group was produced because PMMA has no functional groups including nitrogen. Furthermore, if a C=C double bond is formed, there is a dehydration reaction between the O-CH_3 groups in the side chain of two PMMA molecules. However, this phenomenon unlikely occurs because this functional group is less reactive than the carbonyl group.

It is notable that the peaks at 1143 cm^{-1}, attributed to combination of various ester vibrations and CH_2 rocking modes, and 1724 cm^{-1}, attributed to the stretching vibration

mode of carbonyl group, were reduced as compared with pure PMMA.

Figure 3.9 shows the normalized ATR spectra using a peak height 1434 cm^{-1} [6] in the wavenumber region of 1640 to 1780 cm^{-1} of PMMA, PMMA/$LiCF_3SO_3$, and PMMA/LiBr with 0.07 molar ratio of salts.

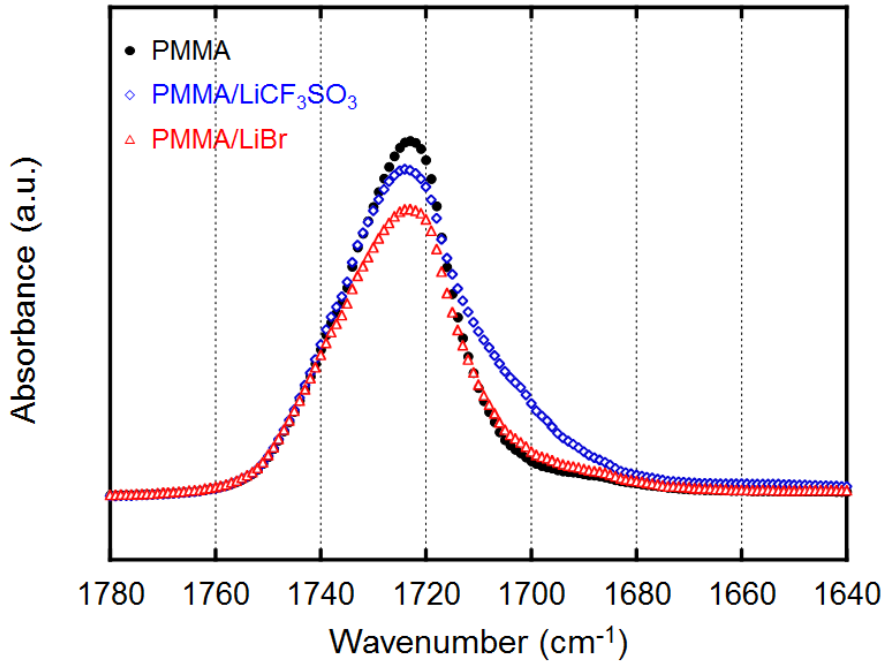

Figure 3.9. ATR spectra normalized with a peak height at a wavenumber of 1435 cm^{-1} of (black) PMMA, (blue) PMMA/$LiCF_3SO_3$ ([Li]/[C=O] ratio of 0.07), and (red) PMMA/LiBr ([Li]/[C=O] ratio of 0.07) in the wavenumber range of 1640 to 1780 cm^{-1}.

Comparing the spectra of these blends at 1724 cm^{-1}, the absorption intensity of PMMA/$LiCF_3SO_3$ and PMMA/LiBr was lower than that of pure PMMA. For PMMA/$LiCF_3SO_3$, it was suggested that the decrease in intensity corresponds to the broaden peak in the lower wavenumber region caused by the physical interaction with lithium cations, as described above. In contrast, the broadening of the peak at 1724 cm^{-1} did not occur in

PMMA/LiBr. The peak intensity at 1724 cm^{-1} in PMMA/LiBr also became lower. Furthermore, the peak intensity at 1143 cm^{-1} of PMMA/LiBr was lower than that of pure PMMA, as indicated in Figure 3.8. As shown in Table 3.8, the vibration modes at 1143 cm^{-1} were attributed to the combination of delocalized modes of various ester vibrations and CH_2 rocking modes. Considering above the results, the vibration of the carbonyl group in PMMA was restricted by the addition of LiBr.

The XRD pattern of pressed films of PMMA and PMMA/LiBr with 0.07 molar ratio of lithium ions to PMMA carbonyl groups was shown in Figure 3.10, as an additional information. This graph suggests that LiBr did not recrystallize and precipitate in the blend film even after the compression molding at 200 °C. This result indicated that the LiBr crystals didn't contribute to the prolonged relaxation mode in PMMA/LiBr.

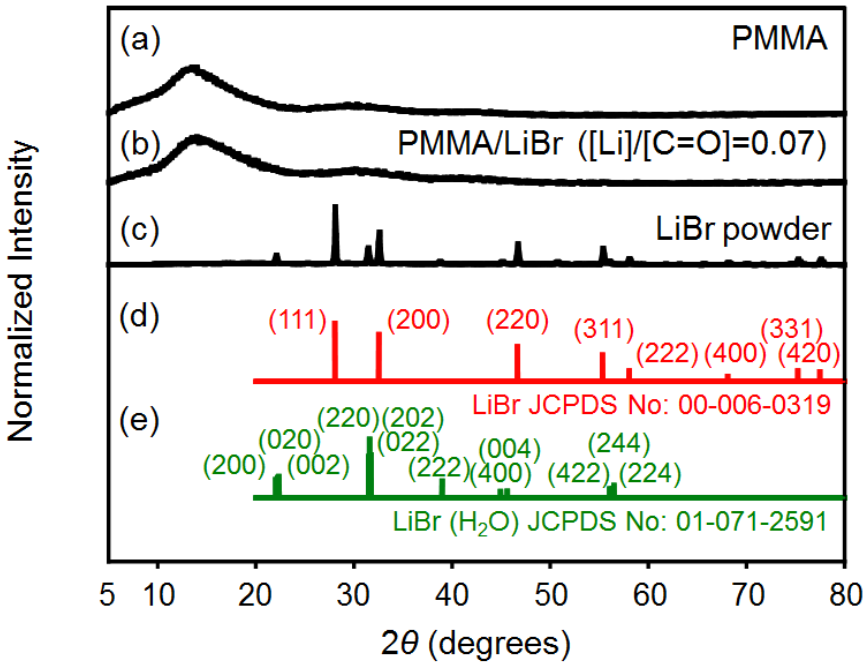

Figure 3.10. XRD pattern of (a) pure PMMA, (b) PMMA/LiBr ([Li]/[C=O] ratio of 0.07), (c) PMMA/LiBr powder, (d) Standard pattern of LiBr (JCPDS 00-006-0319) and (e) Standard pattern of lithium hydrate; LiBr (H_2O) (JCPDS 01-071-2591).

The schematic illustration to describe the origin of T_g enhancement by the LiBr addition is shown in Figure 3.11. The carbonyl groups in PMMA interact with both lithium cations and bromide anions, and thus, vibration modes of carbonyl groups were suppressed.

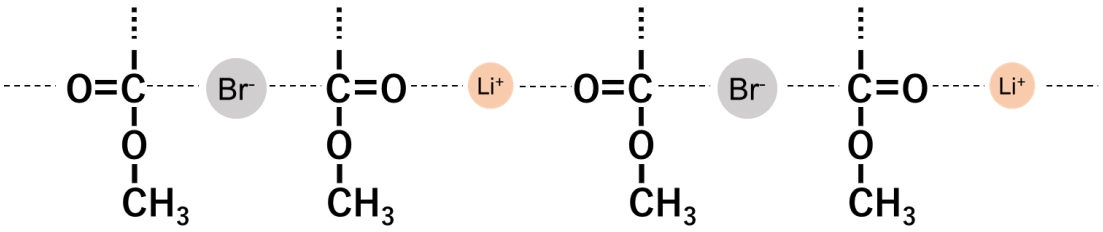

Figure 3.11. Schematic illustration of interaction between ions and carbonyl groups in PMMA/LiBr.

To verify this model, PMMA/LiBr was rinsed with methanol and dried in a draft before the solvent immersion test in THF. The scheme of this experiment is shown in Figure 3.12.

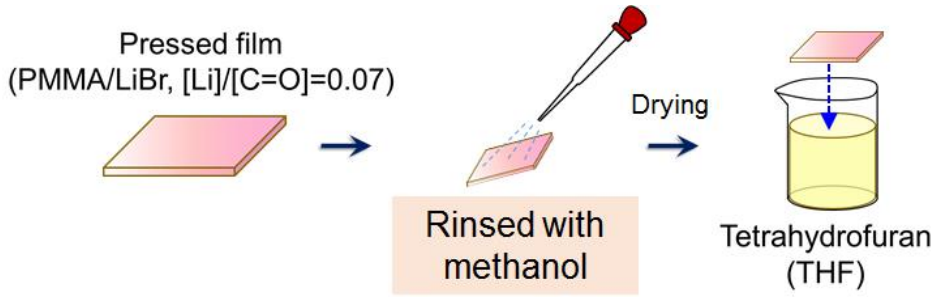

Figure 3.12. Experimental scheme of the solvent immersion tests for the rinsed PMMA/LiBr sample ([Li]/[C=O] ratio of 0.07).

Assuming that chemical crosslinking ocurred in PMMA/LiBr, the sample after washing by methanol will not be dissolved in THF, since methanol only dissolves the salt.

As shown in Table 3.9, insoluble parts were not detected in the rinsed sample by methanol.

Table 3.9. Solubility in THF of PMMA, PMMA/LiBr ([Li]/[C=O] ratio of 0.07), and PMMA/LiBr ([Li]/[C=O] ratio of 0.07) after rinsing with methanol.

Sample	w/o methanol	w/ methanol
PMMA/LiBr	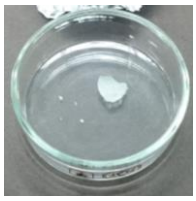 insoluble	dissolved

The sample rinsed with methanol before the solvent immersion test was completely dissolved in THF, suggesting that such strong interaction in PMMA/LiBr is not due to chemical crosslinking, but due to quite strong physical interaction.

Figure 3.13 shows the ATR spectra of pure PMMA, PMMA/LiBr with/without rinsing by methanol.

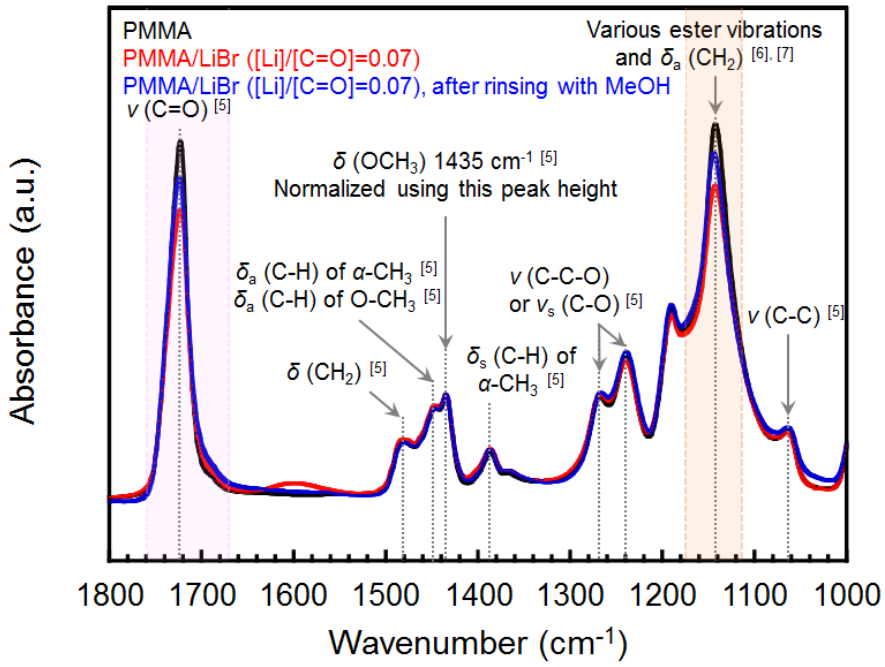

Figure 3.13. ATR spectra normalized with peak height at wavenumber of 1435 cm^{-1} of (black) PMMA, (red) PMMA/LiBr ([Li]/[C=O] ratio of 0.07) and (blue) PMMA/LiBr ([Li]/[C=O] ratio of 0.07) after rinsing with methanol in wavenumber range of 1000 to 1800 cm^{-1}.

PMMA/LiBr still showed low intensities at 1143 and 1724 cm^{-1} with methanol as compared with PMMA. However, it showed higher relative intensities than those of the sample without methanol treatment. Such changes indicate that and the restriction of the carbonyl peaks by the quite strong interaction was relieved because the salt was dissolved into methanol. This phenomenon is described in Figure 3.14.

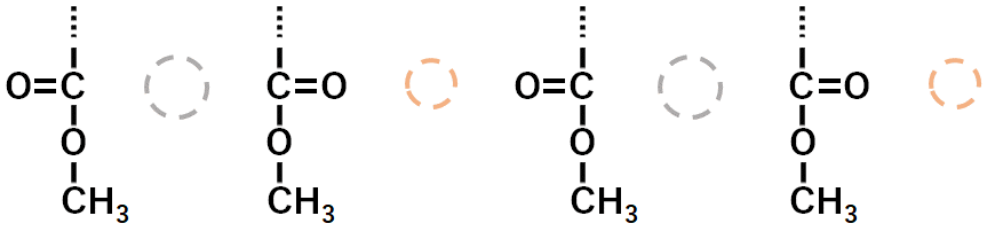

Figure 3.14. Schematic illustration of the relaxation of interaction between ions and carbonyl groups in PMMA/LiBr after rinsing with methanol.

3.4. Conclusion

In the previous chapter, the $LiCF_3SO_3$ addition was found to increase the T_g of PMMA owing to ion–dipole interactions between the lithium cations and the carbonyl groups. However, the addition of the salt also increased moisture absorption. Because water acts as a plasticizer, T_g and elastic moduli were decreased in the PMMA blend with $LiCF_3SO_3$ after being kept in a humid condition. In contrast, the plasticization due to moisture absorption was hardly detected in the case of the blend with LiBr. Therefore, LiBr is more useful for the application in terms of increasing T_g without impairing the quality of PMMA products.

In this chapter, the mechanism of T_g enhancement by the addition of LiBr was investigated. It was found that a strong interaction by both lithium cations and bromide ions with carbonyl groups in PMMA occurred in PMMA/LiBr, leading a prolonged relaxation mode. Furthermore, it was revealed that the prolonged relaxation mode by strong physical interaction is dominant to increase T_g in PMMA/LiBr. This is the first time to report that such quite strong interaction occurs only by the addition of a specific lithium salt.

Furthermore, this technique could be applicable to various functional materials composed of PMMA.

3.5. References

[1] A. Miyagawa, V. Ayerdurai, S. Nobukawa, and M. Yamaguchi, "Viscoelastic properties of poly(methyl methacrylate) with high glass transition temperature by lithium salt addition," *J. Polym. Sci. Part B Polym. Phys.*, vol. 54, no. 22, pp. 2388–2394, 2016.

[2] M. van Gurp and J. Palmen, "Time-temperature superposition for polymeric blends," *J. Rheol. Bull.*, vol. 65, pp. 5–8, 1998.

[3] O. Valentino *et al.*, "Influence of the polymer structure and nanotube concentration on the conductivity and rheological properties of polyethylene/CNT composites," *Phys. E*, vol. 40, no. 7, pp. 2440–2445, 2008.

[4] S. Trinkle and C. Freidrich, "Van Gurp-Palmen-plot: A way to characterize polydispersity of linear polymers," *Rheol. Acta*, vol. 40, no. 4, pp. 322–328, 2001.

[5] H. . Willis, V. J. . Zichy, and P. . Hendra, "The laser-Raman and infra-red spectra of poly(methyl methacrylate)," *Polymer (Guildf).*, vol. 10, pp. 737–746, 1969.

[6] R. H. G. Brinkhuis and A. J. Schouten, "Thin-film behavior of poly(methyl methacrylates). 2. An FT-IR study of Langmuir-Blodgett films of isotactic PMMA," *Macromolecules*, vol. 24, no. 7, pp. 1496–1504, 1991.

[7] S. Havriliak and N. Roman, "The infra-red absorption characteristics of syndiotactic poly(methyl methacrylate) from 1050 cm-1 to 1300 cm-1," *Polymer (Guildf).*, vol. 7, no. 8, pp. 387–400, 1966.

Chapter 4

Improvement of optical properties of poly(methyl methacrylate) by addition of $LiCF_3SO_3$

4.1. Introduction

4.1.1. Application of PMMA for display

It is well known that the refractive index of PMMA is relatively low, 1.49 at the wavelength of 589 nm [1]. Furthermore, PMMA shows a small level of birefringence provided by the mechanical stress in the glassy region, that is so-called photoelastic birefringence. In general, small photoelastic birefringence is necessary for the application of panels in LCD units in Figure 4.1 [1]–[3].

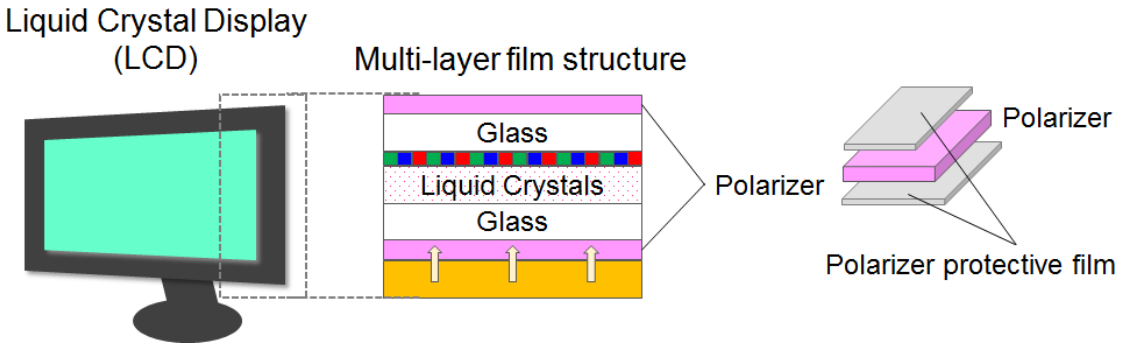

Figure 4.1. LCD unit and polarizer protective film.

When a polarizer protective film, used in an LCD unit as shown in Figure 4.1, is prepared by conventional melt-extrusion process, the molecules orient to the flow direction to some degree. This provides another birefringence, i.e, orientation birefringence. It is known that the orientation birefringence of PMMA is low because of its low value of intrinsic birefringence [1], [4]. Although both photoelastic and orientation birefringences are few for PMMA, further reduction is strategy desired to improve the quality of LCDs.

Moreover, PMMA is a promising material used for a diffusing plate in LCDs as shown in Figure 4.2.

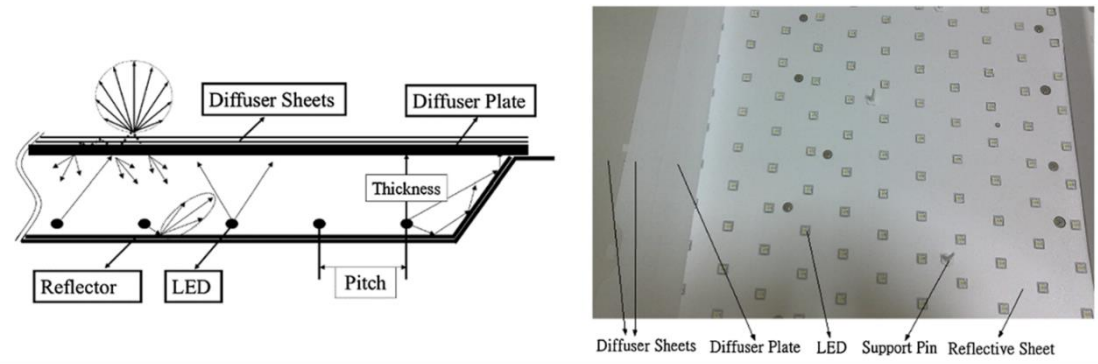

Figure 4.2. LED backlight unit (BLU): (a) diagram of BLU function and (b) diagram of LED BLU structure [5].

Towards the application of PMMA in diffusing plates of LCDs, thermal deformation caused by the heat from backlight units as shown in Figure 4.3 [5], is a serious problem. Therefore, it is important to suppress thermal expansion of such plates especially when it is applied to large LCDs. Considering these circumstances, controlling optical properties of PMMA is carried out in this chapter. Influence of humidity on optical

properties of PMMA is also investigated. There have been few reports about the influence of water absorbency on the optical properties of PMMA. The reason for this is believed that the polarizing plate protective film has a structure sandwiched by other layers in a liquid crystal display and it is hardly affected by water. However, this research is useful for the development of displays to be used under high humidity.

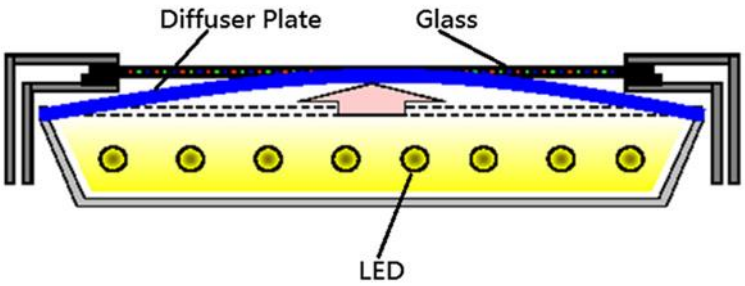

Figure 4.3. Schematic illustration of the diffuser plate under thermal deformation [5].

4.1.2. Purpose

It is known that the addition of low-molecular-weight compounds results in remarkable change on various optical properties of host polymers: e.g. refractive index, photoelastic birefringence, and orientation birefringence [6]–[8]. In a previous study, it was reported that T_g of PMMA is enhanced by more than 40°C by the addition of 30 wt.% of $LiCF_3SO_3$, making it comparable with that of polycarbonate [9], [10], known as another transparent plastic with high heat resistance. Furthermore, it does not affect the transparency up to 60 wt.% of the salt content [11]. In this chapter, the effect of ion-dipole interaction on the optical and thermos-mechanical properties was investigated.

4.1.3. Birefringences

Birefringence is represented by the sum of three terms corresponding to their origins [12]:

$$\Delta n = \Delta n_{\mathrm{O}} + \Delta n_{\mathrm{G}} + \Delta n_{\mathrm{F}} \tag{4.1}$$

where Δn_{O}, Δn_{G}, and Δn_{F} are the orientation birefringence, photoelastic birefringence, and form birefringence, respectively. Each term relates to different physical conformation of polymer chains. The first term relates to the orientation of the polymer chains, which caused by flow/deformation of molecular chains. The second term relates to the localized elastic deformation of the molecular chains in the glassy state. The third term relates to the anisotropic nano/micro-structure, such as array of nanostructured domains and lamellar structures [13].

Because the samples prepared in this study were assumed to be homogeneous, the form birefringence is negligible (*i.e.*, $\Delta n_{\mathrm{F}} = 0$). Therefore, the effects of the addition of $LiCF_3SO_3$ on the orientation birefringence (Δn_{O}) and the photoelastic birefringence (Δn_{G}) were discussed.

Orientation birefringence is provided by the flow field at processing operations. Here, the mechanism of orientation birefringence is briefly explained. When polymer chains are oriented, orientation birefringence is generated. Figure 4.4 represents the schematic illustration of a polymer chain composed of refractive index ellipsoids of monomer units.

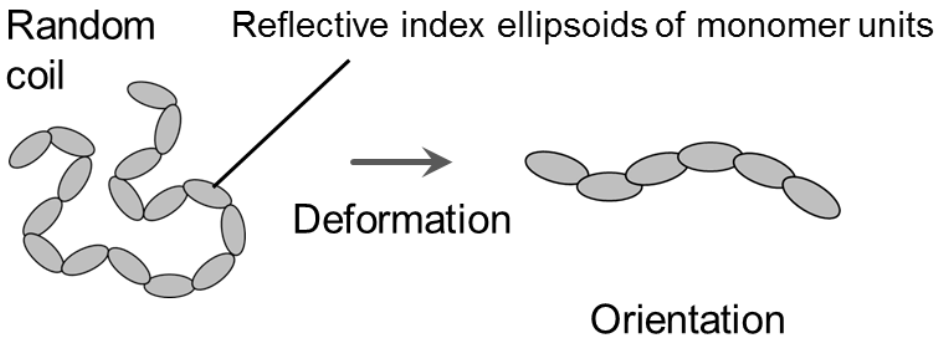

Figure 4.4. Generation of orientation birefringence.

When monomer units are randomly oriented, which is so called a random coil, there are no differences in the refractive index among the directions. In other words, it is an isotropic substance in macroscopic scale. However, when a polymeric material is deformed, polymer chains orient in the direction. As a result, orientation birefringence is generated.

The orientation birefringence becomes positive when the index ellipsoids are aligned parallel to the molecular chains. On the contrary, the orientation birefringence becomes negative when index ellipsoids are aligned perpendicular direction to the molecular chains. Furthermore, the orientation birefringence is given by the following equation [12].

$$\Delta n_{\mathrm{O}} = \Delta n^0 F \tag{4.2}$$

where F is the Hermans orientation function and Δn^0 is the intrinsic birefringence given by the following equation;

$$\Delta n^0 = \frac{2\pi}{9}\frac{\left(\bar{n}^2+2\right)^2}{\bar{n}} N\Delta\alpha_p \tag{4.3}$$

where $\bar{n}$ is the average refractive index, N is the number of molecules in unit volume, and $\Delta\alpha_p$ is the polarizability anisotropy.

Here, Δn^0 is equal to the value of birefringence when main chains are completely

uniaxial oriented (F = 1), and it is determined only by the chemical structure of the monomer unit.

Birefringence is also generated by elastic deformation in the glassy state, known as photoelastic birefringence, which usually causes bad effects on the final product of displays. It is known that the photoelastic birefringence is proportional to stress, as indicated by the equation (4.4) [14].

$$\Delta n_{\mathrm{G}} = C_{\mathrm{G}}\sigma \tag{4.4}$$

where C_{G} the stress-optical coefficient and σ is the stress. C_{G} is an intrinsic value for a material.

PMMA is known to show negative intrinsic birefringence and negative orientation birefringence due to the perpendicular orientation of the side chains to main chains. Both Δn_{O} and Δn_{G} are small.

4.2. Experimental

4.2.1. Chemicals

The polymer utilized in this research was a commercially available PMMA (Acrypet VH; Mitsubishi Chemical Corp.). The number- and weight-average molecular weights, which were estimated using size-exclusion chromatography (HLC-8020; Tosoh Corp.) with chloroform as the solvent, were M_{n} = 54,000 and M_{w} = 120,000 (standard: polystyrene (PS)), respectively. $LiCF_3SO_3$ (purity ≥ 98.0 %; Kanto Chemical Co., Ltd.) was used without further purification.

4.2.2. Sample preparation

Fabrication of blend film

The scheme of the sample preparation was the same way as written in Chapter 2. The molar ratios of lithium ions per 1 mole of carbonyl groups of PMMA were fixed to 0, 0.03, and 0.07 of the lithium salt. These molar ratios were corresponded to 0, 5, and 10 wt.% for $LiCF_3SO_3$. The samples were used for the measurements immediately after compression-molding.

The effect of water absorption on optical properties was evaluated using the samples kept at 25 °C and 50 % relative humidity (RH) in a temperature- and humidity-controlled chamber until the time to reach the equilibrium moisture contents of the samples. The refractive index, glass birefringence and orientation birefringence of the samples after water absorption were measured in the same methods as the samples before water absorption.

4.2.3. Measurements

The temperature dependence of the storage modulus, E', and loss modulus, E'', were measured in the temperatures from 30 to 200 °C by the dynamic mechanical analyzer. The frequency was set at 10 Hz. Heating rate was fixed to 2 °C/min.

The refractive indices of the films with different salt contents were evaluated using an Abbe refractometer (DR-M2; Atago Co., Ltd.) at 589 nm and room temperature. For a contact liquid on the film, 1-bromonaphthalene (purity 97 %; refractive index 1.658; Sigma-Aldrich Co., Ltd.) was used in the measurements.

The stress–strain curves were measured using a tensile machine equipped with a temperature controller (Rheogel-S1000; UBM Co., Ltd.,). The initial length of the rectangular films was 10 mm and the draw ratio was 2. One of the chucks moved at a

constant speed of 0.5 mm/s; i.e., the initial strain rate was 0.05 s^{-1}. The tensile test was performed under the temperature at which the tensile storage modulus at 10 Hz was 100 MPa. After hot-stretching by the tensile machine, the sample was immediately cooled in an air stream and taken out. The retardation (R_e) of the stretched film was measured at room temperature using a birefringence-measuring instrument (KOBRA-WPR; Oji Scientific Instruments Co., Ltd.) at 450, 498, 550, 589, 629, and 751 nm. The photoelastic birefringence in the glassy region was also obtained by the birefringence-measuring instrument under various loads at room temperature.

The linear coefficient of thermal expansion was measured using a thermal mechanical analyzer (TMA4000SA, Bruker AXS Co., Ltd.) in the temperature range from 0 to 100 °C. The sample size was 0.3 mm in thickness and 5 mm × 25 mm in area. The tension load and heating rate were 20 kPa and 5 °C/min, respectively.

ATR measurements using a KRS-5 ATR prism were held to evaluate infrared spectra under nitrogen flow. The accumulation counts were 4 times, and the resolution was 4 cm^{-1}.

4.3. Results and Discussion

4.3.1. Dynamic mechanical moduli

Figure 4.5 shows the temperature dependence of the dynamic mechanical moduli with changing the salt concentration. The storage modulus *E'* decreased slightly in the glassy region and fell down sharply around at 120 °C for pure PMMA, which is attributed to the glass-to-rubber transition, that is, α-relaxation mode. In the tan δ curves, a distinct peak appeared in the temperature range 120–160 °C. In addition, a broad ambiguous peak of tan δ appeared in the temperature range 30–80 °C for pure PMMA as indicated by the arrow, which was ascribed to β-relaxation mode. Several research groups reported that this

is due to the local motion of side chains of PMMA [15]–[18].

It was found that the $LiCF_3SO_3$ addition enhances *E'* and reduces its temperature dependence in the glassy region. Furthermore, the magnitude of tan δ in the glassy region was reduced. This tendency suggests that β-relaxation is suppressed by $LiCF_3SO_3$, which leads to the small level of temperature dependence of *E'*.

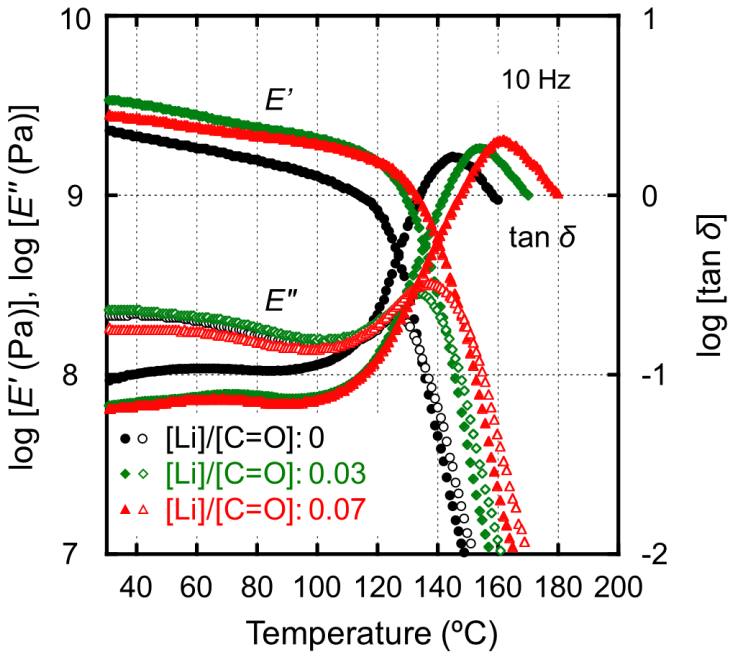

Figure 4.5. Temperature dependence of tensile moduli and loss tan δ at 10 Hz for of PMMA/$LiCF_3SO_3$ ([Li]/[C=O] ratios of 0, 0.03, and 0.07).

Furthermore, T_g was enhanced with the $LiCF_3SO_3$ concentration, as explained in Chapter 2 [11]. The hot-stretching was performed at the temperature when *E'* is 100 MPa at 10 Hz. In this experiment, the orientation birefringence of the stretching film after moisture absorption was studied besides the dried samples.

4.3.2. Refractive index

Because of low refractive index of $LiCF_3SO_3$ due to the large amount of fluorine, the blends had lower refractive indices as the salt concentration increased. Although the refractive index of $LiCF_3SO_3$ has not been elucidated experimentally, it was calculated to be 1.35 [19].

Here, the surface reflectance (*R*) of the blends were estimated using the following equation (4.5) [13].

$$R = \left(\frac{n-1}{n+1}\right)^2 \quad (4.5)$$

where *n* denotes the refractive index [13].

Figure 4.6 shows the refractive indices at 589 nm as a function of the $LiCF_3SO_3$ contents at 25 °C.

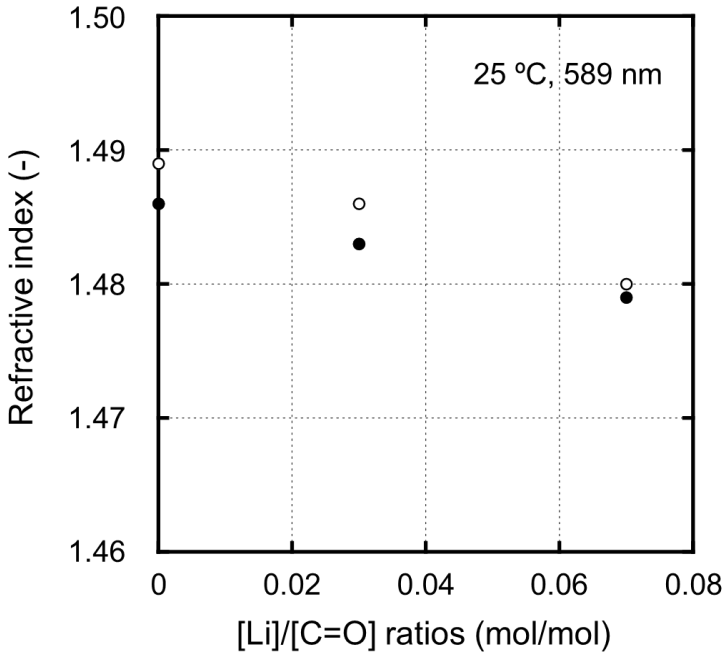

Figure 4.6. Refractive indices at 589 nm for PMMA/$LiCF_3SO_3$ blends ([Li]/[C=O] ratios of 0, 0.03, and 0.07) at 25 °C. Open symbols denote dried blends and closed symbols represent moisture-absorbed blends.

In general, for the transparent plastics such as PMMA (n=1.492 [20]), polycarbonate (PC; n=1.584 [20]), and polystyrene (PS; n=1.592 [20]), light transmittance was one of the most important properties for optical applications mainly determined by the surface reflection.

As shown in Table 4.1, PMMA has originally the lowest refractive index among them. Therefore, the result in Figure 4.6 indicates that the surface reflectance (R) of PMMA can be further reduced by the addition of the salt.

Table 4.1. Refractive indices (*n*) and surface reflections (*R*) at 589 nm for PMMA, PC, and PS [20].

Material	*n* (-)	*R* (%)
PMMA	1.492	3.9
PC	1.584	5.1
PS	1.592	5.2

Furthermore, after storage in a temperature- and humidity-controlled chamber (25 °C and 50 % RH), the refractive indices of the samples decreased. This is reasonable because the refractive index of water is about 1.3. The refractive indices and the surface reflectance of the dried and moisture-absorbed sample are summarized in Table 4.2 and Table 4.3. The blends had lower refractive indices and lower surface reflectance as the salt concentration increased because of the higher equilibrium moisture content in the blends.

Table 4.2. Refractive indices (*n*) and surface reflections (*R*) at 589 nm for PMMA/$LiCF_3SO_3$ films with different salt concentrations ([Li]/[C=O] ratio of 0, 0.03, and 0.07 mol/mol) of dried blends.

[Li]/[C=O] (mol/mol)	*n* (-)	*R* (%)
0	1.489	3.860
0.03	1.486	3.822
0.07	1.480	3.746

Table 4.3. Refractive indices (*n*) and surface reflections (*R*) at 589 nm for PMMA/$LiCF_3SO_3$ films with different salt concentrations ([Li]/[C=O] ratio of 0, 0.03, and 0.07 (mol/mol)) of moisture-absorbed blends.

[Li]/[C=O] (mol/mol)	*n* (-)	*R* (%)
0	1.486	3.822
0.03	1.483	3.784
0.07	1.479	3.734

4.3.3. Orientation birefringence

The stress–strain (S-S) curves at hot-stretching for the blends are shown in Figure 4.7. Here, the stress was calculated assuming that there were no change in the cross-sectional area depending on the applied strain. The strain was the engineering value.

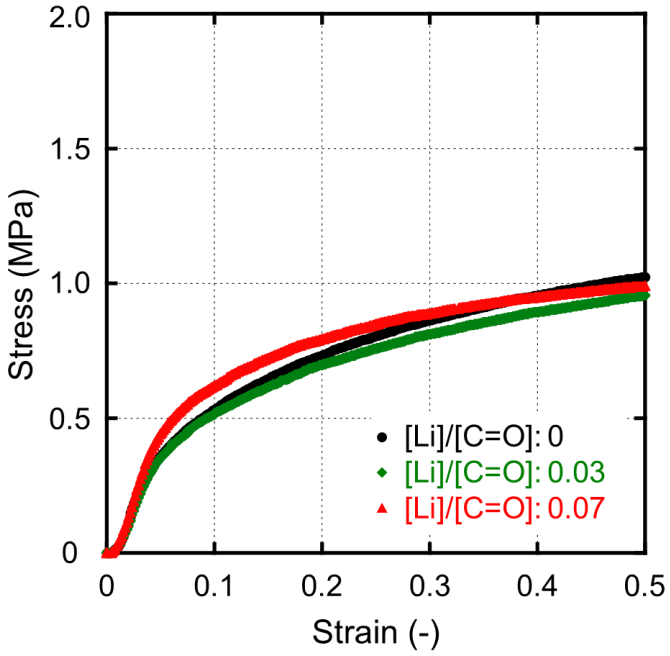

Figure 4.7. Stress-strain curves at hot-stretching for PMMA/$LiCF_3SO_3$ ([Li]/[C=O] ratios of 0, 0.03, and 0.07).

The growth curves of S-S curves and therefore the stress at the strain of 0.5 were identical for all the films. This suggests that the degree of molecular orientation, that is, the orientation function, of the main chains was similar. The orientation birefringence (Δn_O) of each stretched film was measured at room temperature after taking out from the stretching machine.

It is commonly known that PMMA has a small and negative intrinsic birefringence [1]. Therefore, it is reasonable that the negative orientation birefringence was observed in Figure 4.8.

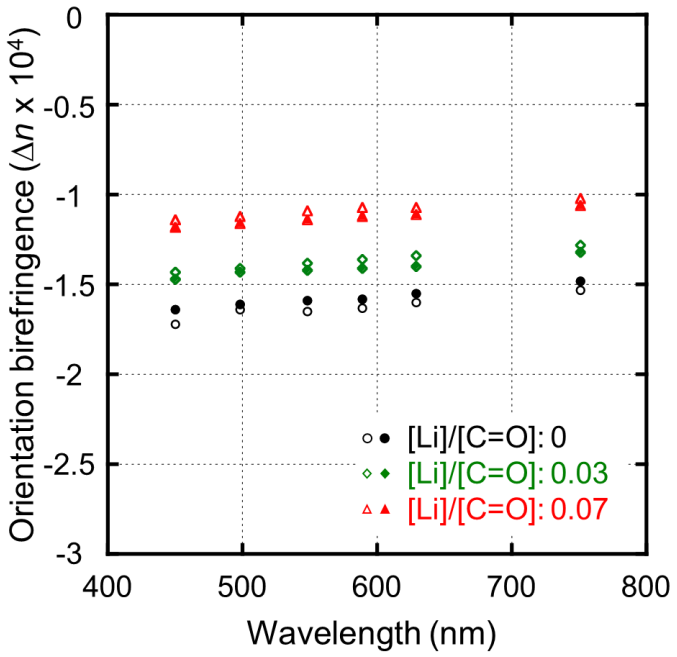

Figure 4.8. Wavelength dispersion of orientation birefringence for PMMA/$LiCF_3SO_3$ films with different salt concentrations. The salt concentrations were 0, 0.03, and 0.07 molar ratios of lithium ions to PMMA carbonyl groups; (black) 0 molar ratio, (green) 0.03 molar ratio, and (red) 0.07 molar ratio of each salt to PMMA carbonyl groups. Open symbols show dried blends and closed symbols show moisture-absorbed blends.

The orientation birefringence was calculated by subtracting the glass birefringence caused by the residual stress from the birefringence after stretching in the stretched film.

Furthermore, the wavelength dispersion was negligible because PMMA has high transparency in visible region, i.e., no/little absorption in the ultraviolet region. As the $LiCF_3SO_3$ concentration increased, the absolute value of orientation birefringence decreased.

In a miscible blend composed of a polymer and a low-molecular-weight compound, orientation correlation (nematic interaction) is induced during deformation or flow [21]–[26]. Because polymer chains make low-molecular-weight compounds align to the flow/deformation direction, the optical anisotropy is decided by the contributions of both polymers and low-molecular-weight compounds. Because of the positive intrinsic birefringence of $LiCF_3SO_3$, the orientation birefringence, Δn_O increased towards positive (the absolute value of orientation birefringence decreased). If the molecular size of the low-molecular-weight compound corresponds to the segment size of the host polymer, the nematic interaction is enhanced [23]–[25]. Another possibility is that intrinsic birefringence of PMMA was affected by the ion–dipole interaction between the lithium cations and the carbonyl groups in PMMA. The orientation birefringence decreased when the polarizability anisotropy was weakened by such ion-dipole interaction, as shown in equation (4.4). The quality of protective films of PMMA can be improved using this technique by reduction of the orientation birefringence with T_g enhancement.

Furthermore, there were no significant changes in the orientation birefringence of pure PMMA and blend films even after water absorption. The influence of water molecules on the orientation birefringences can be negligible because the equilibrium moisture contents were small, as shown in Figure 2.18 and 2.19.

4.3.4. Photoelastic birefringence

Figure 4.9 represents the stress-optical coefficient, which is the ratio of the birefringence to the stress [27], in the glassy region, which determines the photoelastic birefringence (Δn_G).

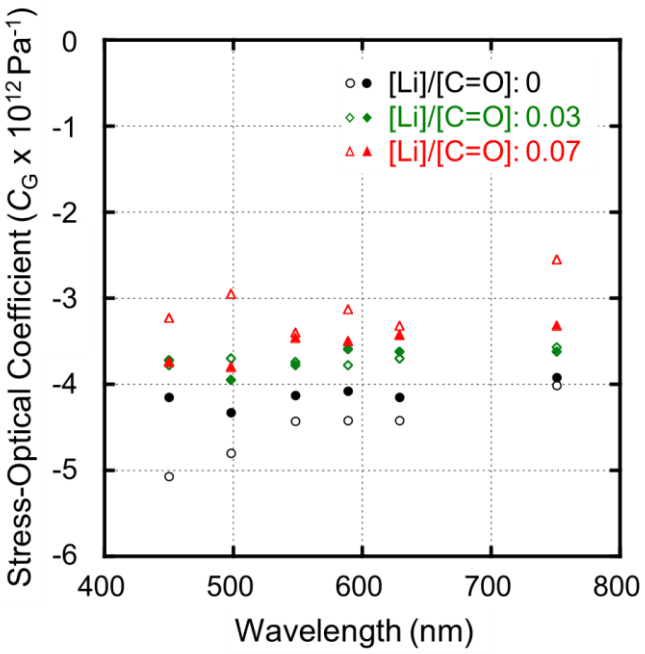

Figure 4.9. Stress-optical coefficient in the glassy region as a function of wavelength for the blends with different salt concentrations. The salt concentrations were 0, 0.03, and 0.07 molar ratios of lithium ions to PMMA carbonyl groups; (black) 0 molar ratio, (green) 0.03 molar ratio, and (red) 0.07 molar ratio of each salt to PMMA carbonyl groups. Open symbols show dried blends and closed symbols show moisture-absorbed blends.

The stress-optical coefficient of pure PMMA was approximately -4.3×10^{-12} Pa^{-1}, which corresponds to the value reported [28]. As the contents of $LiCF_3SO_3$ increased, the photoelastic birefringence was clearly decreased. The reduced local motion, which is predictable from the reduction of β relaxation mode, is responsible for the phenomenon. A recent study implied that filling free volume by adding an antiplasticizer reduces the stress-optical coefficient in the glassy state [29]. This study will lead another good way to reduce the photoelastic birefringence with pronounced heat resistance [11].

Furthermore, the stress-optical coefficient of pure PMMA after water absorption became slightly smaller than that before water absorption. This can be also explained by the hydrogen bonding between water molecules and the carbonyl group of the side chains in PMMA as shown in Figure 4.10, which restricts β relaxation mode of PMMA.

On the other hand, in the case of the PMMA/$LiCF_3SO_3$ blend, the stress-optical coefficients did not change by moisture absorption. The β relaxation mode was suppressed by the ion-dipole interactions between lithium cations and carbonyl groups, even after moisture absorption.

As shown in the ATR spectra, water molecules interact with the carbonyl group by hydrogen bonding in the moisture-absorbed blend, bringing the broadening of the peak at 1724 cm^{-1} attributed to carbonyl stretching vibration mode in the lower wavenumber region. As for the glass birefringence, the effect of ion dipole interaction between carbonyl group and lithium cation on the suppression of β dispersion is supposed to be larger than that of plasticization by water absorption. The influence of water molecules on the photoelastic birefringences can be negligible because the equilibrium moisture contents were small, as

shown in Figure 2.18 and 2.19.

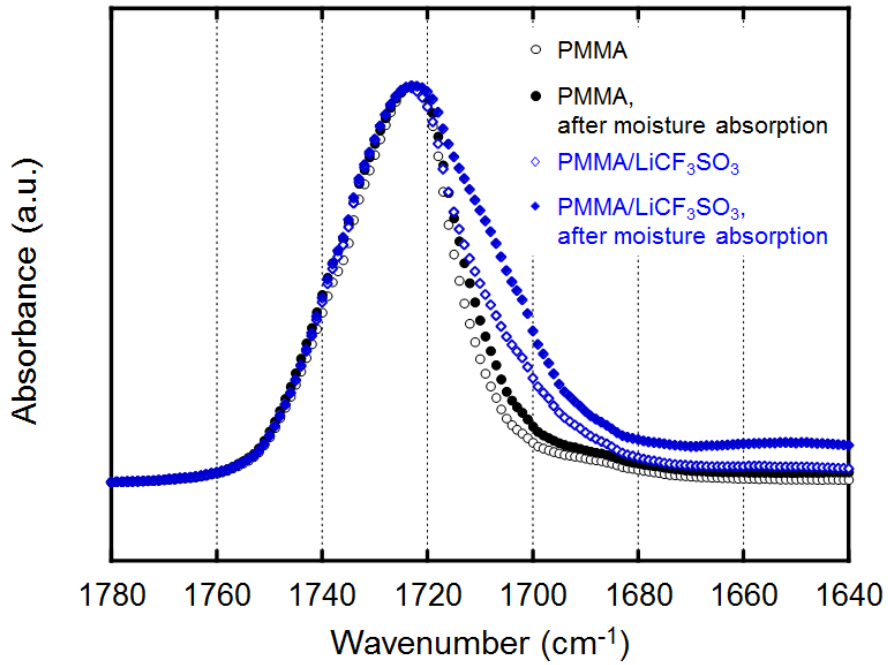

Figure 4.10. Attenuated total reflection (ATR) spectra of (black, open symbols) PMMA, (black, closed symbols) dried PMMA, (blue, open symbols) dried PMMA/$LiCF_3SO_3$ ([Li]/[C=O] ratio of 0.07), and (blue, closed symbols) moisture-absorbed PMMA/$LiCF_3SO_3$ ([Li]/[C=O] ratio of 0.07).

4.3.5. Linear thermal expansion

The linear coefficient of thermal expansion (α) is described by the following equation:

$$\alpha = \frac{1}{l_0}\left(\frac{dl}{dT}\right) \tag{4.6}$$

where l is the length. Figure 4.11 shows the temperature dependence of the linear thermal expansion coefficient. The average values of the linear expansion coefficient are plotted per 10 °C in this figure.

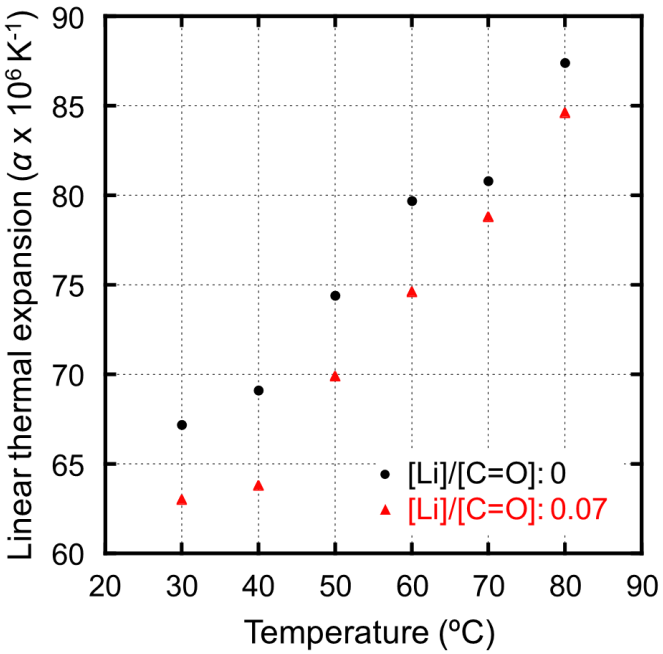

Figure 4.11. Temperature dependence of linear coefficient of thermal expansion α for PMMA/$LiCF_3SO_3$ blends with different $LiCF_3SO_3$ contents ([Li]/[C=O] ratio of 0 and 0.07 mol/mol).

According to Figure 4.11, the thermal expansion was reduced by the addition of $LiCF_3SO_3$. In general, thermal expansion in glassy polymers often becomes a problem because the values are much larger than those of ceramics and metals [30]. To overcome this problem, inorganic fillers are often mixed with polymers [31]. When such fillers are mixed, however, the materials easily lose their optical transparencies. Recently, it was reported that an antiplasticized system shows low thermal expansion [23]. This result indicates that the addition of a metal salt to a polymer is a promising way to suppress thermal expansion especially for optical applications such as laminated films with inorganic glass and polymer films with aluminum frames.

Here, the mechanism of the reduced thermal expansion in the blend film is discussed. In general, the skeletal vibrations of molecular chains dominate the coefficient of linear expansion of polymers [32]. The intermolecular potential energy consists of the attractive force and the repulsive force. The molecular motion is restricted by the addition of $LiCF_3SO_3$ because of ion–dipole interactions. Because the attractive force is increased by introducing ion–dipole interactions, the minimum of the potential well of the intermolecular force deepens. Therefore, the thermal expansion was reduced.

4.4. Conclusion

The optical and thermal properties of the blend films of PMMA with $LiCF_3SO_3$ were investigated in this chapter. The orientation birefringence of films was decreased by addition of $LiCF_3SO_3$ when the film was stretched with the same level of stress. The orientation birefringence of the blend was small since pure PMMA has a small intrinsic birefringence. Moreover, the addition of $LiCF_3SO_3$ reduced the photoelastic birefringence in the glassy state, that is, the stress-optical coefficient. As described in the previous chapter, it was found

that T_g was enhanced with reduced localized segmental motion by the addition of the salt. This may be attributed to the ion–dipole interactions between the lithium cations and the carbonyl groups of the PMMA. The optical properties of the blends after moisture absorption did not show significant change as compared with those of dried blends. The thermal expansion was reduced by the ion-dipole interactions. The modification of properties of PMMA by blending with salts is an attractive choice for optical applications including LCDs.

4.5. References

[1] S. Houran, A. Tagaya, and Y. Koike, "Mechanism of generation of photoelastic birefrengence in methacrylate polymers for optical devices," *J. Polym. Sci. Part B Polym. Phys.*, vol. 45, no. April, pp. 1390–1398, 2007.

[2] M. Yamazaki, "Industrialization and application development of cyclo-olefin polymer," *J. Mol. Catal. A Chem.*, vol. 213, no. 1, pp. 81–87, 2004.

[3] M. Schadt, "Nematic liquid crystals and twisted-nematic LCDs," *Liq. Cryst.*, vol. 42, no. 5–6, pp. 646–652, 2015.

[4] T. J. Hammack and R. D. Andrews, "Temperature dependence of orientation birefringence of polymers in the glassy and rubbery states. II," *J. Appl. Phys.*, vol. 36, no. 11, pp. 3574–3581, 1965.

[5] C. H. Chien, C. C. Chen, T. Chen, Y. M. Lin, and Y. C. Liu, "Thermal deformation of microstructure diffuser plate in LED backlight unit," *J. Soc. Inf. Disp.*, vol. 24, no. 2, pp. 99–109, 2016.

[6] P. Kelly, A. Akelah, S. Qutubuddin, and A. Moet, "Reduction of residual stress in montmorillonite/epoxy compounds," *J. Mater. Sci.*, vol. 29, no. 9, pp. 2274–2280, 1994.

[7] B. Ung, A. Dupuis, K. Stoeffler, C. Dubois, and M. Skorobogatiy, "High-refractive-index composite materials for terahertz waveguides: trade-off between index contrast and absorption loss," *J. Opt. Soc. Am. B*, vol. 28, no. 4, pp. 917–921, 2011.

[8] B. R. Hahn and J. H. Wendorff, "Compensation method for zero birefringence in oriented polymers," *Polymer*, vol. 26, no. 11, pp. 1619–1622, 1985.

[9] N. Shamim, Y. P. Koh, S. L. Simon, and G. B. McKenna, "Glass transition temperature of thin polycarbonate films measured by flash differential scanning

calorimetry," *J. Polym. Sci. Part B Polym. Phys.*, vol. 52, no. 22, pp. 1462–1468, 2014.

[10] Zhu L., Chiu F.C., Fu Q., Quirk R.P., Cheng S.Z.D., "Polymer handbook." p. 26, 1999.

[11] A. Miyagawa, V. Ayerdurai, S. Nobukawa, and M. Yamaguchi, "Viscoelastic properties of poly(methyl methacrylate) with high glass transition temperature by lithium salt addition," *J. Polym. Sci. Part B Polym. Phys.*, vol. 54, no. 22, pp. 2388–2394, 2016.

[12] H. Shimada, S. Nobukawa, T. Hattori, and M. Yamaguchi, "Wavelength dispersion of birefringence of oriented polyethylene films," *Appl. Opt.*, vol. 56, no. 13, pp. 3806–3811, 2017.

[13] M. Born and E. Wolf, *Principles of optics*. New York: Cambridge University Press, 1999.

[14] A. S. Voloshin and C. P. Burger, "Half-fringe photoelasticity: A new approach to whole-field stress analysis," *Exp. Mech.*, vol. 23, no. 3, pp. 304–313, 1983.

[15] E. Muzeau, J. Perez, and G. P. Johari, "Mechanical spectrometry of the beta-relaxation in poly(methyl methacrylate)," *Macromolecules*, vol. 24, no. 16, pp. 4713–4723, 1991.

[16] K. Schmidt-Rohr *et al.*, "Molecular nature of the β relaxation in poly(methyl methacrylate) investigated by multidimensional NMR," *Macromolecules*, vol. 27, no. 17, pp. 4733–4745, 1994.

[17] F. Garwe, A. Schönhals, H. Lockwenz, M. Beiner, K. Schröter, and E. Donth, "Influence of cooperative α dynamics on local β relaxation during the development

of the dynamic glass transition in poly(n-alkyl methacrylate)s," *Macromolecules*, vol. 29, no. 1, pp. 247–253, 1996.

[18] W. J. Davis and R. A. Pethrick, "Mechanical Thermal Analysis," vol. 39, no. 2, pp. 255–266, 1998.

[19] "United States Environmental Protection Agency." [Online]. Available: https://comptox.epa.gov/dashboard/dsstoxdb/results?search=DTXSID3044419#properties.

[20] H. Kawai, "光学用プラスチック材料, Plastic molding materials for precision optics (in Japanese)," 光学, vol. 24, no. 2, pp. 69–75, 1994.

[21] M. Yamaguchi, M. E. A. Manaf, K. Songsurang, and S. Nobukawa, "Material design of retardation films with extraordinary wavelength dispersion of orientation birefringence: A review," *Cellulose*, vol. 19, no. 3, pp. 601–613, 2012.

[22] M. E. A. Manaf, A. Miyagawa, S. Nobukawa, Y. Aoki, and M. Yamaguchi, "Incorporation of low-mass compound to alter the orientation birefringence in cellulose acetate propionate," *Opt. Mater. (Amst).*, vol. 35, no. 7, pp. 1443–1448, 2013.

[23] A. Miyagawa, S. Korkiatithaweechai, S. Nobukawa, and M. Yamaguchi, "Mechanical and optical properties of polycarbonate containing p-terphenyl," *Ind. Eng. Chem. Res.*, vol. 52, no. 14, pp. 5048–5053, 2013.

[24] S. Nobukawa *et al.*, "Strong orientation correlation and optical anisotropy in blend of cellulose ester and poly(ethylene 2,6-naphthalate) oligomer," *J. Appl. Polym. Sci.*, vol. 131, no. 15, p. 40570, 2014.

[25] S. Nobukawa *et al.*, "The effect of flexible chains on the orientation dynamics of small molecules dispersed in polymer films during stretching," *Polym. J.*, vol. 47, no. 4, pp. 294–301, 2015.

[26] A. Kiyama, S. Nobukawa, and M. Yamaguchi, "Birefringence control of solution-cast film of cellulose triacetate," *Opt. Mater. (Amst).*, vol. 72, pp. 491–495, 2017.

[27] D.-S. Ryu, T. Inoue, and K. Osaki, "A simple evaluation method of stress-optical coefficient of polymers," *Nihon Reoroji Gakkaishi*, vol. 24, no. 3, pp. 129–132, 1996.

[28] A. Tagaya, H. Ohkita, T. Harada, K. Ishibashi, and Y. Koike, "Zero-birefringence optical polymers," *Macromolecules*, vol. 39, no. 8, pp. 3019–3023, 2006.

[29] S. Nobukawa, S. Hasunuma, T. Sako, A. Miyagawa, and M. Yamaguchi, "Reduced stress-optical coefficient of polycarbonate by antiplasticization," *J. Polym. Sci. Part B Polym. Phys.*, vol. 55, no. 24, pp. 1837–1842, 2017.

[30] Y. S. Touloukian, R. K. Kirby, R. E. Taylor., and T. Y. R. Lee., *Thermophysical Properties of Matter: Thermal Expansion of Nonmetallic Solids*. New York: Plenum Press, 1975.

[31] L. E. Nielson and R. F. Landel, *Mechanical properties of polymers and composites*. CRC Press, 1994.

[32] D. Porter, *Group Interaction Modelling of Polymer Properties*. New York: Marcel Dekker, Inc, 1995.

Chapter 5

General conclusion

The most important property of PMMA must be its high transparency. Because of this characteristic, PMMA is recognized as one of the most useful plastic glasses. This study was performed to modify PMMA by a novel method to provide high heat resistance and low birefringence without losing transparency. Flowability is also one of the important factors for engineering applications. The film fabrication with the salts to PMMA described in study does not lose thermoprocessability.

In this research, the addition of a lithium salt, e.g., $LiCF_3SO_3$ and LiBr, was employed to modify such thermal and optical properties. Heat resistance of PMMA was evaluated by T_g. The effect of water absorption on the heat resistance, i.e., T_g enhancement, was also evaluated because a salt usually absorbs water.

$LiCF_3SO_3$ is dissolved in PMMA completely, and dissociated to lithium cations and triflate anions. The lithium cations interact with carbonyl groups in PMMA. Thus, the segmental motions of PMMA were restricted by ion-dipole interaction. In this study, it was found that carbonyl groups of PMMA physically interact with both lithium cations and bromide anions.

Chapter2: Improvement of heat resistance of poly(methyl methacrylate) by addition of lithium salts

The effect of the addition of various lithium salts on T_g of PMMA was evaluated. Various lithium salts used for lithium ion batteries, e.g., $LiClO_4$, $LiCOOCF_3$, and $LiCF_3SO_3$ etc., were employed. It was found from the temperature dependence of dynamic tensile moduli that $LiCF_3SO_3$ was the most effective one to enhance T_g. However, $LiCF_3SO_3$ itself has high water absorbency. Since it is well known that the water absorbency greatly affects the physical properties of polar polymers including PMMA, the effect of the water absorption on T_g was investigated. It was found that T_g shifted to low temperature with a low modulus in the glassy state after leaving the sample containing $LiCF_3SO_3$ in the humid condition. This is attributed to the plasticizing effect by water. According to a previous report based on the MD simulation of triflate and bromide anions at the air/water interface, a sample of PMMA containing LiBr has less water absorbency than a sample of PMMA containing $LiCF_3SO_3$. Considering this research, the blend with LiBr was also prepared in the same way as the blend with $LiCF_3SO_3$. As a result, it was revealed that the addition of LiBr enhanced T_g of PMMA and maintained high T_g even after water absorption.

Chapter 3: Effect on T_g enhancement of poly(methyl methacrylate) by addition of LiBr

In this chapter, the effect of the LiBr addition on the viscoelastic properties for PMMA precisely. It was found from the temperature dependence of dynamic tensile moduli that a long-time relaxation mode appears in PMMA/LiBr. This result seems strange because the interaction with the carbonyl group, evaluated by IR, was weak for the blend with LiBr as compared with that with $LiCF_3SO_3$. This contradictory phenomenon can be explained by quite strong interaction in PMMA, which occurred by the addition of LiBr. Mechanism of such strong interaction is due to the interaction of carbonyl groups of PMMA molecules with both lithium cations and bromide anions. The solvent immersion experiments using THF revealed that the strong interaction occurred at heating process for PMMA/LiBr. Subsequent solvent immersion experiments after rinsing with methanol indicated that the strong interaction is not due to chemical crosslinking. According to IR study of PMMA and PMMA/LiBr with/without rinsing by methanol, PMMA/LiBr without rinsing showed lower peak intensities of carbonyl groups than pure PMMA. Because methanol can only dissolve LiBr, rinsing with methanol increased the peak intensities of carbonyl groups in PMMA/LiBr. Although the details in the peculiar behavior of PMMA containing LiBr are unknown, the ionic sizes of LiBr may be suitable to go into the gap between two carbonyl groups in PMMA. Consequently, lithium cations and bromide anions move to the stable positions by heat diffusion during heating process and settled down the places by rapidly cooling.

Chapter 4: Improvement of optical properties of poly(methyl methacrylate) by addition of $LiCF_3SO_3$

PMMA has been commonly utilized for polarizer protective films of LCDs. Therefore, it is necessary to control birefringence. In this chapter, the effect of the $LiCF_3SO_3$ salt addition on photoelastic birefringence in the glassy state and orientation birefringence was studied to reduce the birefringence in both cases. As a result, both birefringences were reduced by the addition of $LiCF_3SO_3$. In the glassy state, it is known that the motion of the carbonyl bond in perpendicular orientation to main chains caused that negative photoelastic birefringence. Based on this, the reduction of the photoelastic birefringence was owing to the reduction of β relaxation mode caused by the ion–dipole interactions.

On the other hand, in rubbery state, it is known that negative orientation birefringence is provided by the perpendicular orientation of C-O-C bond in the side chains to the main chains of PMMA. Therefore, it was assumed that such rotation of the side chain is restricted and thus, orientation birefringence is reduced by the ion-dipole interaction in the blend with $LiCF_3SO_3$. The optical properties of the blends after moisture absorption did not show significant change as compared with those of dried blends.

Thermal expansion is another problem for LCDs, which could lead to thermal warpage of the displays caused by heat of fluorescent lamps in backlight units. Furthermore, the stress given by the thermal expansion produces excess birefringence. These results obtained in this chapter, that is, reduction of orientation birefringence, low stress-optical coefficient in the glassy region, and reduced thermal expansion, will be great benefits for protective films.

Future prospects:

Plastic materials such as PMMA are necessary for our lives because of their versatility. The findings on the improvement of both heat resistance and optical properties by the addition of specific lithium salts would be useful for new material design in the future. There are low barriers to apply this method in industry since it is a very simple method. In addition, this method can be applied to not only PMMA but also various other polymer materials. Furthermore, by combinations of various cations and anions, there are a plenty of possibilities to control the characteristics of a single polymer and to provide new functions. Although the modification of polymer properties has been carried out in various ways, the method proposed in this study has high originality in its simplicity and usefulness. It is expected that further interesting findings can be obtained, not only in the industrial aspect but also in basic research.

Achievements

Publications

Chapter 2, 3

A. Ito, P. Phulkerd, V. Ayerdurai, M. Soga, A. Courtoux, A. Miyagawa, M. Yamaguchi, "Enhancement of glass transition temperature for poly(methyl methacrylate) by salt", *Polym. J., Nature Publishing Group*, Vol. 50, pp. 857-863, 2018. DOI: 10.1038/s41428-018-0080-4

A. Ito and M. Yamaguchi, "Effect of anion species on heat resistance of poly(methyl methacrylate)/lithium salt blends", *In preparation*

Chapter 3

A. Ito, V. Ayerdurai, A. Miyagawa, A. Matsumoto, H. Okada, A. Courtoux, M. Yamaguchi, "Effects of residual solvent on glass transition temperature of poly(methyl methacrylate)",
J. Soc. Rheol. Jpn., The Society of Rheology, Vol. 46, No. 3, pp.117-121, 2018. DOI: 10.1678/rheology.46.117

Chapter 4

A. Ito, R. Maeno, M. Yamaguchi, "Control of optical and mechanical properties of poly(methyl methacrylate) by introducing lithium salt", *Opt. Mater., Elsevier,* Vol. 83, pp. 152-156, 2018. DOI:10.1016/j.optmat.2018.06.001

Other Publications

1. T. Sako, **A. Ito**, M. Yamaguchi, “Surface segregation during injection molding of polycarbonate/poly(methyl methacrylate) blend”, *J. Polym. Res., Springer,* Vol. 24, No. 6, 89, 5 pages, 2017. DOI:10.1007/s10965-017-1251-2

2. N. Tsugawa, **A. Ito**, M. Yamaguchi, “Effect of lithium salt addition on the structure and optical properties of PMMA/PVB blends”, *Polymer, Elsevier,* Vol. 146, pp. 242-248, 2018. DOI:10.1016/j.polymer.2018.05.042

3. Y. Sato, **A. Ito**, S. Maeda, M. Yamaguchi, “Structure and Optical Properties of Transparent Polyamide 6 Containing Lithium Bromide”, *J. Polym. Sci. Pt. B Polym. Phys., Wiley,* Vol. 56, pp. 1513-1520, 2018. DOI: 10.1002/polb.24739

4. P. Phulkerd, Y. Funahashi, **A. Ito**, S. Iwasaki, M. Yamaguchi, “Perpendicular orientation between dispersed rubber and polypropylene molecules in an oriented sheet”, *Polym. J., Nature Publishing Group,* Vol. 50, pp. 309-318, 2018. DOI:10.1038/s41428-017-0017-3

Review

1. S. Maenosono, **A. Ito**, C. Shijimaya, M. Miyata, T. Akatsuka, H. Ono, M. Ohta, "Copper sulfide nanoparticles for thermoelectric materials", *The Journal of the Thermoelectrics Society of Japan,* Vol. **13**, No. 3, 140, 2017 (in Japanese).

Presentations

International Conferences

Peer-reviewed

1. **A. Ito**, C. Shijimaya, K. Higashimine, M. Miyata, D. Mott, T. Akatsuka, H. Ono, M. Koyano, and S. Maenosono, "Wet-chemical Synthesis of Transition Metal Sulfide Nanoparticles as a Sustainable Thermoelectric Material", *The 2016 MRS Fall Meeting*, 29th November 2016, Boston, USA (Oral).

2. **A. Ito**, C. Shijimaya, K. Higashimine, M. Ohta, M. Miyata, D. Mott, T. Akatsuka, H. Ono, M. Koyano, and S. Maenosono, "Thermoelectric Characteristics of Transition Metal Sulfide Nanobulks", *The 2016 MRS Fall Meeting*, 29th November 2016, Boston, USA (Poster).

3. **A. Ito**, R. Maeno, M. Soga, M. Yamaguchi, "Molecular Motion of Poly(methyl methacrylate) Containing Metal Salt", *33rd Annual Meeting of Polymer Processing Society (PPS33)*, 12nd December, 2017, Cancun, Mexico (Poster).

4. **A. Ito**, N. Tsugawa, M. Yamaguchi, "Segmental motion control of poly(methyl methacrylate) by addition of metal salts", *2018 International Conference on Smart Materials Applications (ICSMA 2018)*, 27th January 2018, Singapore (Oral).

5. **A. Ito**, M. Yamaguchi, "Impact of metal salt blending on segmental motion of poly(methyl methacrylate)", *World Polymer Congress MACRO 2018*, 4th July 2018, Cairns, Australia (Oral).

Not peer-reviewed

1. **A. Ito**, A. Miyagawa, M. Yamaguchi, "Control of dynamic mechanical properties for poly(methyl methacrylate) by salt addition", *Plastics Industry, Research & Innovations Forum 2017 (PPES 2017)*, 14-16th December 2017, Bangkok, Thailand (Poster).

Domestic Conferences

1. **A. Ito**, C. Shijimaya, K. Higashimine, M. Ohta, M. Miyata, D. Mott, T. Akatsuka, H. Ono, M. Koyano, S. Maenosono, "Synthesis and Characterization of Transition Metal Sulfide Nanoparticles as Building Blocks for Sustainable Thermoelectric Materials", *The 67th Divisional Meeting on Colloid and Interface Chemistry*, 24th September 2016, Asahikawa, Hokkaido, Japan (Poster).

2. **A. Ito**, C. Shijimaya, K. Higashimine, M. Ohta, M. Miyata, D. Mott, T. Akatsuka, H. Ono, M. Koyano, and S. Maenosono, "Multi-scale structured Thermoelectric Characteristics of Transition Metal Sulfide Materials by Panoscopic approach", *The 97th CSJ Annual Meeting*, 16th March 2017, Hiyoshi Campus, Keio-gijuku University, Yokohama, Japan (Oral).

3. **A. Ito**, M. Yamaguchi, "Enhancement of glass transition temperature by ion-dipole interaction with a metal salt for poly(methyl methacrylate)", *66th Symposium on Macromolecules*, 22th September 2017, Johoku Campus, Ehime University, Ehime, Japan (Poster).

4. **A. Ito**, M. Yamaguchi, "Structure and property of poly(methyl methacrylate) containing metal salt)", *67th SPSJ Annual Meeting*, 23rd May 2018, Nagoya Congress Center, Nagoya, Japan (Oral).

5. **A. Ito**, P. Phulkerd, M. Yamaguchi, "Modification of poly(methyl methacrylate) by addition of metal salt", *67th Symposium on Macromolecules*, 12-14th September 2018, Hokkaido University, Sapporo, Japan (Oral). (Note: This meeting was canceled because of Hokkaido Earthquake).

6. **A. Ito**, M. Yamaguchi, "Material design of poly(methyl methacrylate) with high glass transition temperature", *67th Symposium on Macromolecules*, 12-14th September 2018, Hokkaido University, Sapporo, Japan (Poster). (Note: This meeting was canceled because of Hokkaido Earthquake).

7. **A. Ito**, M. Yamaguchi, "Improvement of poly(methyl methacrylate) by addition of metal salts", JSPP symposium'18, 26-27th November 2018, Grand Hotel Hamamatsu, Hamamatsu, Japan (Poster).

Awards & Honors

1. Best Presentation Award, *2018 International Conference on Smart Materials Applications (ICSMA 2018),* 27th January 2018, Singapore.

2. Adopted as a JSPS fellow of 9th HOPE Meeting by Japan Society for the Promotion of Science (2017).

3. Adopted as a fellow of 69th Lindau Nobel Laureate Meeting (2019).

Grants

1. Doctoral Research Fellow, Japan Advanced Institute of Science and Technology (2016 to 2019).

2. Yoshida Foundation for Science and Technology, *33rd Annual Meeting of Polymer Processing Society (PPS33),* 10-14th December, 2017, Cancun, Mexico.

3. Marubun Research Promotion Foundation, *2018 International Conference on Smart Materials Applications (ICSMA 2018),* 26-28th January 2018, Singapore.

4. Research Grants for JAIST Students, *World Polymer Congress MACRO 2018,* 4th July 2018, Cairns, Australia.